RHEOLOGY AND PROCESSING OF POLY(LACTIDES) AND THEIR ENANTIOMERIC COPOLYMERS AND BLENDS.

by

Norhayani Othman

B. Eng. Universiti Teknologi Malaysia, 2004
M. Eng. Universiti Teknologi Malaysia, 2006

A THESIS SUBMITTED IN PARTIAL FULFILLMENT OF
THE REQUIREMENT FOR THE DEGREE OF

DOCTOR OF PHILOSOPHY

in

The Faculty of Graduate Studies

(Chemical and Biological Engineering)

THE UNIVERSITY OF BRITISH COLUMBIA

(Vancouver)

July 2012

Abstract

Poly(lactide) PLA, a biodegradable thermoplastic produced from corn and other renewable agricultural resources, has received a large share of the interest in biodegradable materials due to environmental concerns and desire to reduce dependence on finite petroleum reserves. In this study, nearly monodisperse controlled microstructure PLA samples synthesized using a novel chiral dinuclear indium catalyst; and studied thermorheologically. Specifically, the effects of molecular structural parameters (*i.e.* weight-average molecular weight (M_w) and different ratios of lactides) on solution and melt rheological properties under shear and extension were studied. The solution properties and linear viscoelasticity (LVE) of melts indicated linear structure behavior. The zero-shear viscosity and relaxation time of PLAs showed a power law scaling of 3.4 with M_w. The K-BKZ constitutive equation was used and proved that strain hardening occurs at low temperatures, which is due to the dynamics of molecular relaxation, when the longest relaxation time exceeded the characteristic time for deformation.

In an attempt to reduce PLA brittleness, copolymers of L-lactide with its enantiomer D-lactide or racemic mixture DL-lactide were synthesized. The effects of M_w and block length ratio on the thermal, rheological and mechanical behavior of the diblock copolymers were investigated. For comparison, blends of PDLLA and PLLA homopolymers of equivalent M_w to the diblock copolymers were prepared. Despite different thermal behavior, the linear viscoelasticity of block copolymers and blends in disordered state are relatively similar. Improvement in elongation at break and tensile strength were observed as compared to their counterpart homopolymer blends.

Furthermore, the wall slip and melt fracture behaviors of four commercial PLAs with M_w in the range of 10^4 to 10^5 g/mol were investigated. PLAs with M_w greater than a certain value slipped. The slip velocity increased with decrease of M_w. The onset of melt fracture for the high M_w PLAs occurred at about 0.2 to 0.3 MPa, depending on the geometrical characteristics of the dies and independent of temperature. Addition of 0.5 wt% of a poly(ε-caprolactone) (PCL) into the PLA that exhibits melt fracture was effective in eliminating and delaying its onset to higher shear rates.

Preface

The work of this thesis consists of three different manuscripts.

Chapter 6 and part of chapter 5 are based on manuscript that has been published. Othman, N., Ramírez, A.A., Mehrkhodavandi, P., Dorgan, J.R., Hatzikiriakos, S.G. (2011). "Solution and melt viscoelastic properties of controlled microstructure poly(lactide)". *Journal of Rheology*, 55(5), 987-1005. I conducted all the experiments and data analysis except the NMR measurements performed by Dr. Alberto Acosta-Ramírez who also synthesized the PLAs. The manuscript was a collaborative effort between my supervisors Prof. Savvas G. Hatzikiriakos and Prof. Parisa Mehrkhodavandi, Dr. Alberto Acosta-Ramírez and myself.

The materials covered in chapters 7 and part of chapter 5 has been accepted for publication. Othman, N., Xu, C., Mehrkhodavandi, P., Hatzikiriakos, S.G. (2012). "Thermorheological and mechanical behavior of polylactides and its enantiomeric diblock copolymers and blends". *Polymer*, 53(12), 2443-2452. I conducted all the experiments and data analysis except the NMR and GPC measurements performed by Cuiling Xu who also synthesized the PLAs. The manuscript was a collaborative effort between my supervisors Prof. Savvas G. Hatzikiriakos and Prof. Parisa Mehrkhodavandi, Cuiling Xu and myself.

Chapter 8 has been published. Othman, N., Jazrawi, B., Mehrkhodavandi, P., Hatzikiriakos, S.G. (2012). "Wall slip and melt fracture of poly(lactides)". *Rheologica Acta*, 51, 357-369. I conducted most of the experiments and data analysis. Bashar Jazrawi co-produced the data of PLA processing under my supervision. The manuscript was a collaborative effort between my supervisors Prof. Savvas G. Hatzikiriakos and Prof. Parisa Mehrkhodavandi, Bashar Jazrawi and myself.

The initial and final drafts of this thesis were prepared by Norhayani Othman, with revisions edited and approved by Prof. Savvas G. Hatzikiriakos and Prof. Parisa Mehrkhodavandi.

Table of Contents

List of Tables

List of Figures

Nomenclature

A	cross-sectional area, mm^2
A_o	initial cross-sectional area, mm^2
$[\alpha]$	specific optical orientations, °
α_T	horizontal shift factor
b	Rabinowitsch correction
b_T	vertical shift factor
C_∞	characteristic ratio
D	capillary diameter, mm
D_b	diameter of barrel, mm
dn/dc	specific refractive index increment, mL/g
E_a	activation energy for flow, J/mol
F	tangential force, N
$F(t)$	instantaneous extensional force at time *t*, N
F_F	frictional force, N
F_d	piston force, N
$G(t)$	stress relaxation modulus, Pa
G'	storage modulus, Pa
G''	loss modulus, Pa
$\lvert G^* \rvert$	complex modulus, Pa
G_d	amplitude ratio in oscillatory shear
G_N^o	plateau modulus, MPa
g_i	generalized Maxwell model parameter, relaxation modulus, Pa
H	gap between plates, mm
$h(\gamma)$	damping function
L/D	length to diameter ratio of the capillary die
L,Lo	capillary length; sample length, mm
n_e	slope of entanglement zone
n_g	slope of glass transition zone

M_n	number average molecular weight, g/mol
M_w	weight average molecular weight, g/mol
M_e	molecular weight between entanglements, g/mol
P	absolute pressure, Pa
P_d	driving pressure, Pa
P_{end}	Bagley correction, Pa
Δp	pressure drop, Pa
P_m	probability of meso
Q	volumetric flow rate, m^3/s
r	capillary radius, m
R	radius of SER windup drums, mm, gas constant, J/K.mol
R_h	hydrodynamic radius, mm
R_g	radius of gyration, mm
T	absolute temperature, K, torque, N.m
T_g	glass transition temperature, °C
T_m	melting temperature, °C
T_{ref}	reference temperature, °C
t	time, s
u_s	slip velocity, m/s

Greek Letters

γ	shear strain
$\dot{\gamma}$	shear rate, s^{-1}
$\dot{\gamma}_A$	apparent shear rate, s^{-1}
$\dot{\gamma}_{A,s}$	apparent shear rate corrected for slip, s^{-1}
$\dot{\gamma}_w$	wall shear rate, s^{-1}
γ_o	strain amplitude in oscillatory shear
δ	phase shift
$\dot{\varepsilon}_H$	Hencky strain rate, s^{-1}

$[\eta]$	intrinsic viscosity, Pa.s
η_o	zero-shear viscosity, Pa.s
η'	dynamic viscosity, Pa.s
η''	out-of-phase component of complex viscosity, Pa.s
η^*	complex viscosity, Pa.s
η^+	steady shear stress growth coefficient, Pa.s
η_E^+	tensile stress growth coefficient, Pa.s
λ_i	generalized Maxwell model parameter, relaxation time, s
λ_c	crossover time, s
$\lambda_{\max}$	longest relaxation time, s
ρ	density, g/cm^3
σ	shear stress, Pa
σ_c	critical shear stress for the onset of melt fracture, Pa
σ_{rz}	shear stress at location *r*, Pa
σ_w	wall shear stress, Pa
σ_o	stress amplitude in oscillatory shear, Pa
ω	frequency rad/s, angular speed s^{-1}
Φ	Flory constant

Abbreviations

BSW	Baumgaertel-Schausberger-Winter
DCM	dichloromethane
DSC	differential scanning calorimeter
GPC	gel permeation chromatography
K-BKZ	Kaye-Bernstein, Kearsley and Zapas
LA	lactide
LVE	linear viscoelastic
PM	parsimonious relaxation spectrum

PLA	poly(lactide) or poly(lactic acid)
PCL	poly(ε-caprolactone)
PHB	poly-3-hydroxybutyrate
ROP	ring-opening polymerization
THF	tetrahydrofuran
TNPP	Tris(nonylphenyl)phosphite
SER	Sentmanat Extensional Rheometer
SSP	solid state polymerization
XRD	X-ray diffraction
WLF	Williams-Landel-Ferry

Acknowledgements

I would like to express my sincere gratitude to my supervisor, Prof. Savvas G. Hatzikiriakos and my co-supervisor, Prof. Parisa Mehrkhodavandi for their skillful guidance, encouragement, patience and great concern which made this work successful.

I am thankful to colleagues from Rheology lab both past and present for giving help in every possible way, making the lab an enjoyable place to work and for their helpful discussions and exchange of ideas. I also thank to Dr. Alberto and Cuiling from Chemistry Department for synthesizing the polymers samples.

A scholarship and study leave granted by Ministry of High Education, Malaysia and Universiti Teknologi Malaysia is also gratefully acknowledged.

Last but not least I wish to express my appreciation and thanks to my parents, friends and co-workers who involved directly and indirectly. Most of all, I thank my husband and son for their endless love, support and understanding. They have been a source of my strength and motivation for success especially in periods of uncertainty and difficulty.

To my family

1 Introduction

Polymers from renewable resources have attracted an increasing amount of attention over the last decades, predominantly due to environmental concerns and the desire to reduce dependence on finite petroleum reserves. Many polymers in the polyester family exhibit biodegradability due to their hydrolysable ester bonds. These include poly(lactic acid) or poly(lactide) (PLA), polyhydroxyalkanoates (PHAs) such as the poly-3-hydroxybutyrate (PHB), polyhydroxyvalerate (PHV) and polyhydroxyhexanoate (PHH), poly(ε-caprolactone) (PCL) and polybutylene succinate (PBS) (Nampoothiri et al., 2010; Witzke, 1997).

PLA is a biodegradable thermoplastic produced from corn and renewable agricultural resources. In the past few years the use of PLA as a packaging material particularly for short shelf life products such as fruit and vegetable packaging including containers, drinking cups, salad cups, overwrap and lamination films and blister packages has increased across Europe, Japan and North America. The production and consumption of PLA is expected to increase substantially in the next ten years (Auras et al., 2004). This could be a technical and economic solution to the problem of the eventual disposal of the large amount of plastic packaging used over the world. More than 20% of the garbage thrown out by households is plastic packaging (www.rcbc.bc.ca). PLA also has medical applications such as suture, bone fixation materials, drug delivery and tissue engineering, where biodegradability and biocompatibility are desired (Nampoothiri et al., 2010). PLA is fully biodegradable by hydrolysis to lactic acid by the use of microorganisms decays into natural products, namely water and carbon dioxide.

PLA can be prepared by polycondensation of lactic acid or by ring-opening polymerization (ROP) of lactide (LA), a six-membered lactone (Wu et al., 2006; Dechy-Cabaret et al., 2004). The latter route is the most convenient and efficient method to obtain PLA with controlled molecular weight and narrow molecular weight distribution. LA formed from lactic acid, can be found in four different forms: the enantiopure isomers L- and D-LA, *meso*-LA, and the racemic mixture of L- and D-LA (DL- or *rac*-LA). The ROP of L- or D-LA produces completely isotactic PLAs, while the polymerization of *meso*-LA can produce a variety of stereostructures such as syndiotactic, heterotactic, or atactic PLA. When DL-LA is polymerized by simple Lewis acidic metal salts, atactic PLA is obtained. An important challenge in the last few years has been to control polymer microstructure using discrete

catalyst design (Numata et al., 2007; Hormnirun et al., 2004; Majerska and Duda, 2004; Agrawal and Bhalla, 2003). Discrete metal complexes have been used for controlled LA polymerization (Thomas, 2010). Use of stereospecific catalyst can lead to stereoblock PLA which shows crystallinity and higher thermal stability (Spassky et al., 1996; Ovitt and Coates, 1999). Thus, by controlling the ratio of L and D enantiomers, many important properties can be manipulated.

In this study, controlled microstructure PLA samples synthesized *via* ROP using a chiral indium catalyst were investigated. An indium complex, $[(NN_HO)InCl]_2(\mu\text{-}Cl)(\mu\text{-}OEt)$ **(1)**, was used as an initiator for the living enantioselective polymerization of DL-LA (Acosta-Ramirez et al., 2010; Douglas et al., 2008) to form PLAs with moderate isotactic enrichment and low polydisperity indices (PDIs) (Figure 1.1).

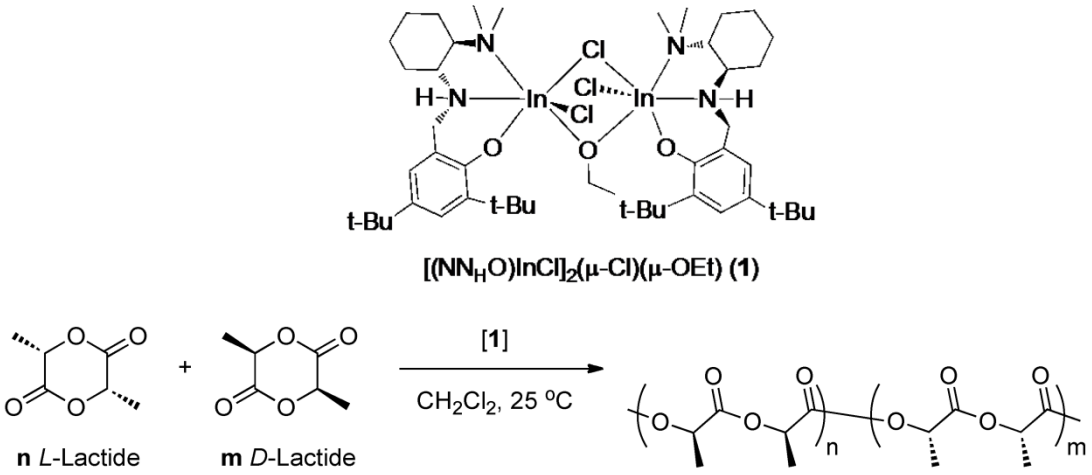

Figure 1.1: Formation of PLA samples with known L-lactide:D-lactide ratios.

PLA is a stiff thermoplastic polymer with properties similar to polystyrene (Witzke, 1997; Garlotta, 2001). Although PLA is a relatively stiff polymer characterized by good mechanical strength, it is considered brittle thus restricting its use in a wide-range of applications particularly in packaging. Numerous approaches such as copolymerizing and blending with plasticizers or a second polymer improve the toughness of PLA. Blending with different biodegradable polymers such as PHB, PCL, poly(ethylene-glycol) (PEG), starch and chitosan offer property improvement without compromising biodegradability (Rasal et al., 2010).

In addition, the thermal stability and mechanical properties of PLA can be improved by blending or copolymerizing PLLA and its enantiomer PDLA or PDLLA (Fukushima and Kimura, 2006; Tsuji and Ikada, 1999). The strong interactions between L- and D-unit sequences form stereocomplex crystals, where PDLA and PLLA chains are packed side by side. The melting point of the stereocomplex crystals with higher compaction of PLA molecules is increased by about 50°C above the corresponding melting point of homocrystallites (Tsuji and Ikada, 1999; Tsuji et al., 1991a; Tsuji et al., 1991b; Tsuji and Ikada, 1993). The presence of stable and strong connection (tie chains) between the crystallites also improves mechanical properties (Tsuji and Ikada, 1999). Copolymerization of crystalline PLLA with amorphous PDLLA or *meso*-LA is another strategy to alleviate the PLLA brittleness and has been proven relatively effective for controlling crystallinity (Bigg, 1996; Bouapao et al., 2009; Ren and Adachi, 2003; Tsuji and Ikada, 1995a; Tsuji and Ikada, 1996).

Rheological properties are useful in evaluating materials performance during processing operations. Rheology is sensitive in identifying and/or detecting any microstructural changes that is directly related to mechanical properties of the final products (Ray and Bousmina, 2005; Lim et al., 2008). Thus, in order for PLA to be processed in standard plastics equipment to produce high yields of molded and film products, the rheological properties must first be understood. Consequently, the processing properties should be studied in order to understand the behavior in extrusion and the occurrence of any flow instabilities that present serious problems in their processing (Kanev et al., 2007). The flow instabilities can be small amplitude periodic distortions known as sharkskin melt fracture (Migler, 2005), alternate distorted and smooth portions, known as stick-slip or oscillating melt fracture (Georgiou, 2005) and gross irregular distortions known as gross melt fracture (Dealy and Kim, 2005). The critical conditions for the onset of melt fractures are important. On the other hand, suitable processing aids should be identified and used to postpone the melt fracture to high shear rates (Amos et al., 2001; Achilleos et al., 2002).

The main theme of this thesis is a study of the thermal, rheological, processing, and mechanical properties of a series of controlled microstructure PLAs as well as some commercial PLAs and the interrelationships between these properties. The effects of

molecular structural parameters (*i.e.* molecular weight and stereochemistry) on their rheology and processability as well as on their mechanical properties are also studied thoroughly.

2 Literature Review

2.1 Poly(lactide) (PLA)

Poly(lactide) (PLA) (Figure 2.1) belongs to the family of aliphatic polyesters derived from alpha-hydroxy acids, a compound found in both plants and animals. Lactide (LA) formed from lactic acid can be found in four different forms: the enantiopure isomers L- and D-LA, *meso*-LA, and the racemic mixture of L- and D-LA (DL-LA or *rac*-LA). There are a number of possible microstructures for PLA due to the different ways of incorporating the isomers of LA into the polymer chain (Figure 2.2). PLAs synthesized from L- and D-lactide are poly(L-lactide) (PLLA) and poly(D-lactide) (PDLA), respectively, and those from racemic monomer are poly(DL-lactide) (PDLLA) (Fukushima and Kimura, 2006). PLLA and PDLA are crystalline, while PDLLA is amorphous.

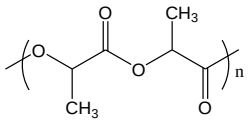

Figure 2.1: The molecular structure of PLA

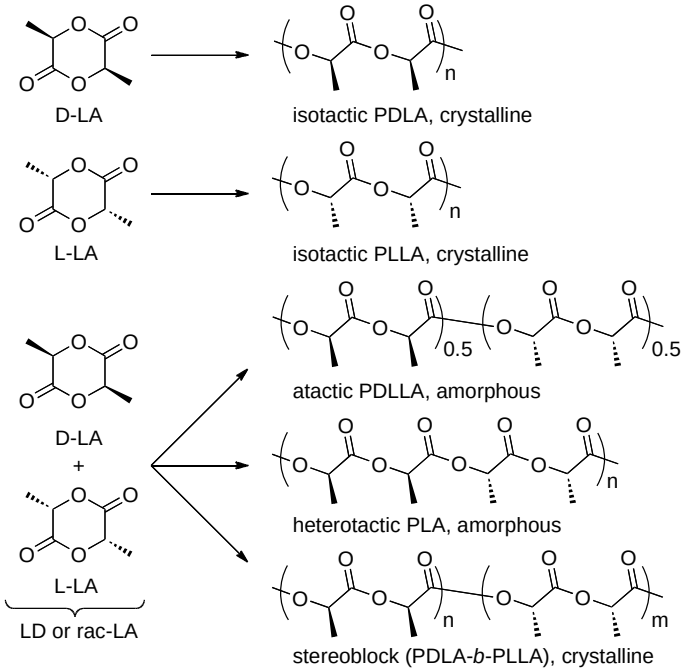

Figure 2.2: Possible PLA microstructures generated from the polymerization of enantiopure or racemic lactide.

2.1.1 Production of PLA

Lactic acid is the basic constitutional unit of PLA. L-lactic acid (2-hydroxy propionic acid) is natural and most common form of the acid that can be found in humans and other mammals. L- and D-lactic acid can also be produced by microorganisms or through bacterial fermentation of sugar from carbohydrates source such as corn, sugarcane and tapioca (Groot et al., 2010)

PLA can be prepared by direct condensation of lactic acid or ring-opening polymerization (ROP) of the cyclic lactide dimer. Direct polycondensation polymerization from lactic acid at reduced pressure and in the presence of catalyst yield low molecular weight PLA because it is hard to remove water completely from the highly viscous reaction mixture. Thus poor mechanical properties are obtained. High molecular weight PLA can be synthesized azeotropically. In this approach, the problem of the removal of water is overcome by manipulating the equilibrium between a monomer and a polymer in an organic solvent and thus lactic acid is polycondensed directly into a polymer of a high molar mass (Sodergard and Stoclet, 2010).

Mitsui Toatsu Chemicals patented an azeotropic dehydrative condensation process that uses a condensation route to produce PLA (Sodergard and Stoclet, 2010). This process uses high temperatures and boiling solvents (200-250°C) in order to remove water and drive the polymerization to completion producing high molecular weight polymers. Another industrial route to PLA, used by NatureWorks LLC., involves the metal-based ring-opening polymerization of lactide (LA) (Nampoothiri et al., 2010). Lactic acid undergoes a continuous condensation to form a low molecular weight prepolymer. The prepolymer is then depolymerized using a tin based metal catalyst that enhances the rate and selectivity of the intermolecular cyclization reaction of production of lactide. After purification by vacuum distillation, the melt lactide undergoes ROP catalyzed by a different tin catalyst to form high molecular weight PLA. Advantage to this polymerization method is that no solvents are used, as all processes are carried out in the melt state (melting point of lactide is 116-119ºC). The metal-based catalysts allows for good control over polymer properties such as molecular weight (Douglas et al., 2008; Witzke, 1997; Tsuji et al., 2006)

There are many routes to ROP lactide including enzymatic, anionic, cationic, organocatalytic, and metal catalyzed polymerizations. Several reviews and reports have been

written, which include details on synthesis and structure of PLA (Douglas et al., 2008; Garlotta, 2001; Witzke, 1997; Gupta and Kumar, 2007).

2.1.2 Thermophysical properties of PLA

The crystallinity of PLA is determined by the proportions of L- and D-LA in the polymer backbone; the greater the optical purity, the higher the crystallinity. PLA can be produced totally amorphous or up to 40% crystalline. PLA containing more than 93% of L-LA is semicrystalline, while PLA with 50-92% L-LA is amorphous (Bigg, 1996). The glass transition temperature, T_g and melting temperature, T_m of crystalline PLA ranges from 50 to 60°C and 145 to 186°C, respectively. Depending on the D-LA content and molecular weight, the cold crystallization temperature, T_c of PLA lies between 95 and 105°C (Tsuji et al., 2006). As the %L content in the polymer is decreased from 100 to 92% the T_m decreased from 180 to 138°C (Reeve et al., 1994; Bigg, 1996).

PLA can be crystallized into various crystalline forms (α, β and γ). Crystallization from solution and melt form α–crystals which is a common polymorph (Hoogsteen et al., 1990; Sawai et al., 2003a; Sawai et al., 2007). The β-crystallites are formed upon tensile drawing at a high temperature and high draw ratio, whereas drawing at a low temperature and/or low draw ratio leads to α-crystallites. Drawn products of PLLA commonly consist of mixture of α- and β-crystallites (Sawai et al., 2003b; Rahman et al., 2009). The β structure that corresponds to a fibrillar morphology melts at a lower temperature than the α structure, however the former bore most of the load during tensile experiments (Hoogsteen et al., 1990).

The density of solid PLA is 1.36 g/cm^3 for crystalline PLLA and 1.25 g/cm^3 for amorphous PLA. The liquid or melt density of L-lactide, *meso*-LA and amorphous LA at particular temperature (T in °C) can be expressed by Witzke (1997):

$$\rho(T) = 1.2836 \exp[-7.7(10^{-4})T] \qquad (2\text{-}1)$$

PLA is a rigid thermoplastic polymer comparable to polystyrene (Perego et al., 1996). The tensile and flexural properties of PLLA and PDLLA, the crystalline and amorphous PLA are slightly different. However PLLA and PDLA exhibit relative equivalent physicochemical

and mechanical properties (Dorgan et al., 2000). The tensile strength of PLLA have been reported in the range of 50-70 MPa, the tensile modulus in the range of 3000-4000 MPa and the elongation at break from 2 to 10%. On the other hand, the tensile strength of PDLLA is typically in the range of 40-53 MPa, much lower than its crystalline counterpart (Perego et al., 1996). Different methods used for specimen preparation and testing affect the measurements of the mechanical properties reported in literature.

2.1.3 Rheology studies on PLA

Extensive rheological studies of several series of PLAs in the melt state were performed by Dorgan and coworkers (Dorgan et al., 1999; Dorgan et al., 2004; Dorgan et al., 2005a; Dorgan et al., 2000; Lehermeier and Dorgan, 2001; Palade et al., 2001). A comprehensive evaluation of the linear viscoelastic properties of linear PLA across a wide range of molecular weights (10^5-10^6 g/mol) and stereo-chemical compositions (100, 80, 50, 0% of L content) were reported. The zero-shear viscosities of thermally stabilized samples were described by the following relationship:

$$\log(\eta_o) = -14.26 + 3.4\log(M_w) \qquad (2\text{-}2)$$

The plateau modulus was measured to be near 1.0 MPa ± 0.2 and in fact varied in a non-systematic way with molecular weight and optical composition. Master curve of PLA with 80:20 L:D and M_w of 570 kg/mol has been presented over nearly 14 decades in frequency obtained *via* time-Temperature superposition (Dorgan et al., 2005a). The modified Havriliak and Negami (HN) model with two-mode best represented the experimental data (Dorgan et al., 2005a). The horizontal shift factor, α_T followed the Williams-Landel-Ferry (WLF) equation:

$$\log \alpha_T = \frac{-C_1(T - T_{ref})}{C_2 + (T - T_{ref})} \qquad (2\text{-}3)$$

with average WLF parameters of C_1=3.24 $K^{-1}$and C_2= 164.9 K which correspond to a Vogel temperature of (T_∞) 288.25 K. The vertical shift factors, b_T were obtained from:

$$b_T = \frac{\rho_o T_o}{\rho T} \tag{2-4}$$

using the known dependence of density, ρ and temperature, T from Equation 2-1 (Witzke, 1997).

The zero-shear viscosity relationship with molecular weight and other melt properties have been reported previously by several research groups for several PLAs of various microstructures (Dorgan et al., 1999; Dorgan et al., 2005a; Dorgan et al., 2000; Palade et al., 2001; Yamane et al., 2004; Grijpma et al., 1994; Cooper-White and MacKay, 1999). However, results from different research groups do not agree in general, due to the different extents of optical copolymers studied, the difficulty associated with measuring the absolute molecular weight of PLA, and the issues of melt thermal stability (Dorgan et al., 2005a).

Ramkumar and Bhattacharya (1998) found that PLAs were susceptible to degradation during testing. Due to low crystallinity, PLA can be easily hydrolyzed and depolymerized to lactic acid. PLA polymers degrade primarily by hydrolysis after exposure to moisture. Also, in PDLLA degradation occurs *via* intra and intermolecular transesterifications, which would be accelerated by the existence of residual monomer, oligomer, and hydroxyl groups.

Unusual behavior of viscosity functions of PLLA melts, which displayed a maximum instead of a horizontal plateau at low frequency, (Arraiza et al., 2007) indicating the effect of thermal degradation process. This implies chain scission leading to a molar mass decrease at long residence times in the rheometer. The thermal degradation of unstabilized PLLA occurred rapidly at temperatures above 230°C and increased with long residence times.

Cicero et al. (2002) and Lehermeier and Dorgan (2001) investigated degradation effect during melt spinning and melt rheology measurements of PLA. Tris(nonylphenyl) phosphate (TNPP) was an excellent stabilizer for PLA over a range of temperatures and lengthens significantly the time available for testing. Excellent superposition of viscoelastic data for stabilized samples within the temperature window explored demonstrated that the use of TNPP as a stabilizer leads to a thermorheologically simple material response (Palade et al., 2001). TNPP acts as a chain extender reconnecting polymer chains that have broken due to moisture and elevated testing temperatures (Cheung et al., 1990). Optimum concentration of TNPP is needed as a too low concentration results in the breakdown of

polymer chains, and a too high concentration results in an increase in the polymer's molecular weight.

Dorgan et al. (2005b) clarified the inconsistency of other fundamental properties of PLA reported in the literature. The authors have confirmed the value of the characteristic ratio, C_∞ of 6.5 ± 0.9 regardless of stereoisomer content, which was determined by solution and melt measurements as well as simulation. Mark-Houwink and Schulz-Blaschke constants, as well as accurate values of specific refractive index increments d*n*/d*c* for dilute solution in chloroform and tetrahydrofuran (THF) were also reported to be 0.08 and 0.042 mL/g respectively, which clarified the inconsistency of values reported previously.

In addition to linear PLA, branched PLA and also the blends of linear and branched PLA also being studied by Lehermeier and Dorgan (2001). The branched PLA studied was produced through peroxide initiation of a linear material by reactive extrusions (Carlson et al., 1998). Higher zero-shear viscosity and stronger shear thinning was observed with the addition of the branched PLA rather than its linear counterpart. The zero-shear viscosities of the blends can be described well by the log additivity rule. The tensile and thermal properties were unchanged within experimental error despite alteration in melt rheology.

Dorgan and coworkers (2001) discovered that PLA with 98% L-content exhibited strain hardening during uniaxial extension in the melt state. Extensional measurements were performed using a Rheometrics RME instrument (Palade et al., 2001). The test was performed at a temperature of 180^{o}C at an elongation rate of 0.1-1 s^{-1} for PLA with M_w of 120 and 110 kg/mol. The Trouton ratio (ratio of extensional to shear viscosity) at small rates was three, which indicates reliability of the experimental data from the two different types of measurement. It was speculated that the observed strain hardening in these linear polymers might be due to the polydispersity and also the stereoregularity of the studied PLA (Palade et al., 2001). The stereoregularity of high L-content PLAs may allow them to form a range of structures when stretched, where helical conformations may form in the melt as a precursor to strain-induced crystallization. Similar result has been reported by Takahashi et al. (1993). The high molecular weight tail and long chain branching contribute to longer relaxation times. Introduction of long relaxation times cause the prominent strain hardening in extensional flow instead of reaching the steady-state value. Even a very small content of very high molecular weight chains results in the prominent strain hardening behavior. On the other

hand, Pearson et al. (1983) reported that star polymers with a narrow molecular weight distribution do not show the strain hardening behavior, while it has been suggested that long chain branched comb and H-shaped polymers show the strong strain hardening behavior.

Moreover, Yamane et al. (2004) observed a strain hardening behavior in biaxial extensional at extension rates of 0.058 to 0.1 s^{-1} for pure PLLA and PLLA\PDLA blends. Stronger strain hardening was observed for the blends due to existence of a stereocomplex as the measurements were performed at a temperature of 190^{o}C, which is below the melting point of the stereocomplex.

2.2 Stereochemically Controlled Polymerization

As mentioned before, polymerization of a racemic mixture of L- and D-LA produces poly DL-LA (PDLLA), which is essentially atactic; an amorphous polymer. Use of a stereospecific catalyst can lead to stereoblock PLA which shows crystallinity (Figure 2.3) (Coates and Ovitt, 1999; Spassky et al., 1996). Ring-opening polymerization (ROP) of LA, with a suitable catalyst results in high molecular weight PLA with useful properties. Different metal catalysts, namely tin, aluminum and zinc have been studied and proven to be effective catalysts for polymerizing LA. However, the polymers produced from these catalysts have large molecular weight distributions, and analysis shows that transesterification is occurring during polymerization (Garlotta, 2001; Douglas et al., 2008).

Advances in the development of metal based chiral catalysts for olefin polymerization have provided some control of the tacticity of the resulting polymers. Stereocomplex PLA can be obtained by stereoselective ROP of DL-LA with chiral complexes. Spassky et al. (1996) introduced the concept of a single-site enantioselective catalyst for polymerization of DL-LA. An aluminum catalyst with a chiral Schiff base ligand was used to produce stereoblock PLA from DL-LA in a one-pot system. However, the molecular weight of the resultant stereoblock PLA has low M_n (12 kDa) and the reaction time were long (200h).

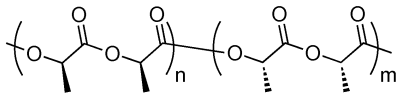

Figure 2.3: Structure of stereoblock PLA

Subsequently, Radano et al. (2000), Zhong et al. (2002) and Coates and Ovitt (1999) have developed a modified catalyst with different ligands that shorten the reaction time and have improved molecular weight distributions, although the sequence control in terms of stereocomplexation ability is unsatisfactory. Majerska and Duda (2004) also have succeeded to synthesize stereoblock of PLLA-*b*-PDLA from DL-LA by sequential addition of two homochiral catalysts.

Coates and Ovitt (1999) have shown that racemic aluminum alkoxide catalysts can be used to polymerize DL-LA at 70^{o}C into stereoblock copolymers with melting temperature of 179^{o}C. This indicated that the resultant block copolymers adopt a stereocomplex morphology in the solid state. The polymerization exhibited living behavior, as evidenced by the correlation between the predicted and observed molecular weights and the narrow molecular weight distribution (MWD). In addition, the narrow MWD suggests that no significant transesterification occurs.

The melting points of the stereocomplexes obtained by the stereoselective polymerization of DL-LA were in the range of 179-210°C which are lower than a 1:1 mixture of the enantiopure homopolymers which are in the range of 210-230°C (Tsuji, 2005).

2.2.1 Stereocomplex formation

Stereocomplexation of macromolecular chains with iso- or syndiotacticity is known for various polymers such as poly(methyl methacrylate), poly(styrene), poly(methyl glutamate) and poly(tert-butylene oxide) (Fukushima and Kimura, 2006). The stereocomplexes are formed in a helical conformation. The interaction between two stereoregular left and right handed helical chains creates a specific chain-packing state that is crystalline in nature. By having different rotations, L-lactic rotates in clockwise, whereas D-lactic acid counterclockwise. Thus the helical chains of PLLA and PDLA can also generate stereocomplexation (Fukushima and Kimura, 2006; Tsuji, 2005).

Ikada et al. (1987) initially discovered the stereocomplexation of PLA from a solution mixture of PLLA and PDLA and then from a melt mixture. Simply mixing PLLA and PDLA of opposite configuration in solution forms a stereocomplex. However the degree of stereocomplexation is affected by the conditions during formation and the molecular weights

of PLLA and PDLA. High molecular weight PLLA or/and PDLA hindered the formation of stereocomplex by homocrystallization. The threshold molecular weight is approximately 6 kDa in a melt mixture, while 40 kDa and 400 kDa for solution casting and precipitation, respectively (Tsuji et al., 1991a; Tsuji et al., 1992; Tsuji and Ikada, 1993). An equimolar ratio is the most favorable for formation of exclusively stereocomplex although polymer compositions of 60/40 to 40/60 form stereocomplexes predominantly without homocrystallization (Ikada et al., 1987). In addition, fast solvent evaporation from cast films induces rapid homopolymer crystallization (Tsuji et al., 1991b). On the other hand, in dilute solution, slow evaporation or isothermally crystallized in a mixture of good and poor solvents yields high molecular weight of stereocomplex PLA (Sawai et al., 2007).

Formation of stereoblock PLA by sequential ring-opening polymerization of L-LA and D-LA is an effective way to obtain exclusive stereocomplexation (Yui et al., 1990). The enantiomeric chains are chemically connected and the chain mixing takes place at the molecular level. First, reported by Yui et al. (1990), stereocomplex PLA with melting temperature of 205°C was obtained with little homopolymer crystallization; however, this material had low molecular weights. An improved technique was developed by Musashino Chemical Laboratory (Japan). They successfully formed high molecular weight (~200 kDa) stereoblock PLA from bulk L- and D-LA capable of stereocomplex crystallization regardless of block ratio (average of 94/6 to 6/94 of PLLA/PDLA was attempted) (Komazawa and Tang, 2008).

2.2.2 Stereocomplex properties

The stereocomplexes formed exhibit a melting temperature almost 50^{o}C higher than that of homopolymers. The unit cell of the stereocomplex crystal is reported by Sawai et al. (2007) to be a trigonal cell with cell constants of a=b=1.50 nm, c=0.823 nm, $\alpha=\beta=90^{o}$, and $\gamma=120^{o}$. PDLA and PLLA with opposite handed helices are packed side by side in parallel fashion and folded to form a lamella. More compact side-by-side crystallization between the two enantiomeric polymers results in a much higher melting point. The T_m increases with increasing molecular weight up to certain value although the effect of molecular weight is not as large as that for PLLA (de Jong et al., 1998). The density of stereocomplex PLA is in the

range of 1.27-1.30 g/cm^3. When an asymmetric blend of PLLA and PDLA is heated up to 200°C, all the homocrystals are in the molten state, while the stereocomplex crystallites stay unmelted because of their high melting temperature.

Intensive studies on the crystallization kinetics have been performed by means of calorimetry and polarizing microscopy. The effects of numerous parameters on the stereocomplex have been intensively investigated by Tsuji and co-workers (*i.e.* blending ratio of the isomeric, molecular weight of isomeric, temperature and time after blending of the two isomeric polymer in solution or after melting the blends, as well as blending mode of the two isomeric) (Tsuji and Ikada, 1993;1999; Tsuji et al., 1991a;1991b;1991c). Polymer solidification by cooling the polymer melt, increase of the polymer concentration of a polymer solution and precipitation of a polymer by pouring the solution into non-solvent promoted the intermolecular interaction for the formation of more stable crystallites. The presence of the stereocomplex affected both the nucleation and the growth of the α-crystals. Depending on the stereocomplex content and the crystallization temperature, α-crystallization can either be enhanced or be inhibited. The effects of crystallization temperature was more pronounced in high M_w PDLA\PLLA blends, which implies a higher ordered structure of stereocomplex, although the crystallinity of stereocomplex was lower than low M_w PDLA\PLLA blends (Rahman et al., 2009).

The complex viscosity, η^* of PDLA\PLLA blends (1-10% PDLA) at low frequency measured at 200°C was higher than that of the pure PLLA. The increment was more pronounced in low M_w PDLA blends compared to high M_w PDLA blends (Rahman et al., 2009). Similar observations were reported by Yamane et al. (2004). This agrees with stereocomplex crystallinity, which is higher in low M_w PDLA blends than high M_w PDLA blends (Tsuji et al., 1991a). The shorter PDLA chains are packed easily into stereocomplex crystals due to their higher mobility. This result clearly indicated that the increase in η^* was due to the existence of stereocomplex crystallites. From the relationship of $\eta_o \propto M_w^{3.4}$ blending of low molecular weight polymer reduces significantly the η^*; however, the results indicate that PLLA\PDLA blends whose molecular weight are lower than pure PLLA show higher viscosities that pure PLLA. The existence of the stereocomplex crystallites as well as

the cross-linking explained the increase in viscosity. It is believed that there are strong interactions between the stereocomplex crystallites.

Tensile strength, Young's modulus and elongation at break of 1:1 PDLA:PLLA blend films were twice as high as those of non-blended PLLA and PDLA films when the molecular weight is in the range of 10^5 to 10^6 g/mol (Tsuji and Ikada, 1999). The increments in those mechanical properties are due to different morphology of those films as a result of formation of many stereocomplex crystallites which act as intermolecular cross-links. It is suggested that the existence of high density tie chain that connecting homocrystallites or stereocomplex micro-crystallites results in better mechanical properties. The density of tie chains increases with increasing molecular weight. On the contrary, non-blended films had larger-sized spherulites of less contact area with the surrounding spherulites.

2.3 Blends and Copolymers of Crystalline and Amorphous PLA

Blending of isotactic and atactic polymers has been reported as a way to improve the properties of polymeric material (Pearce and Marchessault, 1994). Copolymerization of L-LA with *meso*-LA or DL-LA can be used to manipulate and provide a good balance between crystallinity and to produce tough plastic material (Bigg, 1996; Perego and Cella, 2010). The degree of crystallinity and thus the brittleness and mechanical properties can be controlled.

Tsuji and Ikada (1995a) have investigated the effects of different mixing ratios on the thermal and morphological properties of PDLLA (M_w=720 kg/mol) and PLLA (M_w=1330 kg/mol) blends. PLLA and PDLLA blends were miscible in the melt prior to crystallization. The amorphous polymeric molecules (PDLLA) were trapped between the lamellae of spherulites formed from the isotactic PLLA. This agrees with studies by Keith and Padden (1964) and Keith and Padden Jr. (1987) on the morphology and kinetics of spherulites formed from isotactic and atactic blends. Different thermal history also played a role in the crystallization process of the blends. The time required for saturation in PLLA crystallization was shorter for the blends annealed after quenching from melt to 0^oC than for those annealed directly from melt without quenching. PLLA could crystallize from melt and form spherulites when the weight fraction of PLLA in the blend was higher than 0.6. If it became lower than 0.5, the morphology of the blends changed form typical spherullites to less

ordered ones. The presence of PDLLA delayed the induction/nucleation for crystallization of the blends. In spite of difference in the crystallization behavior and morphology among the blends, the melting temperature and the crystallinity of the blends after 600 min annealing were similar. This has also been confirmed by a recent study (Bouapao et al., 2009), that the crystalline form of PLLA remains unchanged in the presence of PDLLA.

The effects of PDLLA molecular weight in equimolar blends have also been studied by the same group (Tsuji and Ikada, 1996). The spherulite structure became more disordered as the molecular weight of PDLLA increased. The size of the spherulites was larger than that of non-blended PLLA, irrespective of the molecular weight of PDLLA. Spherulite growth rate was increased when the molecular weight of the amorphous component was very low (M_w =19 kg/mol). Similar increments of growth rate of spherulites in blends were observed and explained by Abe et al. (1994).

2.4 Rheological Measurements

Rheology is the science of deformation and flow of matter when external forces are applied (Dealy and Wissbrun, 1999). It is a study to understand why a material behaves in a certain way when a force is applied. An important aspect of polymer rheology is the study of the viscoelastic behavior of the molten polymer and its relation with molecular structure. Unlike simple fluids, most polymeric materials are rheologically viscoelastic. Polymeric materials possess rheological properties similar to viscous liquids (they dissipate energy) and similar to elastic solids (they store energy) components which depend on the time scale of the deformation. The meaning of these properties will be discussed in this section as they are central in this thesis.

Concentric and parallel plate rheometers are commonly used to study the viscoelastic properties of polymers (Dealy and Wissbrun, 1999). These are used extensively in industry for quality control purposes because experimental data from the measurements can be collected rapidly to reveal structural information (Dealy and Wissbrun, 1999). The use and operation of such pieces of equipment will also be discussed in these sections as they are extensively utilized in this study.

2.4.1 Rotational rheometer and linear viscoelasticity

A schematic of the parallel plate rheometer is shown in Figure 2.4. In this rheometer, two circular plates are mounted on a common axis of symmetry, and the sample is inserted in the space between them. The upper plate is rotated at a specified angular velocity $\omega(t)$ and as a result the sample is subjected to shear. The motion of the upper plate can be programmed and the resulting torque measured (strain controlled rheometer). In another mode of operation, the torque is fixed and the displacement is measured (stress controlled rheometer).

The most widely used experiments to determine the linear viscoelastic properties of polymers are small amplitude oscillatory shear tests. In practice, most polymeric materials have properties which are a combination of viscous and elastic components.

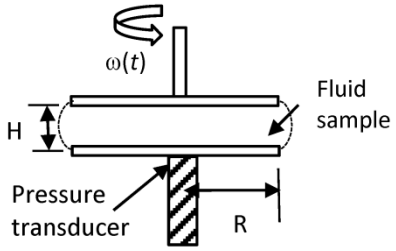

Figure 2.4: Parallel plate rheometer.

During the test, stress or strain are constantly changing, the viscoelastic properties are described in terms of elastic (storage) modulus (G') and viscous (loss) modulus (G'') defined below. In this experiment, the sample is subjected to a simple shear deformation where the shear strain is a function of time given by:

$$\gamma(t) = \gamma_o \sin(\omega t) \tag{2-5}$$

where γ_o is the strain amplitude and ω is the frequency. The stress is then measured as a function of time. For very small strain amplitudes, the shear stress is sinusoidal in time and independent of strain (linear viscoelastic limit) and can be written as:

$$\sigma(t) = \sigma_o \sin(\omega t + \delta) \tag{2-6}$$

where σ_o is the stress amplitude and δ is a phase shift or the mechanical loss angle. Using a trigonometric identity, one can rewrite Equation 2-6 in the following form:

$$\sigma(t) = \gamma_o \left[G'(\omega)\sin(\omega t) + G''(\omega)\cos(\omega t) \right] \quad (2\text{-}7)$$

where $G'(\omega)$ is the storage modulus and $G''(\omega)$ is the loss modulus. These two quantities can be calculated from amplitude ratio, $G_d = \sigma_o / \gamma_o$ and the phase shift, δ as:

$$G' = G_d \cos(\delta) \quad (2\text{-}8)$$

$$G'' = G_d \sin(\delta) \quad (2\text{-}9)$$

There are two other parameters that are frequently used to present the test results. These are the complex modulus (G^*) and the complex viscosity (η^*), defined as:

$$G^*(\omega) = G'(\omega) + iG''(\omega) \quad (2\text{-}10)$$

$$\eta^*(\omega) = \eta'(\omega) - i\eta''(\omega) \quad (2\text{-}11)$$

2.4.2 Extensional rheometer

Another important method in characterizing rheologically polymeric materials is to study their behavior under extensional deformation. In this kind of experiment, the polymer samples are stretched under certain extensional rates. The extensional rheometer used in the present study is the Sentmanat Extensional Rheometer (SER) which is designed as a detachable fixture for commercially available rotational rheometers (Sentmanat et al., 2005; Sentmanat, 2004). This fixture is able to fit within the host oven chamber, thus allowing testing under temperature-controlled conditions. The extensional rheometer consists of a master and a slave windup drums interconnected by means of intermeshing gears (Figure 2.5).

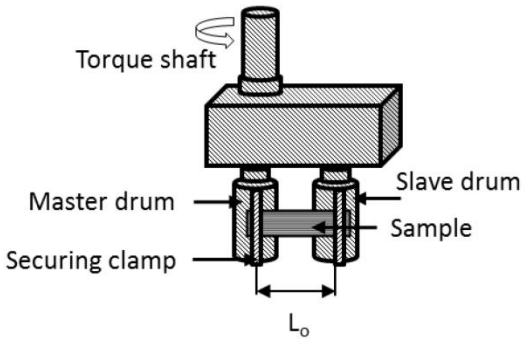

Figure 2.5: A schematic of the Sentmanat Extensional Rheometer (SER).

Rotation of the master drum with an angular speed, ω, results in an equal but opposite rotation of the slave drum. This causes the ends of the affixed sample to be wound up onto the drums resulting in the sample being stretched over an unsupported length, L_o. For a constant drive shaft rotation rate, ω, the Hencky strain rate applied to the sample specimen can be expressed as:

$$\dot{\varepsilon}_H = \frac{2\omega R}{L_o} \tag{2-12}$$

where R is the radius of the windup drums, and L_o is the fixed, unsupported length of the specimen sample being stretched, which is equal to the centerline distance between the master and slave drums (Sentmanat et al., 2005; Sentmanat, 2004).

The material's resistance to stretch is observed as a tangential force, F, acting on the drums which then translated as a torque upon the chassis housing of the assembly. The resultant torque transmitted through the chassis to the torque shaft is determined from the summation of moments about the axis of the torque shaft, yields:

$$T = 2\left(F + F_F\right)R \tag{2-13}$$

where T is the resultant torque measured by the torque transducer, and F_F is the frictional contribution from the bearings and intermeshing gears. With precision bearings and gears, the frictional term is typically quite small (< 2% of the measured torque signal) and can be neglected such that Equation 2-13 may be simplified to:

$$T = 2\left(F\right)R \tag{2-14}$$

(Sentmanat et al., 2005). For polymer melts, if there is no deviation between the nominal and actual strain rates, the instantaneous cross-sectional area, $A(t)$, on the stretched material changes exponentially with time for a constant Hencky strain rate experiment and can be expressed as:

$$A(t) = A_o \exp\left(-\dot{\varepsilon}_H t\right) \tag{2-15}$$

where A_o is the initial cross-sectional area of the unstretched specimen (Sentmanat et al., 2005). For a constant Hencky strain rate, the tensile stress growth coefficient, $\eta_E^+(t)$, of the stretched sample can then be expressed as:

$$\eta_E^+(t) = \frac{F(t)}{\dot{\varepsilon}_H A(t)} \tag{2-16}$$

where $F(t)$ is the instantaneous extensional force at time *t* exerted by the sample as it resists stretch (Sentmanat et al., 2005).

2.5 Time-Temperature Superposition

Rheological properties of molten polymers such as those obtained from parallel plate or capillary rheometer are dependent on temperature. A complete picture of polymer behavior can be obtained by carrying out experiments at several temperatures. Rheological data of thermorheologically simple materials measured at several temperatures can be brought together on a single master curve by means of "time-Temperature superposition" (Dealy and Wissbrun, 1999). This greatly simplifies the description of the effect of temperature. Furthermore, it makes possible the display on a single curve of material behavior covering a much broader range of time or frequency than can ever be measured at a single temperature.

Data for different temperatures can be superposed by introducing a shift factor, α_T, determined empirically. Thus, if one makes a plot of a rheological property versus a quantity with a time unit, α_T is obtained from the horizontal shift necessary to bring the data corresponding to a specific temperature *T* onto the same curve as data corresponding to another temperature, T_{ref}. For example, Figure 2.6 shows storage modulus, G', versus angular frequency, ω, in the range of 10^{-2} to 10^{2} rad/s obtained at three different temperatures from small amplitude oscillatory shear tests for a PLA sample. The frequency is shifted by multiplying the frequency with the horizontal shift factor, α_T and vertically by b_T which is given by the dependence of the density of the material to temperature (Equation 2-1). Figure 2.7 is an example of a master curve prepared from data shown in Figure 2.6. The idea is to shift the data at other temperatures (90 and 130°C) to the selected reference temperature of 110°C. At this temperature, G' is now known over a wider range of frequency.

Note that a shift factor is not required for quantities containing no units of time. This implies that a plot of such a quantity versus another, containing no units of time, will be

temperature independent. The shift factor is a function of temperature, and the WLF equation has been a useful correlation for α_T (Ferry, 1980):

$$\log \alpha_T = \frac{-C_1(T - T_{ref})}{C_2 + (T - T_{ref})} \tag{2-17}$$

where C_1 and C_2 are constants determined at T_{ref} for each material. This equation holds at temperatures very close to glass transition temperature, T_g. At temperatures of at least 100 K above T_g, an empirical relationship, the Arrhenius equation, is valid (Dealy and Wissbrun, 1999):

$$\alpha_T = \exp\{E_a / R(1/T - 1/T_{ref})\} \tag{2-18}$$

where E_a is the flow activation energy, R is the gas constant, and T_{ref} is the reference temperature.

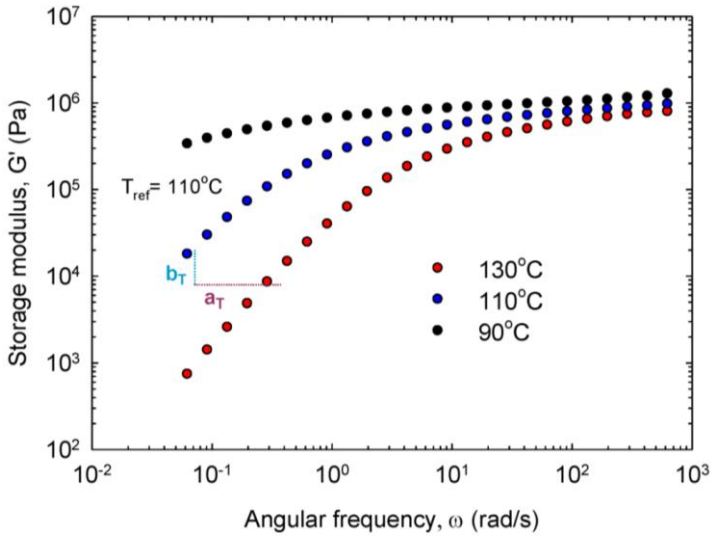

Figure 2.6: Storage modulus measured at different temperatures.

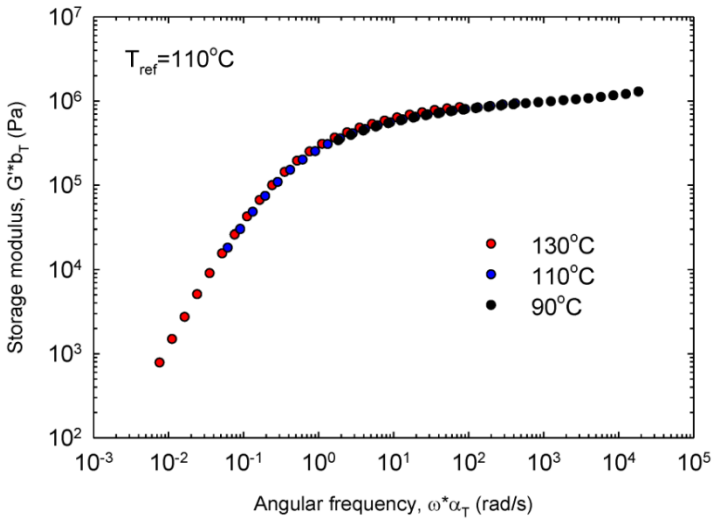

Figure 2.7: An example of a master curve from data in Figure 2.6.

2.6 PLA Processing

2.6.1 Capillary extrusion of PLA

A capillary rheometer is pressure flow type rheometer which primarily is used for measuring viscosity at high shear rates (Dealy and Wissbrun, 1999). It can also be used to assess the processability of polymers in many cases. The capillary rheometer consists of a melt reservoir or barrel in which the polymer is melted and a plunger or piston that forces the melt to flow through a die of known dimensions (*i.e.* diameter, *D*, or length, *L*). The quantities normally measured are the volumetric flow rate, *Q* and the driving pressure, P_d. A schematic diagram of the rheometer and the capillary die is shown in Figure 2.8.

To calculate the viscosity, first the wall shear stress and the wall shear rate must be determined. For an incompressible Newtonian fluid with steady state and fully developed flow, the wall shear stress can be calculated as:

$$\sigma_w = \frac{\Delta pD}{4L} \tag{2-19}$$

where Δp is the pressure drop in the capillary excluding the end pressure (excess pressure needed for flow at the capillary entry).

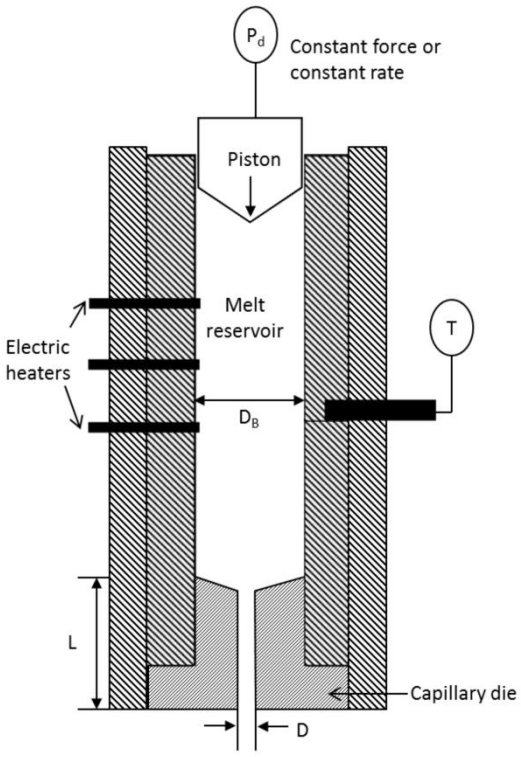

Figure 2.8: A schematic diagram of capillary rheometer.

The wall shear rate of a Newtonian fluid can be calculated as:

$$\dot{\gamma}_w = \frac{32Q}{\pi D^3} \tag{2-20}$$

However for a non-Newtonian fluid, this quantity is called the apparent wall shear rate:

$$\dot{\gamma}_A = \frac{32Q}{\pi D^3} \tag{2-21}$$

At least two corrections should be applied to the capillary experimental data in order to obtain the true values of wall shear stress and rate. First, the pressure drop must be corrected for the additional pressure required for the melt to pass through the contraction between the barrel and the capillary. As mentioned above, in a capillary rheometer the shear stress is determined by monitoring the driving pressure, P_d. The pressure drop (Δp) in Equation 2-19 is then given by $(P_d - \Delta p_{ends})$ where Δp_{ends} is associated by the extra pressure needed for flow at the two ends of the capillary (mainly the entrance). This can be determined by the Bagley method (Dealy and Wissbrun, 1999). This essentially requires the

determination of P_d needed for extrusion from capillaries of various lengths at a fixed apparent shear rate. Extrapolation of the data to zero length yields Δp_{end}. Then the true shear stress can be calculated from:

$$\sigma_w = \frac{\left(P_d - \Delta p_{end}\right)}{4\left(L/D\right)} \tag{2-22}$$

The second, correction is known as Rabinowitsch and it can be calculated by:

$$\dot{\gamma}_w = \left(\frac{3+b}{4}\right)\dot{\gamma}_A \tag{2-23}$$

This correction, *b*, measures the deviation from Newtonian behavior. It equals unity for a Newtonian fluid and 1/n for a power-law fluid. A large amount of data is needed for this technique since differentiation is required to determine *b*:

$$b = \frac{d\left(\log \dot{\gamma}_A\right)}{d\left(\log \sigma_w\right)} \tag{2-24}$$

2.6.2 Processability of polymers (melt fracture)

In the extrusion of thermoplastics, it is desirable that the final products have a smooth and glossy surface to make a useful product. At the same time, the extrusion rates need to be as high as possible and extrusion pressure as low as possible in order to make efficient use of the processing machinery, therefore reducing capital and operational costs. However, in the extrusion process small amplitude periodic and irregular distortions appear on the surface of the extrudates, once the throughput exceeds a critical value. This limits the rate of production to uneconomical levels (Hatzikiriakos and Migler, 2005, Rosenbaum, 1998). These distortions are collectively known as melt fracture. Knowledge about the flow instabilities of commercial biodegradable polyesters is crucial for the design of processing equipment and unit operations. In particular, understanding the origin and occurrence of sharkskin melt fracture (see below) is important for finding methods to eliminate or reduce these irregularities, and thus to minimizing costs by producing high volumes (Dealy and Wissbrun, 1999).

There are various types of distortions that can occur in an extrusion operation. First these can be small amplitude periodic distortions known as sharkskin melt fracture (Migler, 2005). As the apparent shear rate increases, alternate distorted and smooth portions, known as stick-slip or oscillating melt fracture (Georgiou, 2005) and gross irregular distortions known as gross melt fracture (Dealy and Kim, 2005) may also appear. Gross melt fracture affects the entire cross section of the extrudate also known as volume melt fracture, whereas sharkskin only affects the surface of the extrudate often called surface melt fracture. Figure 2.9 show images of extrudates with smooth, sharkskinned and gross fractured appearance (Rosenbaum, 1998).

Kanev et al. (2007) have studied extrusion instabilities of PLA and aliphatic-aromatic copolyester. They observed that with increasing shear rate, PLA exhibits sharkskin and gross melt fracture. The values of the critical shear stress for the onset of sharkskin are 0.14 to 0.18 MPa and 0.36 to 0.4 MPa for gross melt fracture. Experimental results indicate that PLA exhibits extrudate swell up to 28%. This is the only study in the extrusion of PLA and therefore there is a need for further understanding of the melt fracture phenomena in the extrusion of PLAs.

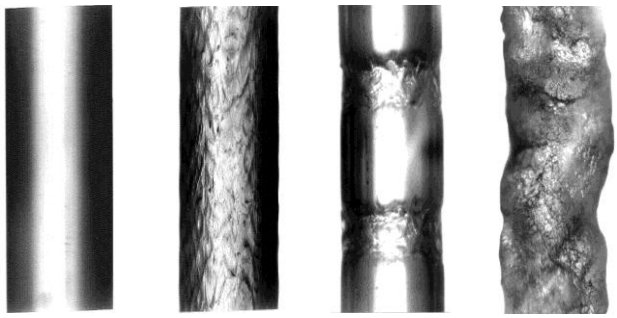

Figure 2.9: Typical extrudates showing (a) smooth surface (b) sharkskin melt fracture (c) stick-slip melt fracture and (d) gross melt fracture (Rosenbaum, 1998).

2.6.3 Wall slip

It is known that polymer melts, particularly from linear polymers slip over solid surfaces under the action of shear stress (Ramamurthy, 1986; Kalika and Denn, 1987; Hatzikiriakos

and Dealy, 1991;1992a; Migler et al., 1993; Kalyon and Gevgilili, 2003; Archer, 2005; Hatzikiriakos, 2012). Slip plays a significant role in correctly determining the rheology of polymers by correcting the data for slip effects (Hatzikiriakos and Dealy, 1991; Gevgilili and Kalyon, 2001) and explaining mismatch of rheological data obtained from various rheometers utilizing different geometries (Hatzikiriakos and Dealy, 1992a; Tang and Kalyon, 2004).

A typical method used to determine and quantify slip in capillary flow is the Mooney technique (Mooney, 1931). Consider steady-state, laminar, incompressible non-Newtonian flow in a capillary of radius *R=D/2* and length, *L*, along the *z*-axis, under wall slip, u_s which is assumed to be solely a function of the wall shear stress. Under these conditions, Mooney (1931) derived the following general equation for the volumetric flow rate, *Q*:

$$Q = \pi R^2 u_s + \frac{\pi R^3}{\sigma_w^3} \int_0^{\sigma_w} \dot{\gamma} \sigma_{rz}^2 d\sigma_{rz} \tag{2-25}$$

where σ_{rz} is the shear stress at location *r* and σ_w is the wall shear stress. The second term in Equation 2-25 is the volumetric flow rate in the absence of slip (u_s=0). It can be easily shown that:

$$\dot{\gamma}_A = \dot{\gamma}_{A,s} + \frac{8u_s}{D} \tag{2-26}$$

where $\dot{\gamma}_A$ is the apparent shear rate defined above, $\dot{\gamma}_{A,s}$ is the apparent shear rate corrected for the effect of slip (solely a function of the wall shear stress), and u_s is the slip velocity (Mooney, 1931). Based on Equation 2-26, the flow curve of a molten polymer becomes a function of capillary diameter in the presence of slip. If such a dependence is observed this equation can be used to quantify slip.

2.6.4 Processing aids

The melt fracture that occurs in the extrusion of linear polymers can be eliminated or postponed to higher rates by the addition of processing aids. Processing aids include different additives, surface coatings and solids which are added at small amounts to help the extrusion of polymers (typical amounts of about 0.1 wt%).

Fluoropolymers and stearates are processing aids that have been used in the extrusion of high-density polyethylenes and linear low-density polyethylenes (Achilleos et al., 2002). Only low concentrations of processing aids (approximately 0.1% of mass fraction of polymer) are usually used in industrial scale (Hatzikiriakos and Migler, 2005). The processing aids act as die lubricants which modify the properties of the polymer-wall interface by increasing the wall slip of the molten polymers, thus reducing pressure drops needed for their flow.

To be effective the processing aid should be able to coat the die wall and in particular the die exit. Coating typically results into a significant decrease of the critical shear stress for the onset of wall slip and an increase of the slip velocity for the polymers. One factor that influences the process of die wall coating is the affinity of the processing aids with the wall and the polymer under processing. The occurrence of slip reduces the energy required for a particular flow rate (Hatzikiriakos and Migler, 2005).

To the author's knowledge, processing aids for processing of PLAs have not been reported in the literature. Therefore, methods to enhance the rate of production by eliminating or postponing melt stabilities to higher shear rates are desirable from the industrial point of view and such processing aids will be investigated in the present work. Thus, identification of suitable and effective processing aids that can eliminate such phenomena (melt fracture) is a key element in this study.

3 Thesis Objectives and Organization

3.1 Thesis Objectives

The ultimate goal of this PhD thesis is to study the effects of molecular weight and stereochemistry on the rheological, processing, and mechanical properties of newly synthesized controlled microstructure PLAs, in addition to several commercial PLAs. Another goal is to improve the properties of PLAs through copolymerization and blending. The particular objectives of this PhD study are as follows:

1. Investigate the rheological behavior of newly synthesized nearly monodisperse PLAs in a systematic way as functions of molecular parameters. First the linear viscoelastic properties of the PLAs will be analyzed over a wide range of temperatures and frequencies. Nonlinear rheological properties such as stress relaxation and viscosity functions will be determined by means of a rotational rheometer. Extensional rheology will also be studied in order to determine the degree of strain hardening if any. The effects of molecular weight on linear viscoelastic behavior of PLAs having different amounts of L- and D-LA changed in a systematic matter will also be studied.
2. Examine the rheological behavior of newly synthesized nearly monodisperse diblock copolymers of PLLA and PDLLA or PDLA with different block length ratios. Corresponding PLLA\PDLLA blends with the same molecular weight and L-/ DL-LA content as the diblock copolymers will be prepared to compare the effects of diblock formation and examine the effects of blending ratio on their thermorheological properties.
3. Evaluate the effects of copolymerization and blending on mechanical properties of PLAs. Mechanical properties to be evaluated include the Young modulus, tensile strength, and elongation at break.
4. Study the rheological behavior of several commercial PLAs and compare to literature reports for other PLAs. The processing of commercial PLAs in capillary flow in terms of slip behavior will be examined as a function of wall shear stress, temperature and molecular weight. The critical conditions for the onset of melt fracture and appropriate processing aids to postpone melt fracture to high shear rates will be investigated.

3.2 Thesis Organization

The organization of this thesis is as follows. Chapter 1 provides an introduction and describes the motivation of this work. In chapter 2, the literature review on PLA is presented. It is includes review of PLA properties particularly rheological and processing. Stereocomplexation and their effects on PLA properties as well as copolymerization of PLA are also reviewed. This chapter also includes a discussions on the rheological methods used in this work. Chapter 3 presents the objectives of the thesis and the thesis organization. In chapter 4, the materials and methods used in this research are discussed in detail. In chapter 5, the characterization of molecular structure and thermal behavior of newly synthesized homopolymers and block copolymers PLAs is presented. The solution and melt rheological properties of the homopolymers with various molecular weight and stereochemistry are presented in chapter 6. Linear viscoelasticity and extensional rheological behavior are discussed. Predictions of the shear and extensional data using the K-BKZ constitutive model are also examined (objective 1). Chapter 7 reports the solution and melt rheological behavior of block copolymers and blends of PLAs. The effects of block length ratio and blends content are discussed. The mechanical properties of the block copolymers and blends are also reported (objectives 2 and 3). Chapter 8 presents the rheological and processing behavior of four commercial PLAs. The effects of molecular weight and temperature on slip and the onset of melt fracture are examined (objective 4). Processing aids for the extrusion of PLAs are also discussed (objective 4). Finally, chapter 9 summarizes the important conclusions from the results of this research and provides recommendations for future work.

4 Materials and Methodology

4.1 Materials

PLAs of controlled molecular weight were synthesized *via* ring-opening polymerization using a chiral dinuclear indium catalyst $[(NN_HO)InCl]_2(\mu\text{-}Cl)(\mu\text{-}OEt)$ as shown in Figure 4.1 (Acosta-Ramirez et al., 2010; Douglas et al., 2008). Different ratios of L- to D-LA of 100:0, 90:10, 75:25, 50:50, and 0:100 and weight-average molecular weights in the range of 10^4–10^5 g/mol were synthesized. The PLAs are denoted by the type of lactide and molecular weight, i.e. LD190 denotes a DL-LA with a weight average molecular weight of about 190 kg/mol, with the exact values shown in Table 4.1.

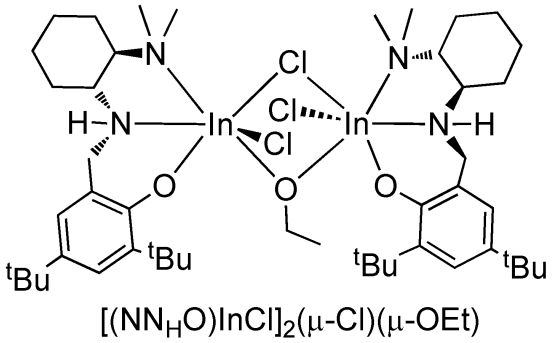

Figure 4.1: Dinuclear indium catalyst $[(NN_HO)InCl]_2(\mu\text{-}Cl)(\ \mu\text{-}OEt)$.

Table 4.1: PLA samples (homopolymers) synthesized.

Entry	*Samples*	%L:%D	*equiv*	M_{ncal} (kg/mol)[a]	M_w (kg/mol)	M_n (kg/mol)	*PDI*	P_m[b]
1	L40	100:0	292	42.0	39.5	37.9	1.04	1
2	L90	100:0	480	69.2	90.6	84.7	1.07	1
3	L130	100:0	1390	200.2	133. 6	128.3	1.04	1
4	L190	100:0	1042	150.0	192.4	176.3	1.09	1
5	L200	100:0	1262	181.8	197.9	180.6	1.10	1
6	L240	100:0	1568	226.0	240.3	229.5	1.05	1
7	L90D100	90:10	695	100.1	104.7	94.2	1.11	0.75
8	L75D40	75:25	418	60.2	43.6	39.3	1.11	0.62
9	L75D100	75:25	695	100.1	100.6	87.6	1.15	0.60
10	LD40	50:50	418	60.2	41.3	38.9	1.06	0.57
11	LD50	50:50	534	77.0	47.7	43.4	1.10	0.60
12	LD85	50:50	480	69.5	85.5	81.1	1.06	0.60
13	LD90	50:50	511	73.6	93.7	90.2	1.04	0.61
14	LD100	50:50	695	100.1	88.4	84.4	1.05	0.56
15	LD160	50:50	1390	200.2	165.6	141.8	1.17	0.59
16	LD170	50:50	1262	181.8	173.7	166.8	1.04	0.62
17	LD190	50:50	1042	150.0	185.2	173.6	1.07	0.60
18	LD50 A	50:50	292	42.0	39.8	38.5	1.03	0.50
19	D100	0:100	695	100.1	98.3	81.5	1.21	1
20	D120	0:100	1390	200.2	111.7	108.2	1.03	1

(a) Equivalents of monomer × 144
(b) P_m is the probability of isotactic enrichment determined by homonuclear decoupled ^{1}H NMR spectroscopy

Three nearly monodisperse diblock copolymers PLLA-*b*-PDLLA were synthesized with different block length ratio with the same molecular weight (Table 4.2, entries 1-3). These block copolymers are denoted by their composition and their overall molecular weight *e.g.* 75L-b170-25LD denotes a block copolymers with an overall molecular weight of about 170 kg/mol (exact value is listed in Table 4.2) with a block of PLLA (75% of the total

molecular weight) and a block of PDLLA (about 25% of the total molecular weight). Other diblock copolymers was synthesized to have a long PLLA block and a lower molecular weight (Table 4.2, entry 4). In addition, two diblock copolymers PLLA-*b*-PDLA were also synthesized with different block length ratio (Table 4.2, entries 5 and 6).

Table 4.2: Diblock copolymers synthesized.

	Samples	***monomer***	***L-LA content***	$[\alpha]_{sample,}$°	M_{ncal} ***(kg/mol)***	M_w ***(kg/mol)***	M_n ***(kg/mol)***	***PDI***
1	75L-b170-25LD	L-, DL-LA	0.75[a]	-121.7±0.7	150.2	177.5	163.3	1.09
2	50L-b170-50LD	L-, DL-LA	0.50[a]	-81.8±0.9	148.6	176.8	163.2	1.08
3	25L-b170-75LD	L-, DL-LA	0.30[a]	-49.6±0.9	147.8	175.1	165.6	1.06
4	84L-b150-16LD	L-, DL-LA	0.87[a]	-142.3±1.4	137.5	156.9	149.5	1.05
5	50L-b170-50D	L-, D-LA	0.49[b]	-4.4±2.1	170.0	169.0[c]	150.9	1.12
6	75L-b170-25D	L-, D-LA	0.71[b]	-73.8±1.5	170.0	173.1[c]	149.2	1.16

(a) Calculated by $[\alpha]_{sample}= x(-162.6)+(1-x)(-0.99)$, where x is L-LA content.
(b) Calculated by $[\alpha]_{sample}= x(-162.6)+(1-x)(+148.6)$, where x is L-LA content.
(c) Samples dissolved in chloroform.

The homopolymer blends were prepared and designed to mimic the three diblock copolymers PLLA-*b*-PDLLA. For each component in the blending, the molecular weight and composition were calculated to match the same molecular characteristics with the corresponding copolymers, namely the overall molecular weight, the ratio of the contents of L-LA and DL-LA and the ratio of the chain lengths of PLLA and PDLLA. For example, for blends 50L190\50LD190 (Table 5.2, entry 5), 1.172 g of PLLA (M_n = 176.3 kDa, PDI = 1.09) and 1.165g of PDLLA (M_n = 173.6 kDa, PDI = 1.07) were dissolved together in dichloromethane (DCM). The solution was stirred for 30 min, then the DCM was removed and the blending mixture was dried *in vacuum* overnight. The weight average molecular weights of the blends were calculated by $M_{w,blend}= x_{PLLA}M_{wPLLA}+(1-x)M_{wPDLLA}$, where x is the weight fraction of PLLA.

In addition, triblock copolymers of lactide isomers, PLLA-*b*-PDLLA-*b*-PLLA and PLLA-*b*-PDLLA-*b*-PDLA as well as PLLA-*b*-aPHB-*b*-PDLA with different length ratio and same molecular weight of about 170 g/mol (exact values are listed in Table 4.3) were also

synthesized. Crystalline PLA (PLLA with PLLA or PDLA) were incorporated in the outer blocks and amorphous polymer either PDLLA or atactic poly-3-hydroxybutyrate (aPHB) in the middle block. Details on synthesizing of PHB can be found in Xu (2012).

Table 4.3: Triblock copolymers PLLA-*b*-PDLLA-*b*-PLLA, PLLA-*b*-PDLLA-*b*-PDLA and PLLA-*b*-aPHB-*b*-PDLA synthesized.

	Samples	***monomer***	M_{ncal} ***(kg/mol)***	M_w ***(kg/mol)***	M_n ***(kg/mol)***	***PDI***
1	37.5L-25LD-37.5L	L-, DL, L-LA	168	179.1	169.1	1.06
2	25L-50LD-25L	L-, DL, L-LA	157	235.3	190.3	1.24
3	37.5L-25LD-37.5D	L-, DL, D-LA	170	175.8 [a]	152.9	1.15
4	25L-50LD-25D	L-, DL, D-LA	157	177.5 [a]	153.0	1.16
5	42.5L-15BBL-42.5D	L-LA,BBL,D-LA	170	-	-	-
6	37.5L-25BBL-37.5D	L-LA,BBL,D-LA	170	174.4 [a]	153.0	1.14

(a) samples dissolved in chloroform.

General Considerations: Unless otherwise indicated, all air and/or water-sensitive reactions were carried out under dry nitrogen using either an MBraun glove box or standard Schlenk line techniques. BrukerAvance 300 MHz or 400 MHz NMR spectrometers were used to record spectra. For determination of polymer tacticity, a BrukerAvance 600 MHz was used to run homonuclear decoupled ^{1}H spectra for polylactide. DCM was degassed and dried using 3 Å molecular sieves in an MBraun Solvent Purification System and distilled from CaH_2. The catalyst, $(NN_HO)InCl]_2(\mu\text{-}Cl)(\mu\text{-}OEt)$, was synthesized according to previously published procedures (Acosta-Ramirez et al., 2010; Douglas et al., 2008). DL-, L- and D-LA were donated by Purac Biomaterials and recrystallized twice in toluene. β-butyrolactone, purchased from Aldrich, was stirred with calcium hydride (CaH_2) for 48 hours, distilled under vacuum degassed through free-pump-thaw cycle and kept in the freezer at -30°C. Tetrahydrofuran (THF) with BHT as stabilizer for GPC analysis was purchased from J. T. Baker. Tris(nonylphenyl)phosphite (TNPP) was purchased from Sigma-Aldrich.

Synthesis of PLA homopolymers: In a typical experiment of synthesis of PLA homopolymers, in a glove box, 22.1 mg of catalyst was weighed and dissolved in DCM. The solution was transferred to a round bottomed flask. While stirring, a solution of L-LA (3.0 g

L-LA dissolved in DCM) was slowly added in and the solution stirred at room temperature overnight. The next day, the reaction mixture was quenched with 0.5 mL hydrogen chloride/diethyl ether (HCl/Et_2O). A few drops of the mixture were removed to check conversion (by ^1H NMR spectroscopy). The rest was concentrated and the polymer was precipitated from cold MeOH. The resulting polymer was washed with 3 × 3 mL cold methanol (MeOH) and dried *in vacuo*. The polymer was redissolved in dry DCM and the thermal stabilizer was added (TNPP, 30 mg) and then the solvent was removed *in vacuo* overnight.

Synthesis of diblock copolymers: In a typical experiment of synthesis of diblock copolymers, in a glove box, 18.3 mg catalyst was weighed and dissolved in DCM. The solution was transferred to a round bottomed flask. While stirring, a solution of L-LA (1.810 g L-LA, dissolved in DCM) was slowly added in. The polymerization was allowed to stir overnight at room temperature to ensure that all the L-LA was converted and the conversion verified by removal and testing (by ^1H NMR spectroscopy) of two drops of the mixture. Subsequently, a solution of second monomer DL-LA (0.690 g DL-LA, dissolved in DCM) was added to the reaction. The reaction was again stirred overnight at room temperature. Then the reaction was quenched with 0.5 mL HCl/Et_2O. A few drops of the mixture were removed to check conversion (by ^1H NMR spectroscopy). The rest was concentrated and precipitated in cold MeOH. The resulting polymer was washed with 3 × 3 mL cold MeOH and dried *in vacuo*. The polymer was redissolved in dry DCM and the thermal stabilizer was added (TNPP, 20.5 mg) and then the solvent was removed *in vacuo* overnight.

Synthesis of triblock copolymers: In a typical experiment of synthesis of triblock copolymers, in a glove box, 22.7mg catalyst was weighed and dissolved in DCM. The solution was transferred to a round bottomed flask. While stirring, a solution of L-LA (1.27 g L-LA, dissolved in DCM) was slowly added in. The polymerization was allowed to stir for several hours at room temperature to make sure that all the L-LA was converted. Then a solution of second monomer DL-LA (0.966 g DL-LA, dissolved in DCM) was added to the reaction. The polymerization was allowed to stir overnight at room temperature to make sure that all the DL-LA was converted. Next day, a solution of the third monomer D-LA (1.27 g D-LA, dissolved in DCM) was added to the reaction. The reaction was allowed to stir overnight at room temperature. Then the reaction was quenched with 0.5 mL HCl/Et_2O. A

few drops of the mixture were pipetted out and run on NMR to check conversion. The rest was concentrated and precipitated in cold MeOH. The resulting polymer was washed with 3 mL cold MeOH for three times and dried under vacuum. The polymer was then redissolved in dry DCM and the thermal stabilizer, TNPP (35.0 mg) was added and then the solvent was removed under vacuum overnight. Parallel experiments of the synthesis of only the first block and the first two block polymers were carried out under the same condition to get information of the molecular weight of each block.

In addition to the newly synthesized samples, four commercial PLAs (PLA 7001, 2002D, 3051D and 3251D) of different molecular weights (in the range of 10^4-10^5 g/mol) and about the same polydispersity (~1.8) were studied in this work. All samples are obtained from NatureWorks LLC. The properties are summarized in Table 4.4. A commercial poly(ε-caprolactone) (PCL) obtained from Perstorp (Capa® 6500) with molecular weight of 55.5 kg/mol and polydispersity of 1.22 also used as a potential processing aid.

Table 4.4: Properties of commercial PLAs used in this study

Sample	M_w **(kg/mol)**	M_n **(kg/mol)**	***PDI***	T_g(°C)	T_m(°C)
PLA 7001D	110.1	69.2	1.59	57.1	149.0
PLA 2002D	106.9	58.7	1.82	56.5	152.4
PLA 3051D	92.5	50.8	1.82	55.0	150.0
PLA 3251D	55.4	34.2	1.62	58.8	167.9

4.2 Characterization Techniques

4.2.1 Gel permeation chromatography (GPC)

Molecular weights, polydispersity indices, characteristic radii (radius of gyration, R_g, and hydrodynamic radius, R_h), and intrinsic viscosity [η] of the PLA samples were determined by triple detection gel permeation chromatography (GPC-LS) using a Waters liquid chromatograph equipped with a Waters 515 HPLC pump, Waters 717 plus autosampler, Waters Styragel columns (4.6 × 300 mm) HR5E, HR4 and HR2, Waters 2410 differential refractometer, Wyatt tristarminiDAWN (laser light scattering detector) and a Wyatt

ViscoStar viscometer. A flow rate of 0.5 mL/min was used and samples were dissolved in THF or chloroform (ca. 2 mg/mL). The measurements were carried out at laser wavelength of 690 nm, at 25°C. The data were processed using Astra software provided by Wyatt Technology Corp. The specific refractive index increment, d*n*/d*c* values were determined by measuring the refractive index of PLA solutions with different concentrations at 25°C using OptilabrEX (Wyatt Technology Corp) at the wavelength of the light 690 nm. At least five different concentrations, $0.5 < c < 6$ g/mL of PLAs in tetrahydrofuran (THF) were measured.

4.2.2 Differential scanning calorimeter (DSC)

A differential scanning calorimeter (DSC) Q1000 (TA Instruments) was employed to measure the glass transition (T_g) and melting (T_m) temperatures of the synthesized samples. Approximately 2-3 mg of the samples were weighed and sealed in an aluminum pan. The experiments were carried out under a nitrogen atmosphere. The samples were heated at a rate of 10°C/min, then held isothermally at high temperature for 5 min to destroy any residual nuclei before cooling at 5°C/min. The glass transition, melting temperatures, enthalpies of melting and crystallization were obtained from a second heating sequence, performed at 10°C/min.

4.2.3 Optical rotational measurement

Specific optical rotations of the block copolymers were measured at a concentration of 1 ± 0.1 mg/mL in chloroform. The measurements were carried out using Jasco P-2000 Polarimeter under a wavelength of 589 nm at room temperature. Five times measurements were carried out for each sample and the average and standard deviation are reported.

4.3 Sample Preparation

Tris(nonylphenyl)phosphate (TNPP) was added as a stabilizer against thermal degradation. The optimum TNPP concentration used to stabilize the polymers was 0.35 wt. %, also reported by (Palade et al., 2001). The samples for the rheological testing were prepared as

follows: weighed quantities of the polymers were dissolved in DCM and then dried in vacuum for at least 2 h. To ensure that the solvent is completely removed, the samples were left in the vacuum oven for 5 min at a temperature above the melting temperature (~190°C) for the crystalline samples (100% L or 100% D) or 110°C for the amorphous samples. The samples were then molded by compression molding at the same temperatures as used in vacuum oven for about 20 min before being cooled. The molded discs for shear measurements were ~0.6 mm in thickness and 8 mm in diameter.

4.4 Rheological Measurements

4.4.1 Linear viscoelasticity

Shear measurements were performed using a MCR 501 rheometer (Anton Paar), equipped with 8 mm parallel plates. The dynamic linear viscoelastic measurements were carried out within the linear viscoelastic regime at temperatures in the range from 70 to 210°C. The limit of linear viscoelasticity was first determined by a set of strain amplitude sweep tests, performed at frequencies equal to 0.1, 1, and 10 Hz at 180°C and 190°C.

The dynamic measurements were conducted in the range of 0.01–100 rad/s at a strain of 2%. Gaps of 0.3–0.6 mm were used to minimize edge effects and ensure a reasonable aspect ratio of plate radius and gap. Dynamic time sweep measurement was carried out at an angular frequency of 1 rad/s and 180°C to examine the thermal stability of the samples. Step shear strain measurements were performed at 150°C to determine the shear damping function for the constitutive modeling.

4.4.2 Extensional rheology

Uniaxial extensional measurements were performed using the Sentmanat extensional rheometer (SER-2) which extensional fixture attached to MCR 501 (Anton-Paar) rheometer. Full description of this unit can be found elsewhere (Sentmanat et al., 2005). Rectangular samples with dimensions of 16 × 50 mm and thickness 0.4–0.6 mm were prepared by the same procedure used for shear samples. Individual polymer specimens were then cut to a width of 3.4–6.4 mm. Measurements were conducted at temperatures close to the transition

and melting temperature for amorphous and crystalline sample respectively, to ensure that the viscosities of the samples were high enough to prevent sagging. The extensional stress growth coefficients were measured at various Hencky strain rate in the range of 0.01-10 s^{-1}. All the rheological measurements were performed under nitrogen atmosphere to minimize degradation of the polymer samples during testing.

4.4.3 Constitutive rheological modeling of PLA

The Wagner integral constitutive model, Kaye-Bernstein, Kearsley and Zapas (K-BKZ) model was used to analyze the linear and nonlinear viscoelastic behavior of PLA. The damping and memory functions were evaluated based on the results of the stress relaxation experiments and the linear and nonlinear viscoelastic behavior of PLA. The ability of the above mentioned model in predicting the nonlinear behavior of PLA was studied using the experimental data from the successive start-up of steady state shear, and oscillatory flow experiments. An aspect of particular interest is the prediction of strain hardening that been reported for PLAs in literature (Palade et al., 2001; Yamane et al., 2004). Using such a model in the analysis of the experimental results might shed more light into the origin of strain hardening in linear polymers.

4.4.4 Processing study

The processability and shear viscosity at high apparent shear rates were studied by using a pressure driven Instron capillary rheometer equipped with a barrel having a diameter of 0.95 mm. A series of dies having a fixed diameter of 0.76 mm and various length to diameter (*L/D*) ratios were used to correct for the entry effects (Bagley correction) and assess the effect of pressure on viscosity. Two additional series of dies having different diameters of 0.43 and 1.22 mm and constant *L/D* ratios were used to detect slip effects through the Mooney analysis (Hatzikiriakos and Dealy, 1992a; Ramamurthy, 1986). All dies had an entry angle of 180°. These are summarized in Table 4.5 along with their characteristic dimensions. The Bagley and Mooney corrections were applied to the data to obtain the true viscosity of the samples (Dealy and Wissbrun, 1999) in order to compare them with viscosity data from

the parallel plate rheometer. The extrudates from the capillary extrusion experiments were inspected by Olympus MIC-D microscope to detect any visual defects known as melt fracture phenomena (Hatzikiriakos and Dealy, 1991; Hatzikiriakos and Dealy, 1992b; Ramamurthy, 1986). A commercial PCL was used as a potential processing aid to eliminate/ postpone melt fracture phenomena (Achilleos et al., 2002; Amos et al., 2001).

Table 4.5: Characteristic dimensions of capillary dies used.

Diameter (mm)	***L/D***	**Entry angle (^{0})**
0.43	16	180
0.76	1.8	180
0.76	5.3	180
0.76	16	180
0.76	33	180
1.22	16	180

4.5 Tensile Measurements

Tensile tests were performed using COM-TEN 95 series tensile testing equipment (COM-TEN Industries) at ambient conditions. Tensile specimens were cut from compression-molded films. Specimen of 36.6 mm in width and 90 mm in length were cut from the middle portion of the compressed films to avoid edge effects and edge imperfections. The films were compressed in a hot press at 190°C for 30 min before being cooled. A gage length of 40 mm, crosshead speed of 25 mm/min and a 40 pound (178 N) capacity of load cell was used for testing all samples. To eliminate specimen slippage from the grips, double adhesive masking tape was used to wrap around the top and bottom portions of the sample. For each sample five tests were run. The average modulus, tensile stress and elongation at break were calculated from the resultant stress-strain measurements and these are reported below along with standard deviations shown by the plotted error bars.

5 Materials Characterization

In this chapter, we examined the molecular structure of the newly synthesized PLAs. These include PLAs with different ratios of L- to D-lactide (LA) of 100:0, 90:10, 75:25, 50:50, and 0:100 and weight-average molecular weight (M_w) in the range of 10^4 to 10^5 g/mol, diblock and triblock copolymers of different length ratio of PLLA to PDLLA or PDLA at fixed M_w ~170 g/mol. The thermal properties of the newly synthesized PLAs are also discussed in this chapter.

5.1 Molecular Structure

5.1.1 Homopolymers

Polymerization of a mixture of 50:50 D- and L-LA in dichloromethane (DMC) produces polymers with moderated isotacticity with probability of a meso linkage in polymers (P_m values) between 0.56 and 0.6 (entries 10-17, Table 4.1). P_m values close to one indicate entirely isotactic PLA. When tetrahydrofuran (THF) was used as a solvent, atactic PLA (P_m=0.5) was obtained (entry 18, Table 4.1). This catalyst is capable of living polymerization of lactide as indicated by the parity between the theoretical and experimental number-average molecular weight values (M_n). GPC measurements from different mixtures of PLA samples from 50:50 to 75:25 or 90:10 show very close agreement between theoretical and observed M_n values (entries 7-17 in Table 4.1). Finally, when pure L- or D-LA were used as monomers, completely isotactic PLA was obtained (entries 1-6 and 19-20 in Table 4.1). In all cases, high conversions (>97%) and yields (>90%) as well as narrow PDIs were obtained.

5.1.2 Diblock copolymers

As reported previously, the dinuclear indium complex $[(NN_HO)InCl]_2(\mu\text{-}Cl)(\mu\text{-}OEt)$, is an active and living catalyst for the ring opening polymerization of LA (Acosta-Ramirez et al., 2010; Douglas et al., 2008). In particular, 200 equivalents of LA are converted to PLA in 30 min (25°C, DCM, >90% conversion). No chain termination events are observed. Kinetic observation of sequentially adding two copies of 100 equivalents LA to the polymerization solution shows that the polymerization rate remains the same for the second aliquot LA,

indicating that the catalyst retains its activity over multiple additions (Douglas et al., 2008). Thus, it is possible to synthesize well-defined diblock copolymers of PLLA and PDLLA with this catalyst system by sequential addition.

The diblock polymers discussed in this study, such as 75L-b170-25LD (Table 4.2, entry 1), were synthesized in a two-step process. In the first step L-LA (755 equivalents) was added to a solution of the catalyst and the reaction was stirred at room temperature overnight. The conversion (>98%) and molecular weight (M_{ncalc}= 108.8 kg/mol, M_{nexp} = 124.4 kg/mol, PDI = 1.08) of the PLLA were measured. DL-LA (288 equivalents) was added only after L-LA was fully converted so that each block only contained the expected amount of the corresponding monomer. The conversion (>98%) and molecular weights of the resulting copolymers were measured to ensure that a true diblock was formed. Overlayed GPC traces (Figure 5.1) of 75L and 75L-b170-25LD (M_{ncalc} =150.3 kg/mol) show that the peak corresponding to 75L-, is not observed after addition of 25LD, confirming that chain termination did not occur.

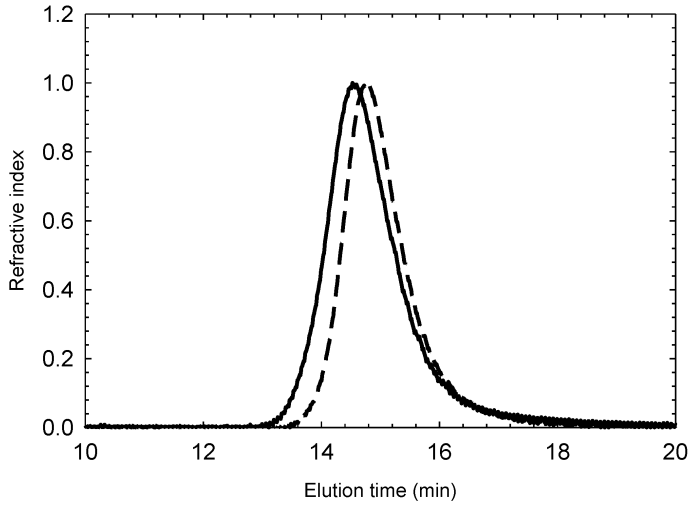

Figure 5.1: GPC trace of the diblocks. Left (solid line): PLLA-*b*-PDLLA (M_n = 163.3 kg/mol, PDI = 1.09); right (dash line): PLLA block in the copolymer (M_n = 124.4 kg/mol, PDI = 1.08).

Formation of stereoblock polymers PLLA-*b*-PDLA causes a significant decrease in polymer solubility in THF at room temperature. The stereoblocks can be dissolved slowly in dichloromethane or chloroform with heating and sonication. Therefore, the measurement for

entries 5 and 6 in Table 4.2 were performed using GPC equipped with refractive index detector using chloroform as the solvent.

Specific optical rotations of the diblock copolymers are listed in Table 4.2. The specific optical rotations, [α] of homopolymers LD30, L210 and D220 were also measured having values of 0.99 ± 0.3°, -162.6 ± 0.1° and +148.6 ± 0.5° respectively, which are close to literature values ($[\alpha]_L$ = -151°, ($[\alpha]_D$ = +151°) (Yui et al., 1990). These values are used as a reference to calculate the L-LA content and determine the ratios of respective monomers in the copolymers. The ratios of monomers calculated from optical rotation agreed well with the nominal values, *i.e*. the feeding ratios in synthesis. The formation of well-defined polymers with predicted constitution is also a result of living polymerization with our catalyst.

5.1.3 Triblock copolymers

The triblock copolymers were synthesized in three steps. All the polymerizations were carried out overnight at room temperature, with conversion over 99%. The molecular weights of the resulting copolymers after addition of each block were measure to ensure that a true block was formed. Overlayed GPC traces (Figure 5.2) of 25L, 25L-50LD and 25L-50LD-25L (M_{ncalc} =157 kg/mol) show that the peak corresponding to 25L and 25L-50LD are not observed after the second and third additions, respectively, confirming that no chain termination event occurred.

Triblock copolymers with PLLA and PDLA at the outer block were highly insoluble in THF at room temperature (Table 4.3, entries 3- 6). Therefore, the GPC measurements were performed in chloroform. However, copolymers entry 5 in Table 4.3 was highly insoluble in chloroform thus we were unable to determine the molecular weight of the polymers with our existing facilities. While the measurements performed using different GPC facilities, the results were within experimental error (10% difference).

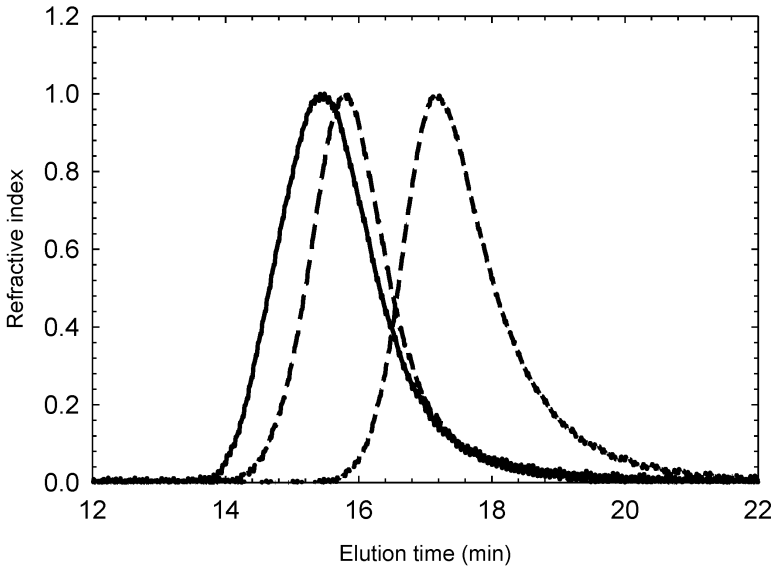

Figure 5.2: GPC trace of the triblocks. Left (solid line): PLLA-*b*-PDLLA-*b*-PLLA (M_n = 190.3 kg/mol, PDI = 1.24); middle (long dashed line): PLLA-*b*-PDLLA block in the copolymers (M_n = 140.2 kg/mol, PDI = 1.12); right (short dash line): PLLA first block in the copolymers (M_n = 44.4 kg/mol, PDI = 1.14).

5.2 Thermal Properties

5.2.1 Homopolymers and blends

As can be seen from Table 5.1, isotactic PLAs from enantiopure isomers L- and D-LA exhibits a peak melting temperature (T_m) in the range of 170 to 180°C and glass transition temperature (T_g) between 50 and 65°C. However, the PLAs produced from L- and D-mixtures are amorphous and exhibit a T_g between 50 and 55°C.

Figure 5.3 shows the thermograms of the second heating sequence of PLLA, (a) L240 PDLLA, (e) LD90 and their blends at different compositions (b, c and d). LD90 does not exhibit crystallization and melting, hence it is concluded that the material is completely amorphous. The T_g's of L240 and LD90 are 61°C and 52.6°C respectively. The thermograms for a blend of L240 and LD90 (Figure 5.3) show a single peak and no broadening of the T_g can be seen, indicating that L240 and LD90 are miscible in the molten state. When the percentage of L240 in the blends is decreased, the intensity of melting peak decreases. The continuing presence of a single melting peak indicates continued miscibility. These observations agree well with previous studies on PLLA\PDLLA blends (Ren and Adachi, 2003; Tsuji and Ikada, 1995a; Xu et al., 2005). The presence of a single T_m peak indicates

that the incorporation of PDLLA did not vary the final crystalline thickness and form of PLLA. These results are in agreement with work by Bouapao et al. (2009) who show that the crystalline form of PLLA remains unchanged in the presence of PDLLA. Simply, the crystal composition decreases with increasing amount of PDLLA as determined from the value of the enthalpy of melting, ΔH_m in Table 5.2.

Table 5.1: The T_g, T_m, ΔH_c and ΔH_m of homopolymers PLA studied in this work.

Entry	***Samples***	T_g***(°C)***	T_m ***(°C)***	$\Delta H_c (Jg^{-1})$	$\Delta H_m (Jg^{-1})$
1	L40	55.9	169.4	21.4	37.4
2	L90	53.6	178.1	10.3	42.2
3	L130	54.8	176.8	-	22.2
4	L190	59.2	179.5	11.7	32.7
5	L200	60.3	180.7	23.0	33.9
6	L240	61.0	183.1	-	45.1
7	L90D100	54.0	-	-	-
8	L75D40	51.7	-	-	-
9	L75D100	53.6	-	-	-
10	LD40	51.3	-	-	-
11	LD50	51.5	-	-	-
12	LD85	51.5	-	-	-
13	LD90	52.6	-	-	-
14	LD100	52.4	-	-	-
15	LD160	52.6	-	-	-
16	LD170	52.6	-	-	-
17	LD190	53.2	-	-	-
18	LD50 A	49.5	-	-	-
19	D100	57.2	170.7	16.0	23.9
20	D120	64.9	176.1	-	29.6

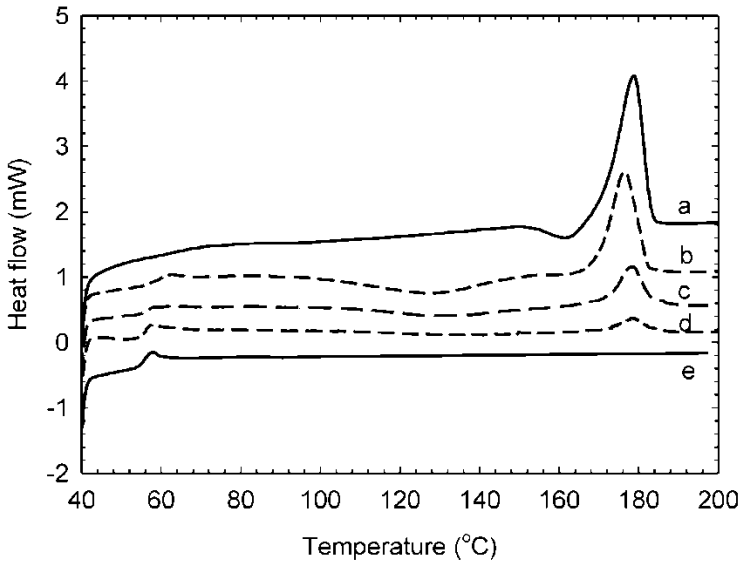

Figure 5.3: DSC thermograms of L240(a), LD90(e) and their blends with different L240 weight fractions 0.75(b),0.5(c) and 0.25(d).

Table 5.2: The T_g, T_m, ΔH_c and ΔH_m of PLA blends studied in this work.

Entry	***Samples***	***M_w (kg/mol)***	***T_g(°C)***	***T_m (°C)***	***$\Delta H_c (Jg^{-1})$***	***$\Delta H_m (Jg^{-1})$***
1	75L240\25LD90	203.7	60.0	175.8	20.5	38.9
2	50L240\50LD90	167.0	56.0	177.4	-	19.6
3	25L240\75LD90	130.4	55.9	177.7	-	7.3
4	75L200\25LD85	166.0	57.0	179.2	20.5	28.5
5	50L190\50LD190	188.8	56.3	179.0	14.2	19.8
6	25L90\75LD170	150.7	57.0	-	-	-

Similar observations were also found for blends, entries 4 to 6 in Table 5.2. The blends that consists of shortest and smallest M_w of PLLA was completely amorphous (Figure 5.4).

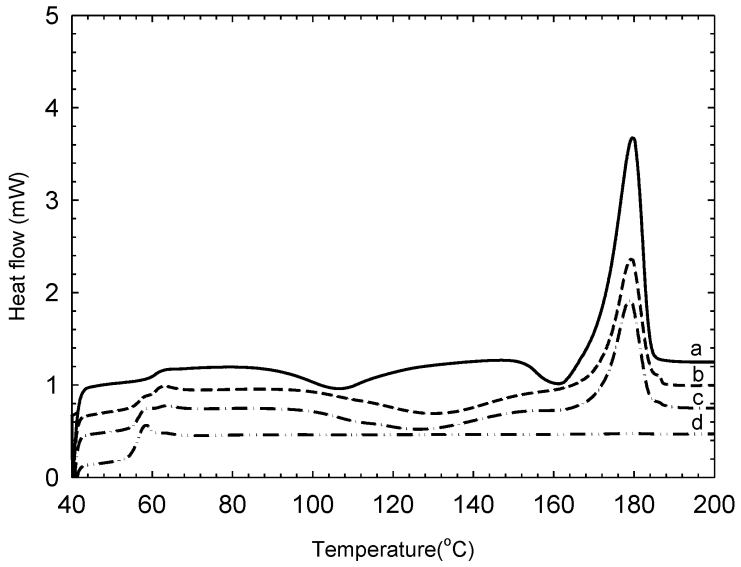

Figure 5.4: DSC thermograms of PLLA\PDLLA blends entries 4 to 6 in Table 5.2 (a) L190 (b)75L200\25LD85 (c)50L190\50LD190 (d)25L90\75LD170.

5.2.2 Diblock copolymers

Figure 5.5 depicts the thermograms of diblock copolymers with the same molecular weight and different block compositions (entries 1 to 3 in Table 5.3). For comparison the thermograms of PLLA with about the same molecular weight, L190 (entry 4 in Table 5.1) is shown as well. The presence of PDLLA block (amorphous) shifts the T_m to lower temperatures with an increase of the PDLLA block. With a large enough PDLLA block length (75%), the T_m peak disappears and the diblock copolymer becomes completely amorphous. The depression of T_m in diblock copolymers is due to shorter PLLA lengths in the diblock copolymers.

Symmetric diblock copolymers with similar lengths of PLLA and PDLLA show small broad melting peaks (see inset in Figure 5.5). The value of ΔH_m for diblock copolymers (entry 2 in Table 5.3) is much lower (0.9 Jg^{-1}) than the corresponding value for the blends (entry 5 in Table 5.2) which is 19.6 Jg^{-1}. The reduced degree of crystallinity of diblock copolymers compared to that of the corresponding blend is attributed to the segmental connection between PLLA and PDLLA chains, which somehow hinders the free movement of the PLLA chains of the diblock copolymers during crystallization. Tsuji et al. (2010) have reported that the nucleation constant values calculated from Hoffman's nucleation theory for

copolymers were higher than those for corresponding blends. This indicated that the crystallite growth mechanism in copolymers PLLA-*b*-PDLA are different from that in the corresponding blends (Tsuji et al., 2010).

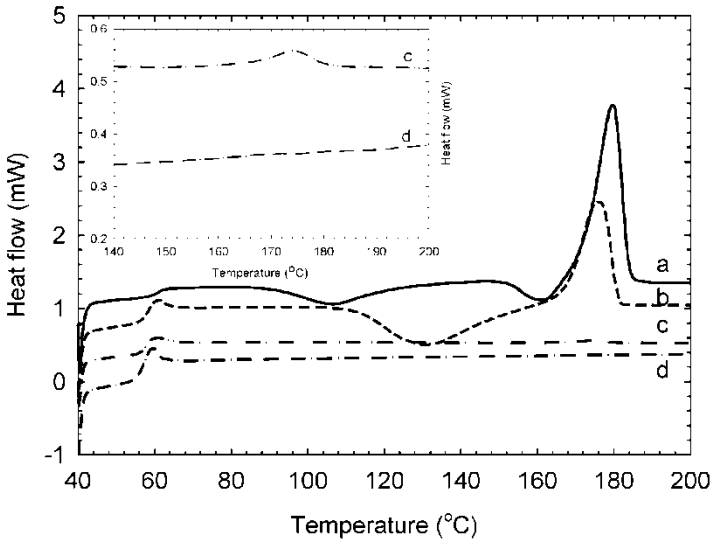

Figure 5.5: DSC thermograms of diblock copolymers with different block length ratio (a)L190 (b)75L-b170-25LD (c)50L-b170-50LD (d)75L-b170-25LD.

Table 5.3: The T_g, T_m, ΔH_c and ΔH_m of diblock copolymers studied in this work.

Entry	***Samples***	T_g (°C)	T_{m1} (°C)	T_{m2} (°C)	ΔH_c (Jg^{-1})	ΔH_{m1} (Jg^{-1})	ΔH_{m2} (Jg^{-1})
1	75L-b170-25LD	58.5	176.0	-	29.8	30.1	-
2	50L-b170-50LD	56.8	174.0	-	-	0.9	-
3	25L-b170-75LD	55.2	-	-	-	-	-
4	84L-b150-16LD	59.9	170.9	-	30.8	33.7	-
5	50L-b170-50D	55.0	162.0	210.0	7.2	1.8	34.7
6	75L-b170-25D	53.0	169.0	204.0	22.1	9.3	17.8

PLLA-*b*-PDLA diblock copolymers possess double melting peaks (Table 5.3, entries 5 and 6); the low melting point is detected at about 170°C and the high melting temperature peak at about 210°C (Figure 5.6). The lower melting temperatures are close to the melting temperature of pure PLLA (α-form crystallites). The higher melting temperatures for the diblock copolymers are attributed to the fusion of PLA crystallized in stereocomplex form,

which is in agreement with reported values for copolymers and blends containing both lactic acid stereoisomers (Fukushima and Kimura, 2006; Fukushima et al., 2007; Li et al., 2004; Rahman et al., 2009; Sarasua et al., 2005; Spassky et al., 1996; Tsuji and Ikada, 1999; Tsuji et al., 1991a; Tsuji and Ikada, 1993; Tsuji et al., 2010; Woo and Chang, 2011; Yamane et al., 2004)

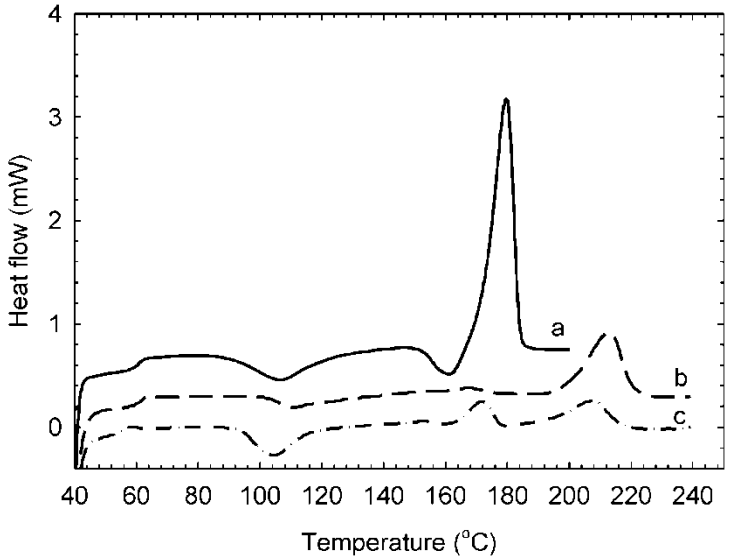

Figure 5.6: DSC thermograms of diblock copolymers with different block length ratio (a)L190 (b)50L-b170-50D (c)75L-b170-25D.

It has been reported in the literature that 1:1 molar ratios of PLLA and PDLA in chiral mixtures prefer to form a stable stereocomplex, as the packing between PLLA and PDLA is most accessible when the molecules of the two opposite chiral configurations are equal in number. The fraction of complexes decreases steadily as the molar ratio deviates from 1:1 ratio (Tsuji et al., 1991a; Li et al., 2004; Opaprakasit and Opaprakasit, 2008). Similar results have been reported by Li et al. (2004) for PLLA-*b*-PDLA diblock copolymers. The symmetric diblock copolymers crystallize in the stereocomplex form, however, as the block ratio deviates from 1:1 coexistence of homocrystal phase can be found at low crystallization temperatures.

In the case of symmetric diblock copolymer PLLA-*b*-PDLA, (Figure 5.6b) a broad low temperature peak can be observed, while the high temperature peak that corresponds to stereoblock crystallites is clearer. This indicates that both homocrystallites and stereocomplex crystallites are formed. The 50L-b170-50D diblock has a high molecular

weight sufficient to form stereocomplex crystallites species as well as homocrystallites. The critical value of M_w below which only stereocomplex crystallites are formed is approximately 10 kg/mol (Tsuji et al., 1991a; Tsuji et al., 2010). When the molecular weights of PLLA and/or PDLA are increased above the upper critical values and in a molecular weight range of over 200 kg/mol, only homocrystallites are formed (Tsuji and Ikada, 1999; Tsuji et al., 1991a; Tsuji et al., 2010). The high molecular weight of block copolymers increases the domain sizes of the PLLA or PDLA chains, resulting in delayed stereocomplex crystallization.

5.2.3 Triblock copolymers

Triblock copolymers of PLLA-*b*-PDLLA-*b*-PLLA having almost 40% PLLA at each end show a melting temperature at 168.9°C. However as the PLLA length decreases to 25% the copolymer becomes amorphous as no melting peak detected during second heating (Table 5.4).

Figure 5.7 shows the DSC thermograms of triblock copolymers PLLA-*b*-PDLLA-*b*-PDLA. Unlike diblock PLLA-*b*-PDLA, the triblock of PLLA-*b*-PDLLA-*b*-PDLA possess exclusively stereocomplex crystallites (only one melting temperature can be observed). Similarly, the melting temperature and crystallinity of the stereocomplex decreases with decrease of the PLLA and PDLA length (Table 5.4). The presence of PDLLA in the middle block shortens both PLLA and PDLA end block thus ease stereocomplex formation.

On the other hand, copolymers with atactic PHB as the middle block instead of PDLLA, display two melting temperatures, which are the low melting temperatures of homocrystalline followed by high melting temperature of stereocomplex (Figure 5.8). Similar observations by Chang and Woo (2011) show that the crystallization of stereocomplex PLA in the blends was significantly hindered with addition of PHB. Furthermore, less perfect crystals were found with increasing PHB contents (Chang and Woo, 2011). However, the melting temperatures of stereocomplex in these triblocks were higher than that of triblock with PDLLA in the middle.

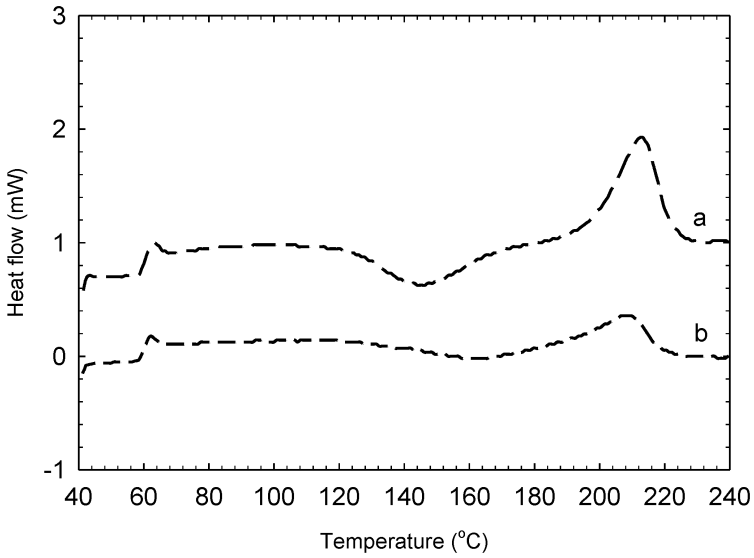

Figure 5.7: DSC thermograms of triblock copolymers with different block length ratio (a)37.5L-25LD-37.5D (b)25L-50LD-25D.

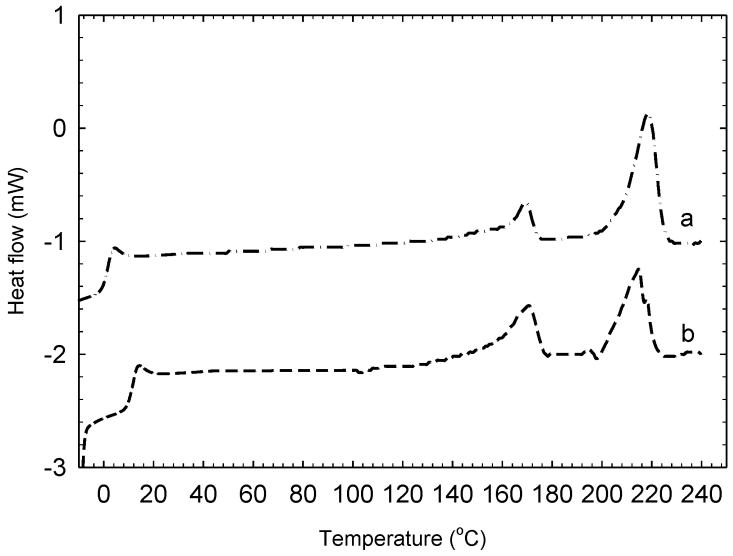

Figure 5.8: DSC thermograms of triblock copolymers with different block length ratio (a)42.5L-15BBL-42.5D (b)37.5L-25BBL-37.5D.

Table 5.4: The T_g, T_m, ΔH_c and ΔH_m of triblock copolymers studied in this work.

Entry	***Samples***	T_g (°C)	T_{m1} (°C)	T_{m2} (°C)	ΔH_c (Jg^{-1})	ΔH_{m1} (Jg^{-1})	ΔH_{m2} (Jg^{-1})
1	37.5L-25LD-37.5L	53.3	168.9	-	-	4.6	-
2	25L-50LD-25L	57.3	-	-	-	-	-
3	37.5L-25LD-37.5D	62.8	-	212.8	20.6	-	32.9
4	25L-50LD-25D	62.8	-	208.4	11.1	-	17.6
5	42.5L-15BBL-42.5D	4.6	169.2	218.4	-	3.9	34.0
6	37.5L-25BBL-37.5D	9.2	170.5	214.8	-	18.0	21.7

5.3 Summary

The molecular structure and thermal properties of homopolymers, blends and block copolymers were examined. High conversion (>98%) and nearly monodisperse PLAs were obtained *via* ring-opening polymerization of lactide using dinuclear indium complex as initiator. GPC measurements after addition of each block proved that no chain termination occurred and the well-defined polymers with predicted constitution were synthesized.

PLA synthesized from enantiopure L- or D-LA show melting temperature in range of 170-180°C. On the other hand, PLAs synthesized from L- and D-mixtures are amorphous with glass transition temperature in the range of 50-60°C.

The crystalline content in the blends of PLLA\PDLLA decreased with addition of amorphous PDLLA, while the melting points remain unchanged. The crystallization of diblock copolymers was different from that of equivalent blends as a result of the covalent connection between PLLA and PDLLA chains that restricts molecular flexibility for ease of molecular orientation. As a result, the crystallinity of diblocks decreases compared to that of the corresponding blends.

For PLLA-*b*-PDLA diblocks, formation of stereocomplex crystallites lead to a high melting point (>200°C). On the other hand, triblock copolymers of PLLA-*b*-PDLLA-*b*-PDLA with amorphous PLA in the middle block crystallized into exclusively stereocomplex crystal. In contrast, triblock copolymers with amorphous PHB in the middle block exhibit two melting temperatures of homocrystallites and stereocomplex crystallites.

6 Rheology of PLA Homopolymers

In this chapter a series of newly synthesized controlled microstructure PLAs (nearly monodisperse listed in Table 4.1 from known mixtures of L- and D-LA is studied rheologically (Acosta-Ramirez et al., 2010; Douglas et al., 2008). The solution properties as well as the melt rheological properties are studied in order to determine relationships between molecular characteristics and rheological properties for comparison with previous studies (Cooper-White and Mackay, 1999; Dorgan et al., 2005a; Dorgan et al., 2005b; Palade et al., 2001; Yamane et al., 2004). The extensional viscosity measurements for PLAs are presented over a broader range of Hencky strain rate and temperature than previously reported (Palade et al., 2001; Yamane et al., 2004). Modeling is also performed using the K-BKZ constitutive equation based on experimental results. The new data from this set of nearly monodisperse polymers sheds additional light on the dynamics of this important class of polymers.

6.1 Solution Properties

The solution properties of single chain are discussed and related to measurable quantities available from dilute solution viscometry. A crucial input parameter for the determination of the absolute molar mass distribution is the refractive index increment, d*n*/d*c*. This value describes the change in refractive index *n* of a solution with concentration *c* at a fixed wavelength and a fixed temperature. To ensure that the molecular weights were as accurate as possible, the specific refractive index increment (d*n*/d*c*) were measured, yielding d*n*/d*c* of 0.044 ± 0.005 mL/g for various L:D compositions and molecular weights. This agrees with value reported by Dorgan et al. (2005b), thus confidence is gained regarding the reliability of the molecular weight values from light scattering measurements.

The average values of the intrinsic viscosities, $[\eta]$ and the weight-average molecular weight (M_w) obtained from light scattering GPC are plotted in Figure 6.1. Linearity in this plot implies linear random coils. The slope of the linear regression line (exponent of the Mark Houwink equation) is 0.75, which agrees with the values reported by Dorgan et al. (2005b) for PLAs in THF. For linear polymers with random coil conformation, the exponent of the Mark Houwink equation has a value from 0.5 in a poor solvent to 0.8 in a good solvent

(Burchard, 1999). The chain properties and solution characterization of PLAs in three different solvents using few different techniques have been reported by Dorgan and coworkers (Dorgan et al., 2005b).

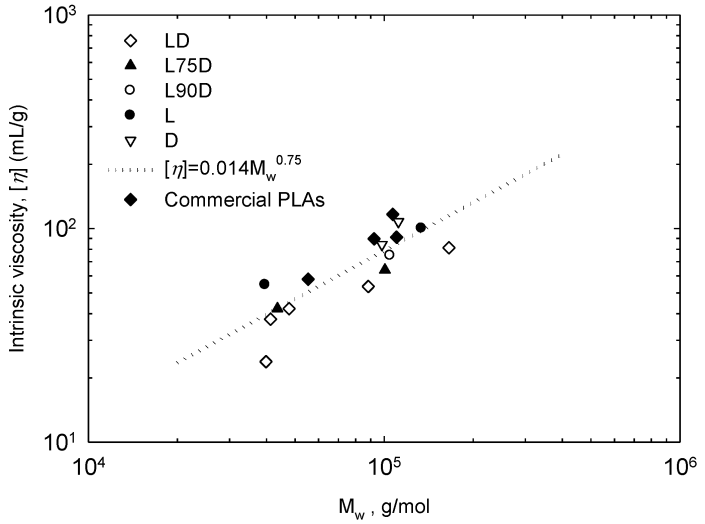

Figure 6.1: The intrinsic viscosities of homopolymers and commercial PLAs versus molecular weight at 25°C. The slope of the straight line is 0.75 (Mark Houwink slope) implying good solvent conditions.

The hydrodynamic radius (R_h) and radius of gyration (R_g) dependence of the weight-average molecular weight of the polymers were determined in the range of 10^4 and 10^5 g/mol (Figure 6.2). Figure 6.2a and Figure 6.2b are log-log plots of R_h and R_g vs. molecular weights respectively. The scaling relation between R_h (Equation 6-2) and M_w can be described as below with minimum scattering:

$$R_h = 0.017\, M_w^{\,0.56} \qquad (6\text{-}1)$$

Conversely, the data for R_g data exhibit a certain degree of scattering (see error bars in Figure 6.2b). This scattering is due to the relatively low molar masses and radii, which are reported as limiting experimental problem for a number of materials (Auhl et al., 2006). However, the values agree well with the value calculated from the molar mass dependence of the intrinsic viscosity using the Flory-Fox equation (Equation 6-3) (Podzimek, 1994). A slope of 0.58 fits with the typical value for flexible polymer chain expected for linear random coils in a good solvent (0.588) (Burchard, 1999).

$$R_h = \left(\frac{3[\eta]M_w}{10\pi} \right)^{1/3} \tag{6-2}$$

$$R_g = \left(\frac{[\eta]M_w}{6^{3/2}\Phi} \right)^{1/3} \tag{6-3}$$

where the Flory constant, Φ is 2.55×10^{23}, (Dorgan et al., 2005b; Miyaki et al., 1980) and by using $[\eta]$ with units of mL/g results R_g in cm.

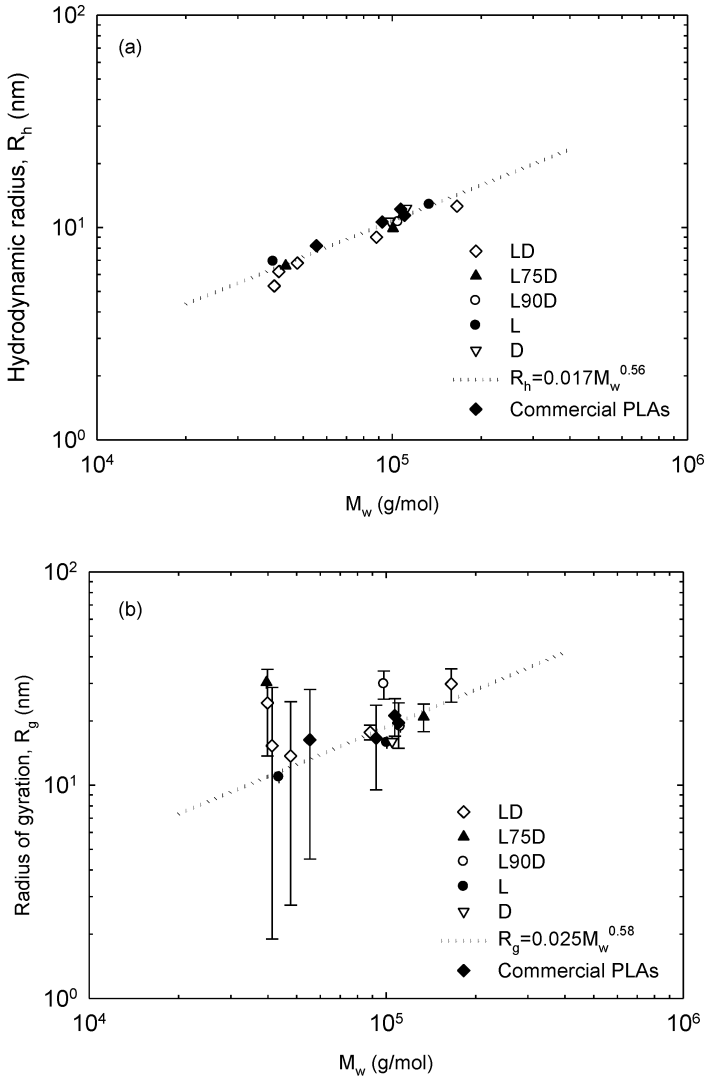

Figure 6.2: The characteristic radius of R_h (a) and R_g (b) as a function of molecular weight for homopolymers and commercial PLAs.

The ratio of R_g/R_h can be used to interpret molecular compactness (Kainthan et al., 2006). The calculated values ranged from 1.80-2.00 with an average of 1.90. A value of 1.78 and 2.05 are reported for random coil, linear chain monodisperse and polydisperse in good solvent respectively (Burchard, 1999). The values obtained here for PLAs solution in THF are close to that type of linear chain, consistent with our expectation. In addition, the Mark Houwink slope (Figure 6.1) has shown the existence of good-solvent conditions.

The solution properties ($[\eta]$, R_h and R_g) of the four commercial PLAs are also plotted in Figure 6.1 and Figure 6.2 as a function of the weight-average molecular weight in order to check the structure of these commercial PLAs. The good agreement of the solution data with those nearly monodisperse PLAs, show that these commercial polymers possess a linear structure.

6.2 Linear Viscoelastic Properties of PLA Homopolymers.

Dynamic time sweeps carried out at the temperature of 180°C, at the fixed frequency of 1 rad/s confirmed that the samples were sufficiently stabilized and did not degrade during the duration of a typical experiment. A representative result for sample LD100 is shown in Figure 6.3 (entry 14, Table 4.1). The consistency of complex modulus during the test (typically last up to 2000 s) indicated that sample degradation had not occurred during the testing time after addition of 0.35 wt% TNPP.

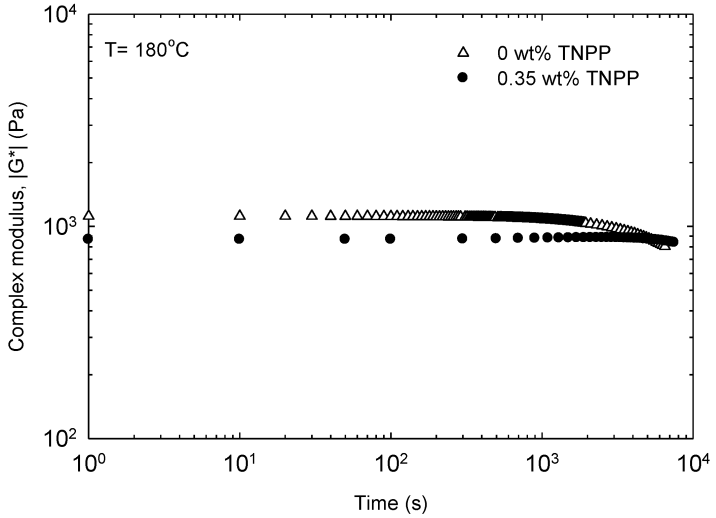

Figure 6.3: The thermal stability of LD100 at 180°C.

Figure 6.4 show the viscoelastic data of LD160 an amorphous sample measured at frequencies in the range from 0.01 to 100 rad/s, at temperatures from 70 to 170°C. Time-Temperature superposition was applied to the data in Figure 6.4 to produce a master curve at the reference temperature of 150°C.

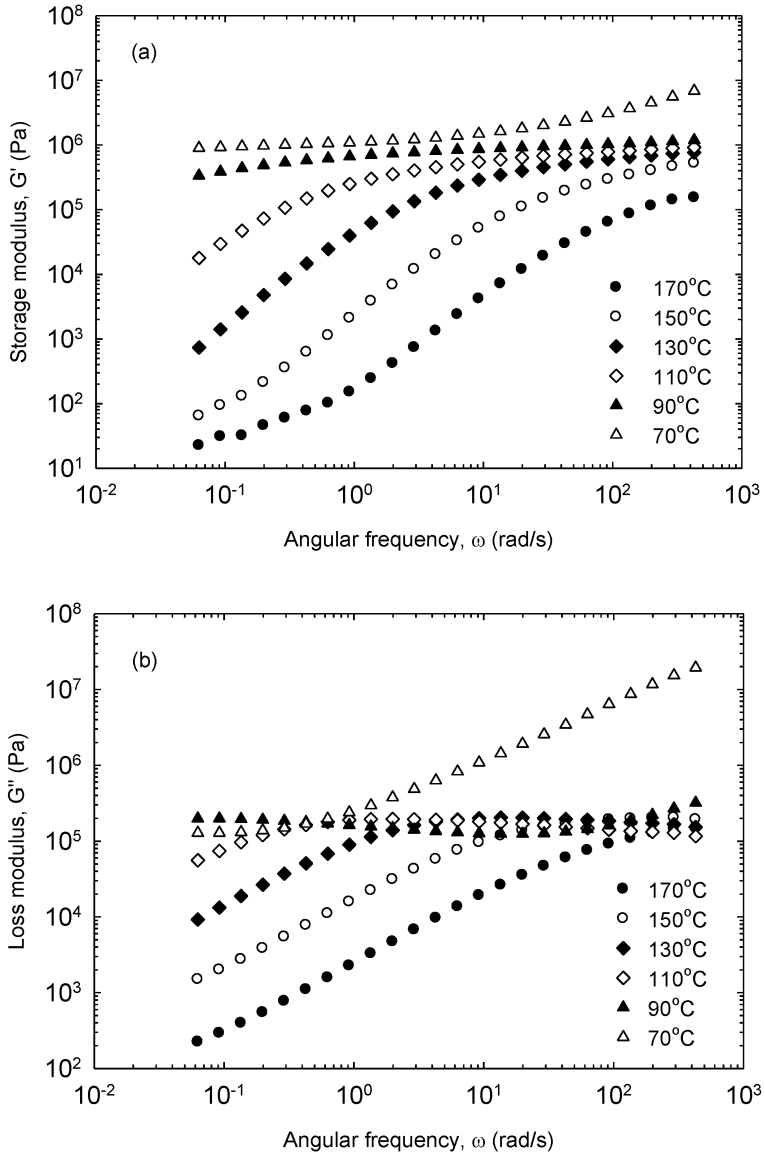

Figure 6.4: Dynamic moduli (a) storage modulus (b) loss modulus of LD160 at various temperatures.

Figure 6.5 and Figure 6.6 show the master curves of linear viscoelastic moduli, G' and G'' and complex viscosity $\left|\eta^*(\omega)\right|$ of amorphous and crystalline samples at the reference temperature of 150 and 180°C respectively. The time-Temperature superposition (for more

detail on this principle see section 2.5) was applied using RHEOPLUS software to obtain the master curves. The superposition of the data was excellent pointing to the thermorheological simplicity of these linear polymers. The terminal zone at small frequencies was reached with the characteristics slopes of 2 and 1 according to the scaling relationships $G' \propto \omega^2$ and $G'' \propto \omega$. Master curves of viscoelastic properties (G', G'' and $|\eta^*(\omega)|$) of all homopolymers studied in this work can be found in Appendix A.

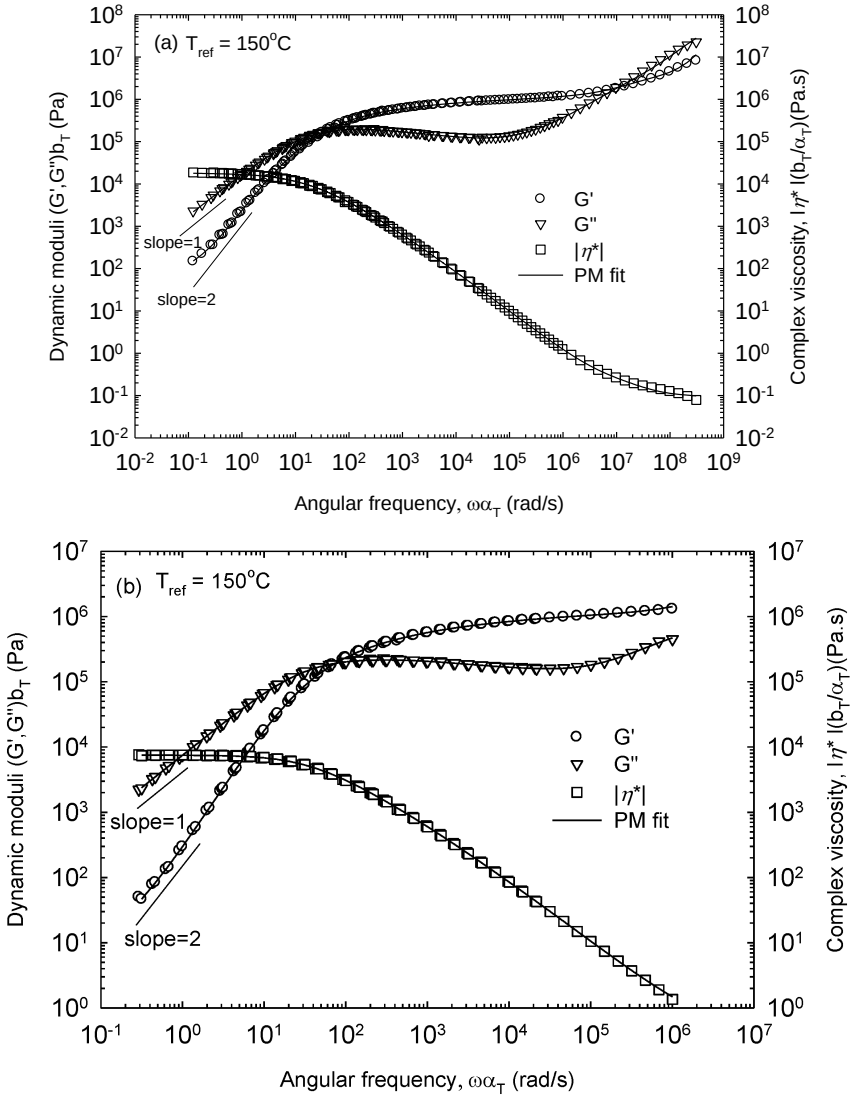

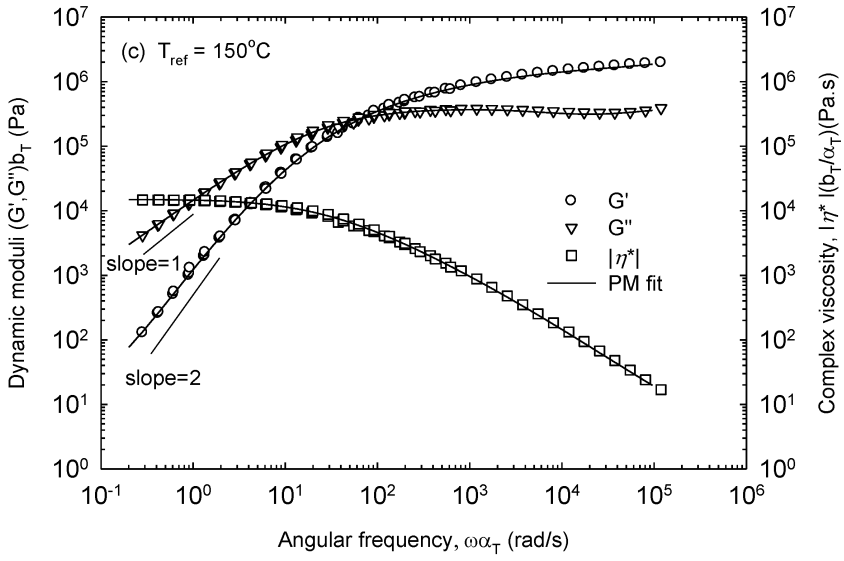

Figure 6.5: Master curves of the linear viscoelastic moduli, G' and G'' and complex viscosity $\left|\eta^*(\omega)\right|$ of amorphous PLAs (a) LD160 (b) L75D100 and (c) L90D100 at the reference temperature of 150°C.

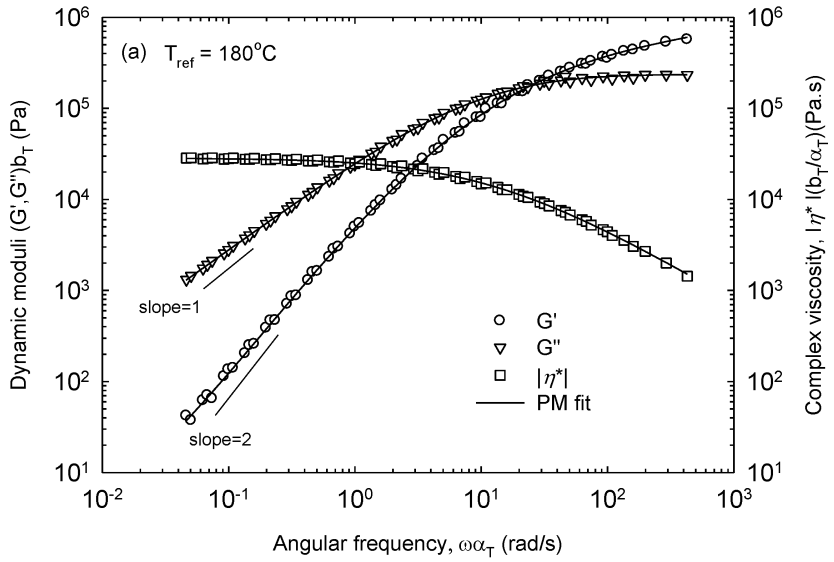

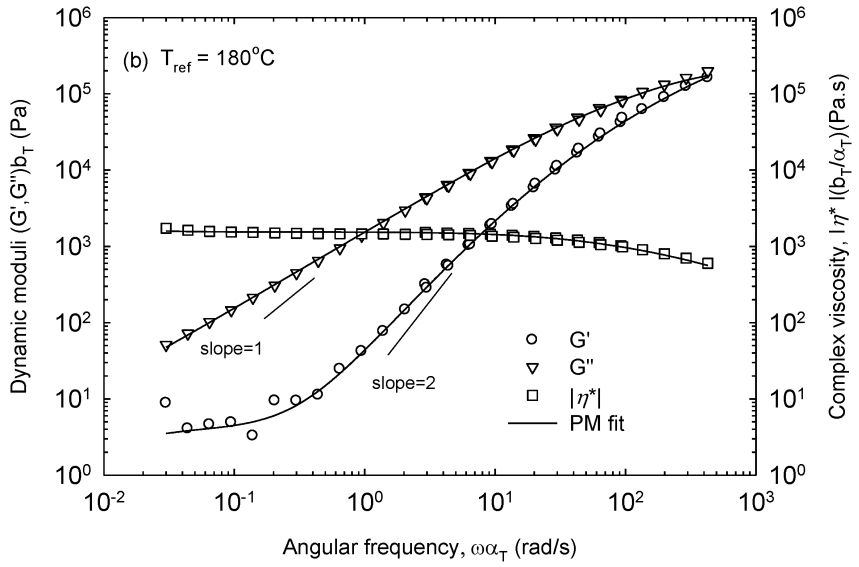

Figure 6.6: Master curves of the linear viscoelastic moduli, G' and G'' and complex viscosity $\left|\eta^*(\omega)\right|$ of crystalline PLAs (a) L240 (b) D120 at the reference temperature of 180°C.

Figure 6.6 show that the range of frequencies over which the linear viscoelastic data could be determined for crystalline samples is narrow as compared to the range of master curves of amorphous PLAs (Figure 6.5).

Vertical, b_T and horizontal α_T shift factors were applied. Typical values of b_T were in the range of 0.98-1.03, which is close to 1 (typically found for other linear polymers) (Cooper-White and Mackay, 1999). Figure 6.7 shows that the horizontal shift factors α_T for all PLAs follow the Arrhenius equation:

$$\alpha_T = \exp\{E_a / R(1/T - 1/T_{ref})\} \qquad (6\text{-}4)$$

where E_a is the activation energy for flow, R is the universal constant of the ideal gas law and T_{ref} is the reference temperature. The activation energy of flow is molecular weight independent. Single straight line fitting of the data results in an average activation energy of 177.65 kJ/mol. However, it has been reported that α_T of amorphous PLA can be described by the Williams-Landel-Ferry (WLF) equation, with average WLF parameters of C_1=3.24 K^{-1} and C_2= 164.9 K at a reference temperature of 180°C (Dorgan et al., 2005a), which is in agreements with data presented in chapter 7.

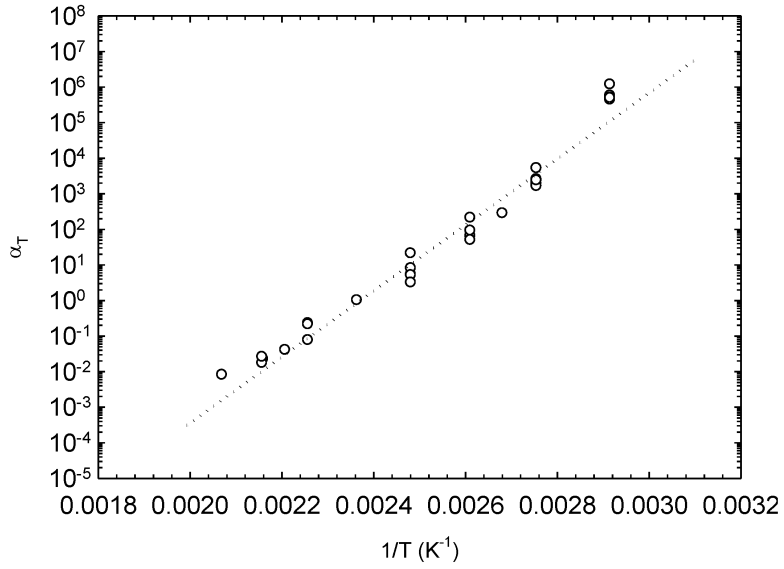

Figure 6.7: The horizontal shift factors, α_T for PLAs at the reference temperature of 150°C. The dotted line represents single fitting of the data.

Figure 6.8a plots the storage modulus, G', of selected PLAs with the same composition (L:D:50:50) and different molecular weight. Figure 6.8b plots the corresponding loss modulus, G'', for this series of polymers. With an increase in molecular weight, the plateau in the storage modulus (Figure 6.8a) becomes more well defined, followed by a transition to the terminal zone which shifts to lower frequencies. At high frequency, the G' and G'' become independent of molecular weight as short segment relaxation plays the dominant role. These observations are typical for linear monodisperse polymer (Jackson et al., 1994; Kainthan et al., 2006).

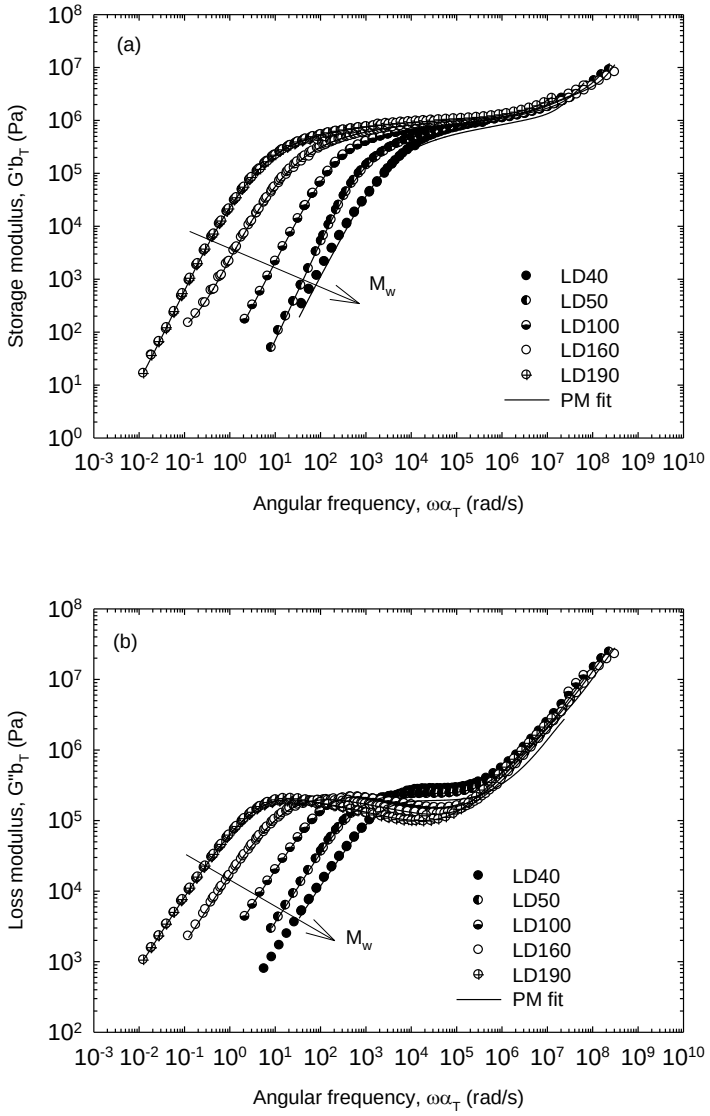

Figure 6.8: (a) The storage modulus of LD samples (b) the loss modulus of LD samples at 150°C.

Figure 6.9 shows the complex viscosity of LD samples at the reference temperature of 150°C. It shows that the terminal zone has been reached and the zero-shear viscosity can be obtained directly. The zero-shear viscosities can also be determined from the fitted relaxation spectrum to the experimental data shown by solid lines in Figure 6.9 (see below for relevant discussion). Figure 6.10 depicts the zero-shear viscosity as a function of the molecular weight for samples listed in Table 4.1. The relationship between the zero-shear viscosity and molecular weight can be described by:

$$\log(\eta_o) = -13.2 + 3.4\log(M_w) \tag{6-5}$$

at the reference temperature of 150°C. The validity of the power of 3.4 for well entangled linear polymers has also been reported by Dorgan et al. (2005a) in their comprehensive study of a wide range of PLAs with different L:D compositions and molecular weights. Good agreement is obtained when the present zero-shear viscosity data are shifted to 180°C using the shift factors reported in Figure 6.7 and compared with the correlation reported by Dorgan et al. (2005a) (Figure 6.10b).

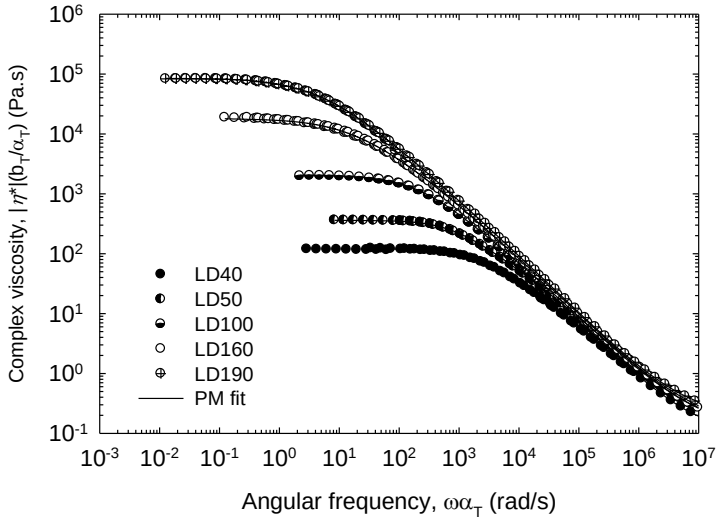

Figure 6.9: The complex viscosity of LD samples at 150°C.

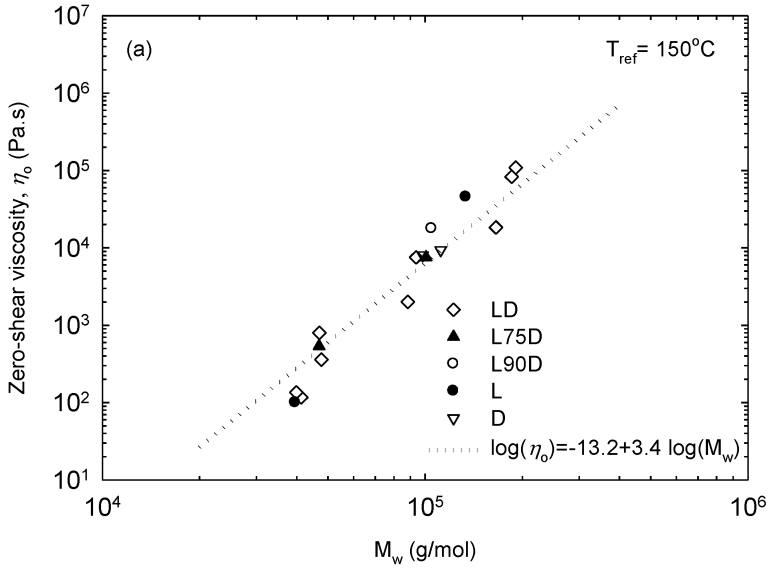

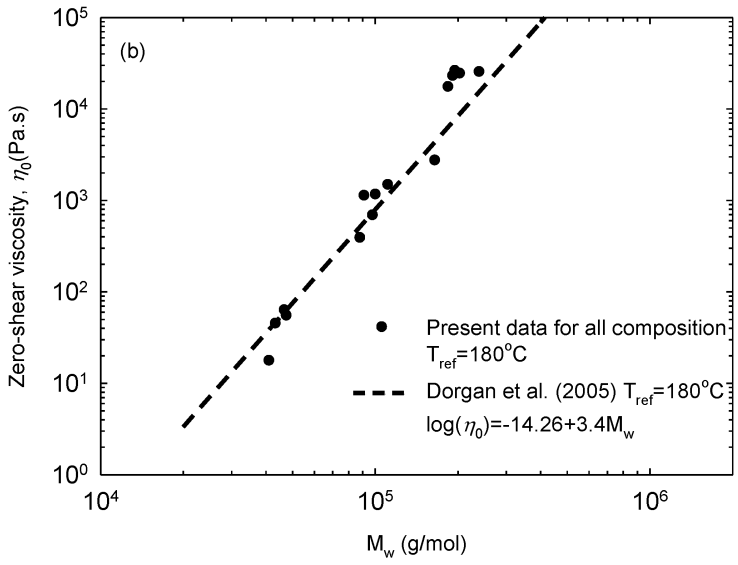

Figure 6.10: The scaling between the zero shear viscosity and M_w of PLAs at the reference temperature of (a) 150°C (b) 180°C.

The plateau modulus, G_N^o is 0.9 MPa ± 0.2 obtained from Van Gurp-Palmen plot (Figure 6.11) (Trinkle and Friedrich, 2001). The minimum in the plot of phase angle versus complex modulus correspond to the G_N^o. One minimum can be seen from Figure 6.11 which agrees with characteristic curvature for narrow distributed amorphous polymers such as poly(styrene) and poly(methymethacylate) (Trinkle and Frienrich, 2001; Fuchs et al., 1996). This value falls within the range reported by Dorgan et al. (2005a) of 1.0 MPa ± 0.2 for all L:D compositions. The molecular weight between entanglements, M_e, can be calculated from the plateau modulus utilizing Equation 6-6:

$$M_e = \frac{\rho_o RT}{G_N^o} \tag{6-6}$$

where ρ_o is melt density (g/cm^3) at the chosen reference temperature. Using the relationship for the PLA density, (T in °C), reported by Witzke (1997):

$$\rho(T) = 1.2836 \exp[-7.7(10^{-4})T] \tag{6-7}$$

the M_e of PLAs is be about 4,400 g/mol at 150°C.

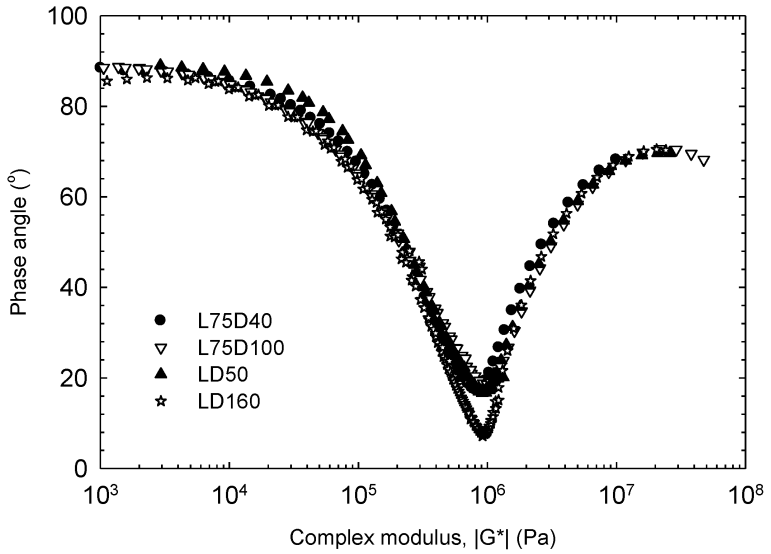

Figure 6.11: Van Gurp-Palmen plots of samples LD and L75D with different molecular weight to obtain G_N^o .

6.3 Relaxation Spectrum of PLAs

The continuous lines in Figure 6.5, 6.6, 6.8 and 6.9 represent the fitting of the parsimonious relaxation spectrum (PM) (g_i, λ_i) calculated from Equations 6-8 and 6-9:

$$G'(\omega) = \sum_{i=1}^{N} g_i \frac{(\omega\lambda_i)^2}{1+(\omega\lambda_i)^2} \tag{6-8}$$

$$G''(\omega) = \sum_{i=1}^{N} g_i \frac{\omega\lambda_i}{1+(\omega\lambda_i)^2} \tag{6-9}$$

where ω is the frequency of oscillation, (g_i, λ_i) are the generalized Maxwell model parameters, relaxation moduli and relaxation times, respectively, and N is the number of relaxation modes. The parameters were determined using a nonlinear optimization program, which follows the algorithm of Baumgaertel and Winter (1989). The input data are the experimental results from the frequency sweeps, and the output gives the (g_i, λ_i). The values for LD160 at different temperatures are listed in Table 6.1, needed for subsequent calculations.

Figure 6.12 plots the PM relaxation spectrum (5 modes) along with the Baumgaertel-Schausberger-Winter (BSW) continuous relaxation spectrum for LD160 given by Equation

6-10. It has been confirmed by Baumgaertel et al. (1990) and Hatzikiriakos et al. (2000) that BSW have shown an excellent agreement with the PM spectrum for linear and star polybutadiene polymers. This allows for an accurate representation of the linear viscoelastic relaxation with the smallest number of parameters as follows:

$$H(\lambda) = n_e G_N^o \left[\left(\frac{\lambda}{\lambda_c} \right)^{-n_g} + \left(\frac{\lambda}{\lambda_{\max}} \right)^{n_e} \right] \qquad (6\text{-}10)$$

where λ_{max} is the longest relaxation time, n_e and n_g are the slopes of the spectrum in the entanglement and glass transition zones respectively, and λ_c is the crossover time to the glass transition (Jackson et al., 1994). The values of the parameters for LD160 calculated from the fitting procedure (Equations 6-8 and 6-9) are shown in Figure 6.12.

Table 6.1: Generalized Maxwell model parameters (g_i, λ_i) for sample LD160 at different temperatures.

150 °C		***130°C***		***110 °C***		***90°C***	
g_i	λ_i	g_i	λ_i	g_i	λ_i	g_i	λ_i
2.46×10^{5}	1.72×10^{-2}	2.55×10^{5}	4.25×10^{-2}	2.11×10^{5}	4.72×10^{-2}	1.48×10^{5}	6.88×10^{-2}
2.48×10^{5}	2.98×10^{-3}	2.27×10^{5}	6.23×10^{-3}	1.77×10^{5}	6.07×10^{-3}	1.84×10^{5}	6.66×10^{-3}
1.04×10^{5}	8.27×10^{-2}	2.43×10^{5}	2.40×10^{-1}	2.52×10^{5}	3.26×10^{-1}	1.91×10^{5}	5.57×10^{-1}
7.77×10^{3}	4.97×10^{-1}	5.22×10^{4}	1.09×10^{0}	2.36×10^{5}	1.94×10^{0}	2.49×10^{5}	4.13×10^{0}
1.42×10^{2}	1.83×10^{1}	2.97×10^{3}	6.46×10^{0}	5.05×10^{4}	9.78×10^{0}	3.85×10^{5}	3.87×10^{1}

The continuous relaxation spectra for LD samples with various molecular weights are shown in Figure 6.13. At short times, the spectra are nearly identical, resulting in the same slope. Similar trends have been reported for monodisperse polystyrenes and polybutadienes (Jackson et al., 1994). The longest relaxation time was taken from the intersection of entanglement power law on the x axis as shown in Figure 6.12. This scales with molecular weight as shown below. The slopes of n_e and n_g are independent of molecular weight (see Figure 6.13) and L:D composition.

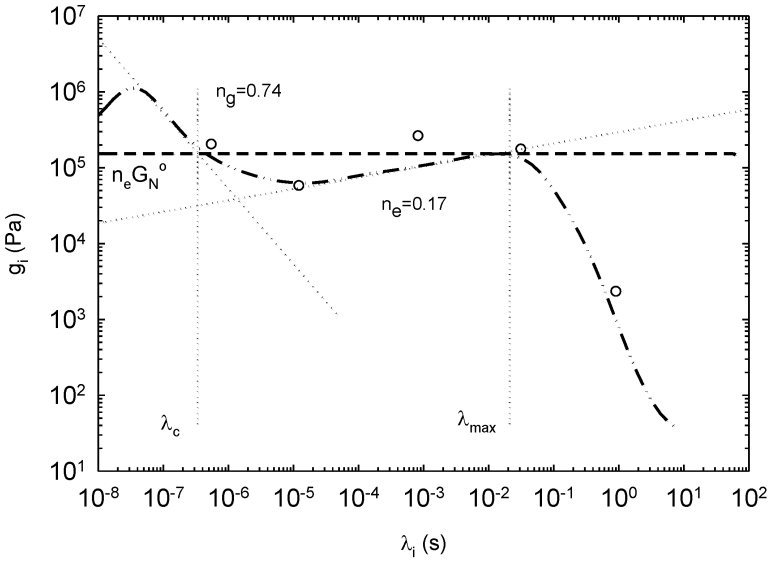

Figure 6.12: The PM along with the relaxation spectrum of LD160 at 150°C.

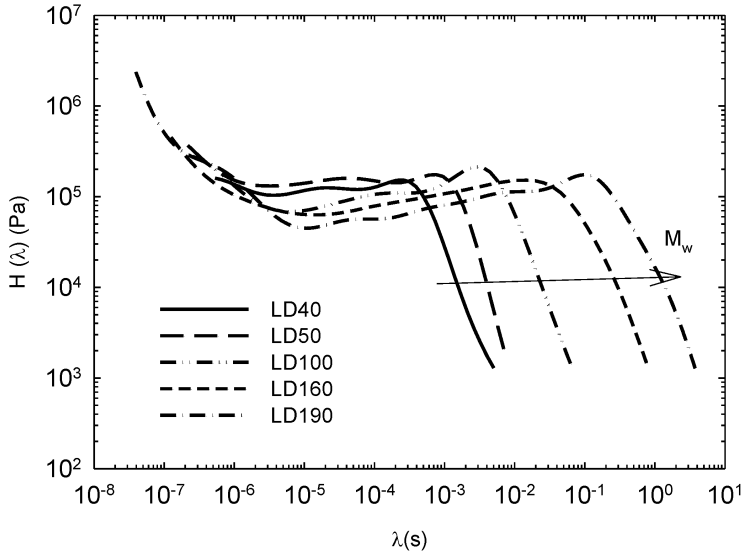

Figure 6.13: The continuous relaxation spectra for LD samples at 150°C plotted with various M_w.

Figure 6.14 depicts the molecular weight dependence of the longest relaxation time for all compositions at 150°C. The slope of the relaxation time versus M_w, is approximately equal to the slope found from the zero-shear viscosity versus M_w, curve. These observations are in agreement with previously reported results for the relaxation spectrum of linear polymers (Baumgaertel et al., 1990).

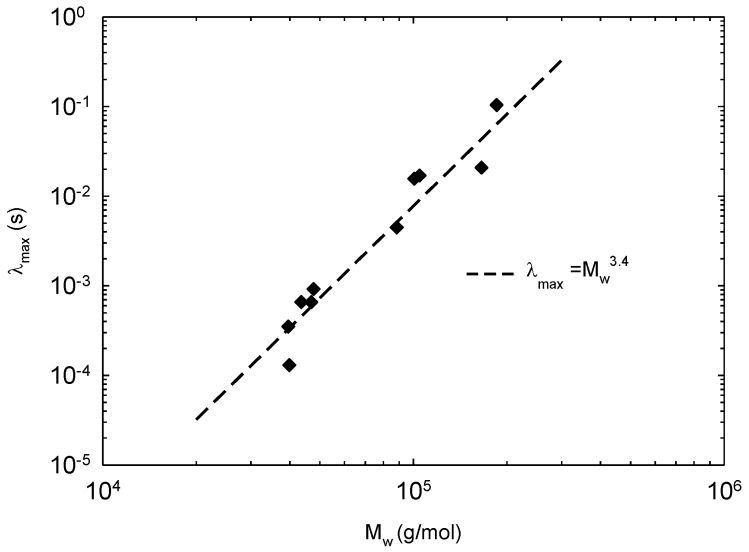

Figure 6.14: The scaling between longest relaxation time and molecular weight of PLAs.

6.4 Extensional Rheology

Figure 6.15a, b and c plot the tensile stress growth coefficient of PLA LD160 in steady uniaxial extension, at several extensional Hencky strain rates measured at 90, 110 and 130°C respectively. The dashed lines represent the linear viscoelastic envelope (LVE) $3\eta^+(t)$, where $\eta^+(t)$ is the shear stress growth coefficient obtained in linear viscoelasticity by a number of different ways. In the present case the coefficient $\eta^+(t)$ was calculated from the parsimonious relaxation spectrum (g_i, λ_i) fitted to linear viscoelastic moduli (G' and G'') using the following expression:

$$\eta^+(t)=\sum_{i=1}^{N}\frac{g_i}{\lambda_i}\left[1-e^{-t/\lambda_i}\right] \qquad (6\text{-}11)$$

At the lowest Hencky strain rate of 0.01 s^{-1} and short time, the extensional data is superposed well with the LVE indicating the consistency between the two sets of experimental data, namely shear and extensional. However, at the higher values of the Hencky strain rate of 1 s^{-1} and 10 s^{-1}, a clear strain hardening effect can be observed (see Figure 6.15a and b) *i.e.* at the longer times the tensile stress growth coefficient clearly deviates from the linear viscoelastic behavior. This strain hardening at high Hencky strain

rate becomes less pronounced or completely disappears with increasing temperature (see Figure 6.15c).

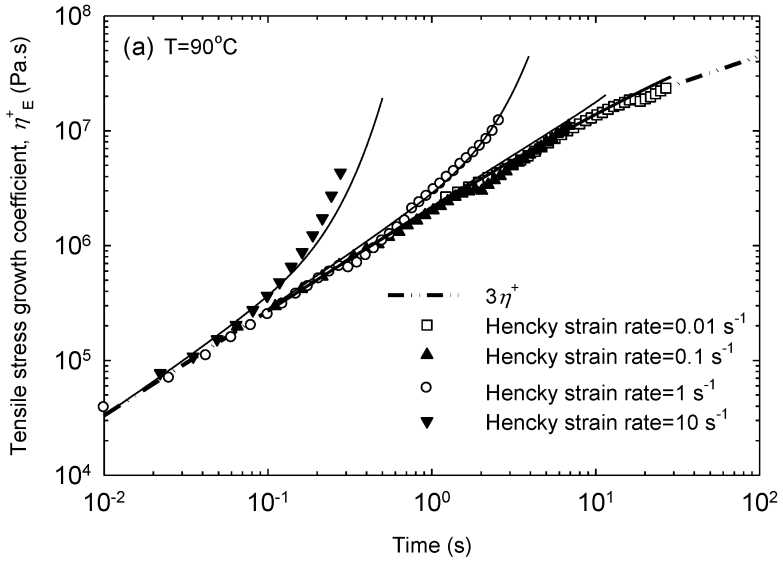

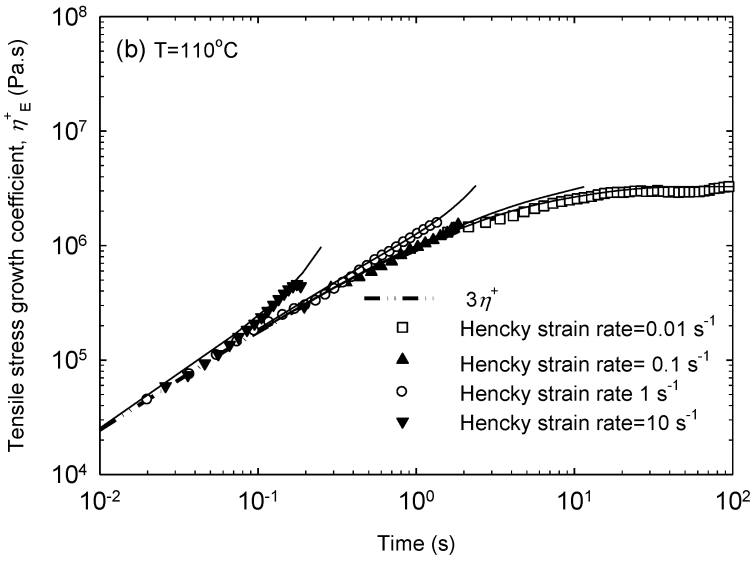

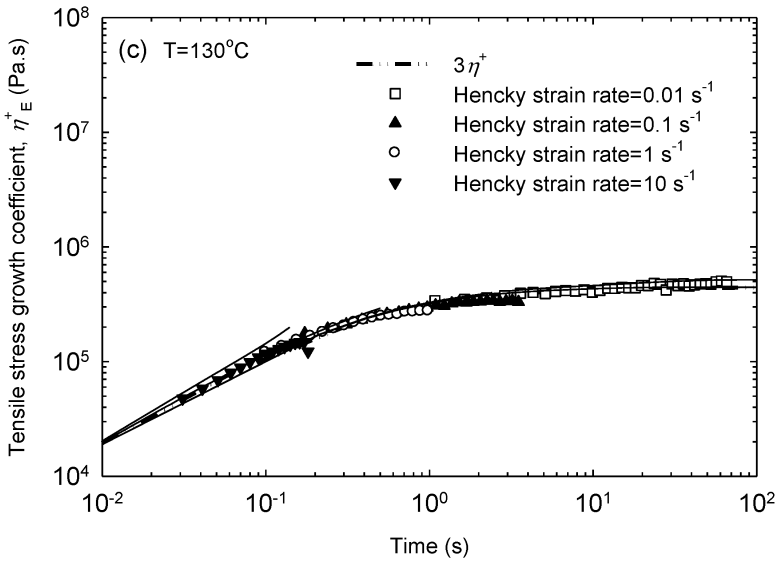

Figure 6.15: Tensile stress growth coefficient as a function of time measured at various Hencky strain rates for LD160 at (a) 90°C, (b) 110°C and (c) 130°C.

Strain hardening for linear PLA polymers has been observed and reported by others (Palade et al., 2001; Yamane et al., 2004). In their study of uniaxial extensional behavior of PLLA, Palade et al. (2001) have observed a strain hardening at a Hencky strain rate of 0.1 s^{-1} measured at the temperature of 180°C. Moreover, Yamane et al. (2004) observed a strain hardening in biaxial extensional flow at extensional rate of 0.1 to 0.006 s^{-1} for PLLA and PLLA\PDLA blends at 190°C. Such PLAs (100% L or 100% D homopolymers) are readily crystallizable and since the temperature used was well above the T_m, the hardening effect was solely attributed to the dynamics of the polymers. Similar observations have been noted by Stamboulides and Hatzikiriakos (2006) and van Ruymbeke et al. (2010) for linear commercial poly(methyl methacrylate) and dendritic poly(methyl methacrylate) respectively. It has been reported that the strain hardening for these polymers was due to wide polydispersity and presence of branching respectively.

In the present study, differential scanning calorimeter (DSC) and X-ray diffraction (XRD) were used to understand the strain hardening behavior that occurred at relatively low temperatures, in other words to examine if the strain hardening observed was due to stress induced crystallization or stretching induced orientation of chains. These tests were performed on un-stretched and stretched samples that were quickly quenched in order to freeze any crystallinity formed during stretching. No evidence of crystallinity or other

supermolecular structure was detected in our samples by DSC and XRD studies. This could be attributed to very low crystallinity, since it been reported that at high strain rates the onset of crystallization is delayed (Zhang et al., 2011). Mahendrasingam and co-workers (2000) found that the crystallization of polymers at different strain rates starts at different stages during the extension process (Blundell et al., 2000; Mahendrasingam et al., 2000; Mahendrasingam et al., 2003; Mahendrasingam et al., 2005). The fast strain rate may delay the onset of crystallization of deformed PLA. In particular, studies of poly(ethylene terephthalate) showed that when the deformation rate was faster than the chain retraction relaxation mechanism, the onset of crystallization was delayed until the end of the deformation (Blundell et al., 2000; Mahendrasingam et al., 2003). Therefore, it can be concluded that the strain hardening effect observed in the present study is solely due to the dynamics of the polymers.

It has been reported in the literature that independent of molecular architecture, strain hardening behavior can be observed when the rate of the deformation exceeds the rate of molecular relaxation (Kasehagen and Macosko, 1998). At the high strain rates, the chain deformation rate is faster than that of chain reptation, which promotes the chain orientation. When the chain orientation reaches the critical value where crystals can be formed, the crystallization of polymers happens, and proceeds faster than chain relaxation can occur (Mahendrasingam et al., 2005). In other words, strain hardening always occurs when the characteristic time for molecular relaxation (longest relaxation time) is longer than the characteristic time of the deformation (inverse of Hencky strain rate).

The longest relaxation times obtained from Figure 6.12 for LD160 for the three temperatures are listed in Table 6.2. The strain hardening effect observed in this study occurs when the longest relaxation time is larger than the deformation time applied. For example at 130°C, the longest relaxation time (0.065 s) is smaller than the characteristic times (0.1 to 100 s) of Hencky strain rates from 0.01 to 10 s^{-1} and therefore strain hardening effects are not present. At high temperatures chain mobility increases leading to chain relaxation and results in a lower degree of segment orientation for a given draw ratio.

On the other hand at 90°C, the longest relaxation time is 7.63 s, which is larger than most of the characteristic times of the deformation 1 and 0.1 s for the Hencky strains of 1 and 10 s^{-1} and therefore strain hardening are obtained. This was the case for the great majority of

the available experimental data obtained for other PLAs studied here (see Appendix B). In all these cases strain hardening has been observed at relatively low temperatures and this disappears gradually as the temperature increases.

Table 6.2: The longest relaxation times for LD160 at various temperatures.

Temperature (°C)	Longest relaxation time (s)
90	7.63
110	0.98
130	0.065

6.5 Constitutive Equation Modeling

In an effort to understand the origin of the strain hardening behavior from the molecular point of view, a macro-molecular K-BKZ (Kaye-Bernstein, Kearsley and Zapas) constitutive model is used. The K-BKZ constitutive model can be written as:

$$\boldsymbol{\sigma} = \int_{-\infty}^{t} m(t-t')\, h(I_1, II_2)\, \mathbf{B}(t,t')\, dt' \tag{6-12}$$

where, $\boldsymbol{\sigma}$ is the stress tensor, $\mathbf{B}(t-t')$ is the Finger strain tensor, which represents the material strain history, $m(t-t')$ is the memory function and $h(I_1, II_2)$ is the damping function which in the general case can be expressed in terms of the first and second invariant of the Finger strain tensor. This constitutive equation has been found to accurately fit both shear and extensional data of molten polymers (Dealy and Wissbrun, 1999; Kasehagen and Macosko, 1998; Papanastasiou et al., 1983).

The memory function in Equation 6-12 may be expressed as a summation of the exponentials obtained from the relaxation spectrum determined by fitting the linear viscoelastic moduli by means of Equations 6-8 and 6-9:

$$m(t-t') = \frac{dG(t-t')}{dt'} = \sum_i \frac{g_i}{\lambda_i} \exp\left(-\frac{(t-t')}{\lambda_i}\right) \tag{6-13}$$

where *G(t-t')* is the stress relaxation modulus determined from linear viscoelasticity where g_i and λ_i are the relaxation strengths and times respectively.

The damping function $h(\gamma)$ was determined experimentally by step strain relaxation tests using the MCR 501 rheometer equipped with the cone-and-plate geometry having a plate diameter of 25 mm and a cone angel of 4°. Five different shear strain values were used in the step strain tests at the temperature of 150°C since at lower temperatures wall slip limits the accuracy of measurement. The stress relaxation results are plotted in Figure 6.16, along with the linear viscoelastic modulus, *G(t),* calculated from the linear viscoelastic moduli using the PM relaxation spectrum listed in Table 6.1. It is noted that the PM relaxation spectrum curve calculated from Equation 6-14 matches the data for γ=0.05, indicating that this strain can be used as the limit of linear viscoelasticity.

$$G(t) = \sum_i g_i \exp\left(-\frac{(t)}{\lambda_i}\right) \tag{6-14}$$

The stress relaxation curves plotted in Figure 6.16, were vertically shifted, $G(t,\gamma)/h(\gamma)$, for strain values γ>0.05 to determine the shift factors ($h(\gamma)$) that best superpose the relaxation moduli data (Dealy and Wissbrun, 1999). The shift factors for the damping function are plotted in Figure 6.17. The $h(\gamma)$ values agree well with the functional form proposed by Papanastasiou et al. (1983) with α=3.66 suggested by the Doi and Edwards (1986). The same damping function and alpha value was used by Palade et al. (2001) in their study to predict the non-linear viscoelastic behavior of molten PLAs.

$$h(\gamma) = \frac{G(\gamma,t)}{G(t)} = \frac{\alpha}{\alpha+\gamma^2} \tag{6-15}$$

It is noted that the damping function $h(I_1, II_2)$ in Equation 6-12 reduces to Equation 6-15 once the forms of I_1 and II_2 for simple shear flow are replaced.

For start-up of steady shear, Equation 6-12 with Equation 6-15 can be written as:

$$\eta^+(t) = tG(t)\left(\frac{\alpha}{\alpha+(\dot{\gamma}t)^2}\right) + \int_0^t sm(s)\left(\frac{\alpha}{\alpha+(\dot{\gamma}s)^2}\right)ds \tag{6-16}$$

Figure 6.18 depicts the comparison between prediction of Equation 6-16 shown by lines and experimental data for LD160 at 150°C. The K-BKZ constitutive model predicts the start-up of steady shear viscosities considerably well. This has been reported previously by Palade et al. (2001) for PLLA at 180°C.

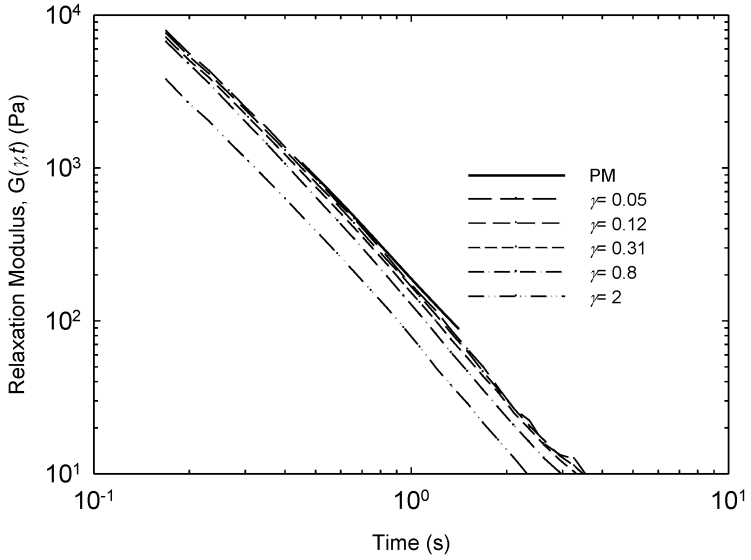

Figure 6.16: Step-strain relaxation tests performed at different strain values for LD160 at 150°C.

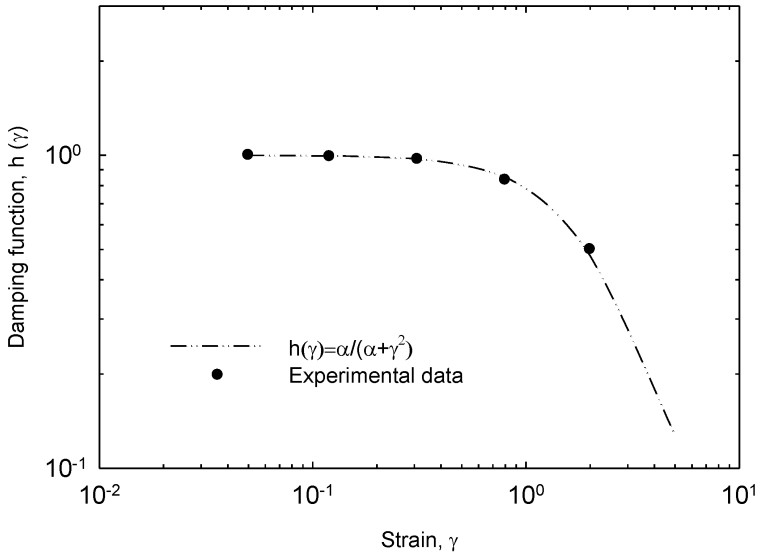

Figure 6.17: The damping functions of LD160 at 150°C.

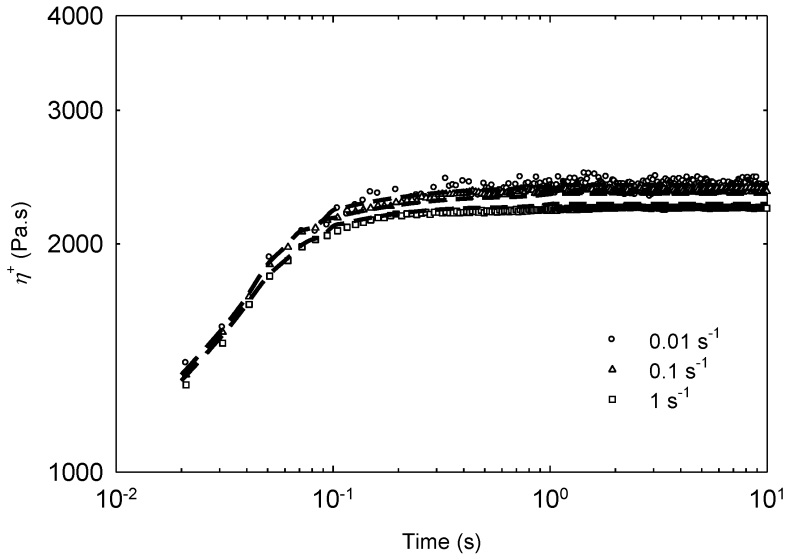

Figure 6.18: The shear stress growth coefficient of LD160 for various shear rates at 150°C. The lines represent the K-BKZ constitutive model predictions.

The theoretical predictions for the extensional viscosity are based on Equation 6-17 which from Equation 6-12 with Equation 6-15 for uniaxial extension. These (predictions) are plotted in Figure 6.15a, b and c as solid lines, indicating an excellent agreement with the extensional rheological data.

$$\eta_E^+(t) = \frac{\alpha}{\dot{\varepsilon}}\left[\frac{\left(e^{2\dot{\varepsilon}t} - e^{-\dot{\varepsilon}t}\right)G(t)}{(\alpha-3)+\left(2e^{\dot{\varepsilon}t} - e^{-2\dot{\varepsilon}t}\right)} + \int_0^t \frac{\left(e^{2\dot{\varepsilon}s} - e^{-\dot{\varepsilon}s}\right)m(s)}{(\alpha-3)+\left(2e^{\dot{\varepsilon}s} - e^{-2\dot{\varepsilon}s}\right)}ds\right] \qquad (6\text{-}17)$$

The predicted strain hardening behavior by the K-BKZ equation disappears when the longest relaxation time becomes lower than the deformation time at increasing temperature. This clarified the strain hardening behavior, which can be observed in linear polymers when the rate of chain relaxation is slower than the rate of deformation. Similar results were obtained for other PLAs as shown in Appendix B. The K-BKZ constitutive model predicts the transient extensional viscosities of PLAs very well.

6.6 Summary

The solution and melt rheological properties of PLA have been investigated for different optical compositions and molecular weights. Values of the Mark Houwink parameters and

characteristic radii agreed well with values reported for other PLAs as well as other linear flexible polymers. The time-Temperature superposition applies well on the linear viscoelastic data of stabilized PLAs indicating that PLAs are themorheologically simple fluids. On melt rheology, the plateau modulus of PLAs is 0.9 MPa ± 0.2, which is independent of molecular weight and optical compositions. The PLA melts have a molecular weight between entanglements of approximately 4,400 g/mol that was determined from their plateau modulus. The zero-shear viscosity, as well as the longest relaxation time of PLAs have shown a scaling of $\eta_o \propto M_w^{3.4}$, $\lambda_{\max} \propto M_w^{3.4}$ with the exponent of 3.4 to be consistent with those reported for other well-entangled linear macromolecular.

Furthermore, it was demonstrated that strain hardening can be obtained for these linear polymers where the longest relaxation time is larger than the characteristic time of deformation. Significant strain hardening is observed at low temperatures, which gradually disappears with increase in temperature and decrease of Hencky strain rate. The K-BKZ constitutive equation was successfully used to predict the strain hardening behavior of PLAs and that such behavior (strain hardening) was due solely to the dynamic of molecular relaxation.

7 Rheology and Mechanical Properties of Block Copolymers and Homopolymer Blends

In this chapter, the solution and melt rheological properties of newly synthesized nearly monodisperse diblock and triblock copolymers of PLLA and PDLLA with different block length ratios are examined. Corresponding PLLA\PDLLA blends with the same molecular weight and L-/ DL-LA content as the diblock copolymers were also prepared to compare the effects of diblock form and examine the effects of blending ratio. Furthermore, the mechanical properties of the diblock copolymers and their equivalent blends are also compared. In addition, nearly monodisperse PLLA-*b*-PDLA diblock copolymers, that expected to have superior mechanical properties as their blends (Fukushima and Kimura, 2006; Sarasua et al., 2005; Tsuji and Ikada, 1999), were also synthesized and compared with blends and diblock copolymers of L-LA and DL-LA. Finally, the rheological and mechanical properties of triblock copolymers with amorphous middle block, PLLA-*b*-PDLLA-*b*-PDLA and PLLA-*b*-aPHB-*b*-PDLA are also examined.

7.1 Solution Properties

Figure 7.1 plots the intrinsic viscosities, $[\eta]$ of copolymers PLLA-*b*-PDLLA and PLLA-*b*-PDLLA-*b*-PLLA as well as those reported previously by Othman et al. (2011) as a function of the weight-average molecular weight (M_w). The data agree well with nearly monodisperse PLAs reported previously and the linearity in this plot implies linear random coils. The slope of the linear regression line (exponent of the Mark Houwink equation) is 0.75, which agrees with the values reported in literature for PLA and linear polymers in a good solvent, which is 0.736 ± 0.023 (Dorgan et al., 2005b; Othman et al., 2011).

Figure 7.2a and 7.2b depict the dependence of hydrodynamic radius (R_h) and radius of gyration (R_g) on the M_w respectively. The agreement with data reported by Othman et al. (2011) for nearly monodisperse PLA homopolymers is excellent. The scaling relation between R_h and M_w can be described by:

$$R_h = 0.017 M_w^{0.56} \qquad (7\text{-}1)$$

The data for R_g show significant scatter; however, the exponent value is in good agreement with the value calculated from the molar mass dependence of the intrinsic viscosity using the Flory-Fox Equation. The scaling of R_g with M_w is:

$$R_g \propto M_w^{0.58} \tag{7-2}$$

which is in agreement with the exponent of 0.588 typical reported value for flexible polymer chain expected for linear random coils in a good solvent (Dorgan et al., 2005b). The good agreement of the solution data with those reported previously on nearly monodisperse PLAs (Othman et al., 2011), show that these diblock and triblock copolymers possess a linear molecular structure.

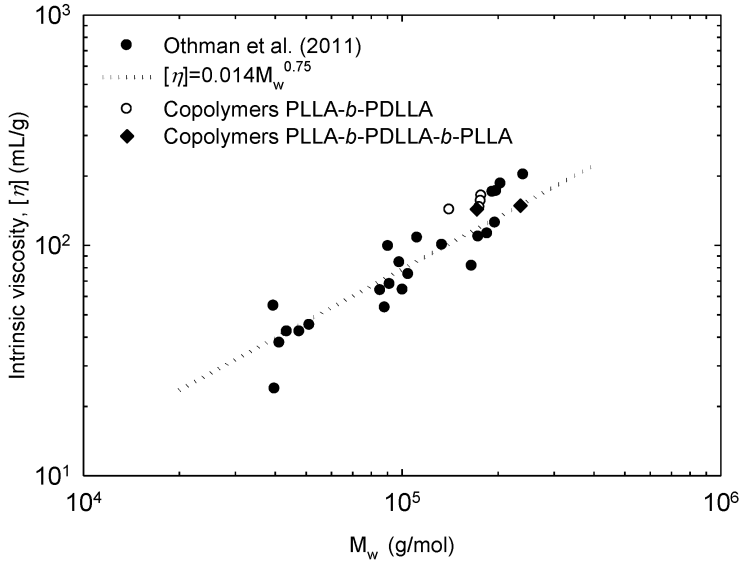

Figure 7.1: The intrinsic viscosities of homopolymers, PLLA-*b*-PDLLA and PLLA-*b*-PDLLA-*b*-PLLA block copolymers versus molecular weight at 25°C. The slope of the straight line is 0.75 (Mark Houwink slope) implying good solvent conditions.

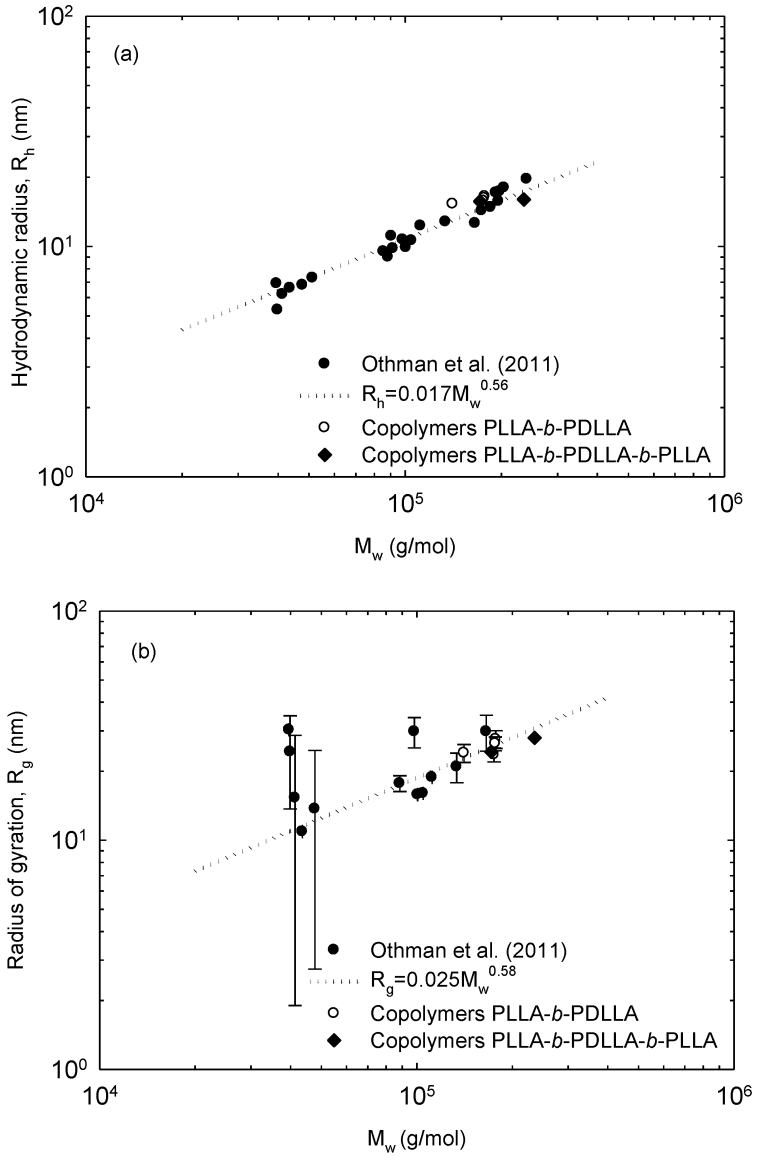

Figure 7.2: The characteristic radii of (a) R_h and (b) R_g of homopolymers, PLLA-*b*-PDLLA and PLLA-*b*-PDLLA-*b*-PLLA block copolymers as functions of molecular weight.

7.2 Linear Viscoelasticity

7.2.1 Homopolymers and blends

Figure 7.3 shows the complex viscosities of a set of PLA blends with different composition ratio at the reference temperature of 180°C. The two basic components were the crystalline PLLA of molecular weight equal to 240 kg/mol and the amorphous PDLLA of molecular weight equal to 90 kg/mol. It is clearly shown that the terminal zone has been reached as the

zero-shear viscosities can be deduced directly from the experimental data. The zero-shear viscosity decreased with increasing the PDLLA content, which possess the smaller molecular weight of the two PLAs in the blends. As was discussed in section 5.2.1, these blends are miscible in the molten state.

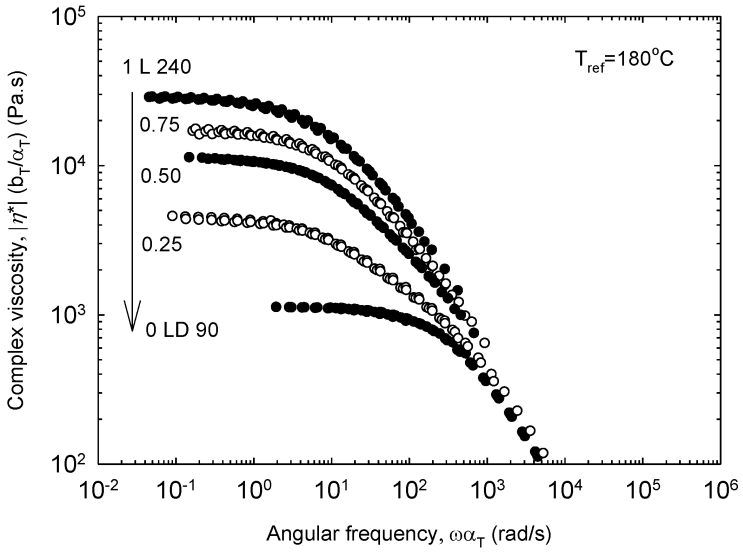

Figure 7.3: The complex viscosity of L240 and LD90 and their blends at 180°C.

Figure 7.4 plots the zero-shear viscosities of the blends of Figure 7.3 as a function of the weight fraction of LD90. The zero-shear viscosities of the blends calculated from the log-additivity and the Tsenoglou mixing rules (Tsenoglou, 1988) are also plotted in Figure 7.4. The data shows a positive deviation from the log-additivity and can be described by the Tsenoglou mixing rule reasonably well. The clear positive deviation from the log-additivity rule indicates miscible blends. Due to specific polymer-polymer interactions, in homogenous blends the zero-shear viscosity of the blends is expected to be higher than that predicted from the log-average viscosity of the neat resins (Utracki, 1986). Therefore, these blends of polymers of different molecular weights are miscible down to molecular level. Similar complex viscosity were obtained for other blends that have similar molecular weight, shown in Figure 7.5.

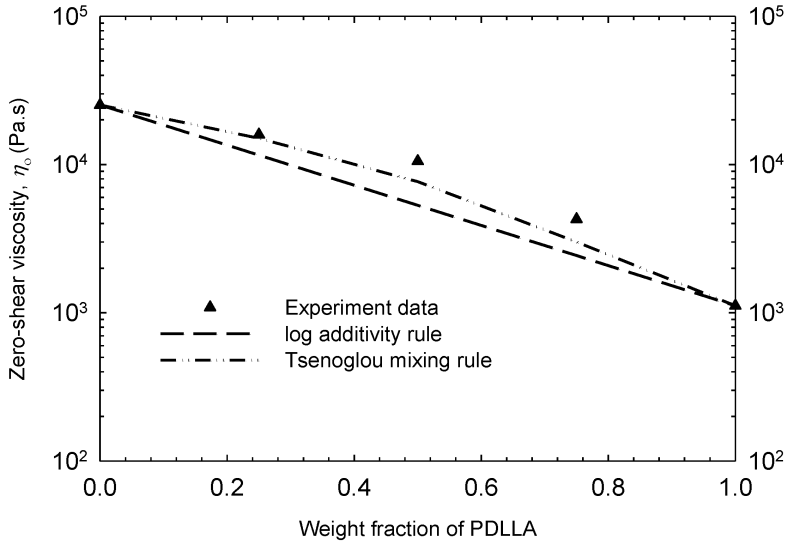

Figure 7.4: The zero-shear viscosities of the blends (entries 1 to 3 in Table 5.2) as a function of PDLLA weight fraction.

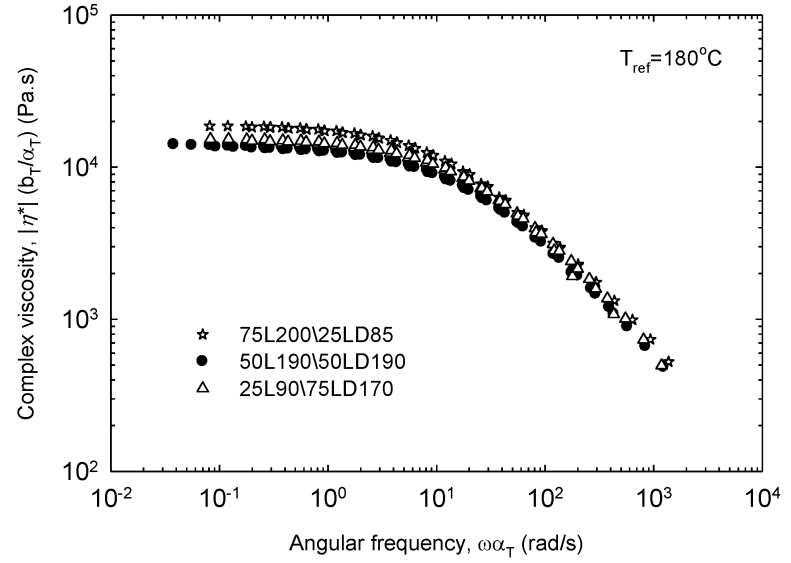

Figure 7.5: The complex viscosity of blends entries 4 to 6 in Table 5.2 at 180°C.

7.2.2 Diblock copolymers

Figure 7.6a shows the master curves of the linear viscoelastic moduli and the complex viscosity of diblock copolymers 25L-b170-75LD (entry 3 in Table 5.3) and its equivalent (similar total molecular weight) blends having components similar to those of the two blocks in the copolymer. The rheological behavior in terms of linear viscoelasticity is quite similar –

small differences are due to small differences in the molecular weights of blends and block copolymers.

Similar linear viscoelastic behavior was found for the other diblocks having different block composition (entries 1 and 2 in Table 5.3), which are plotted in Figure 7.6b and c respectively along with the viscoelastic behavior of corresponding blends. These figures show that diblock copolymers and their corresponding equivalent blends exhibit similar rheological behavior. As a reminder, the thermodynamic behavior of diblock copolymers was different than the corresponding blends, as the diblock copolymers exhibited a lower melting point and also a lower enthalpy of melting (see section 5.2.2 for more details). The linear viscoelastic properties of the diblock copolymers not presented in this chapter are shown in Appendix C.

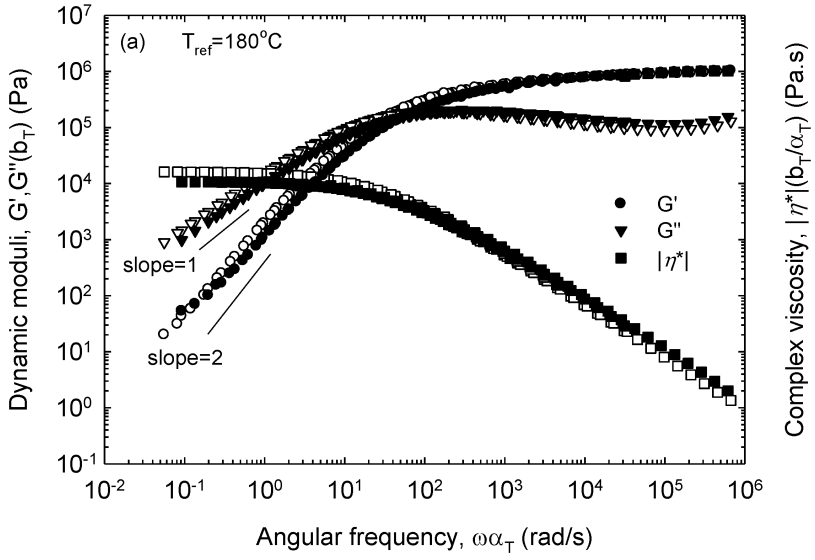

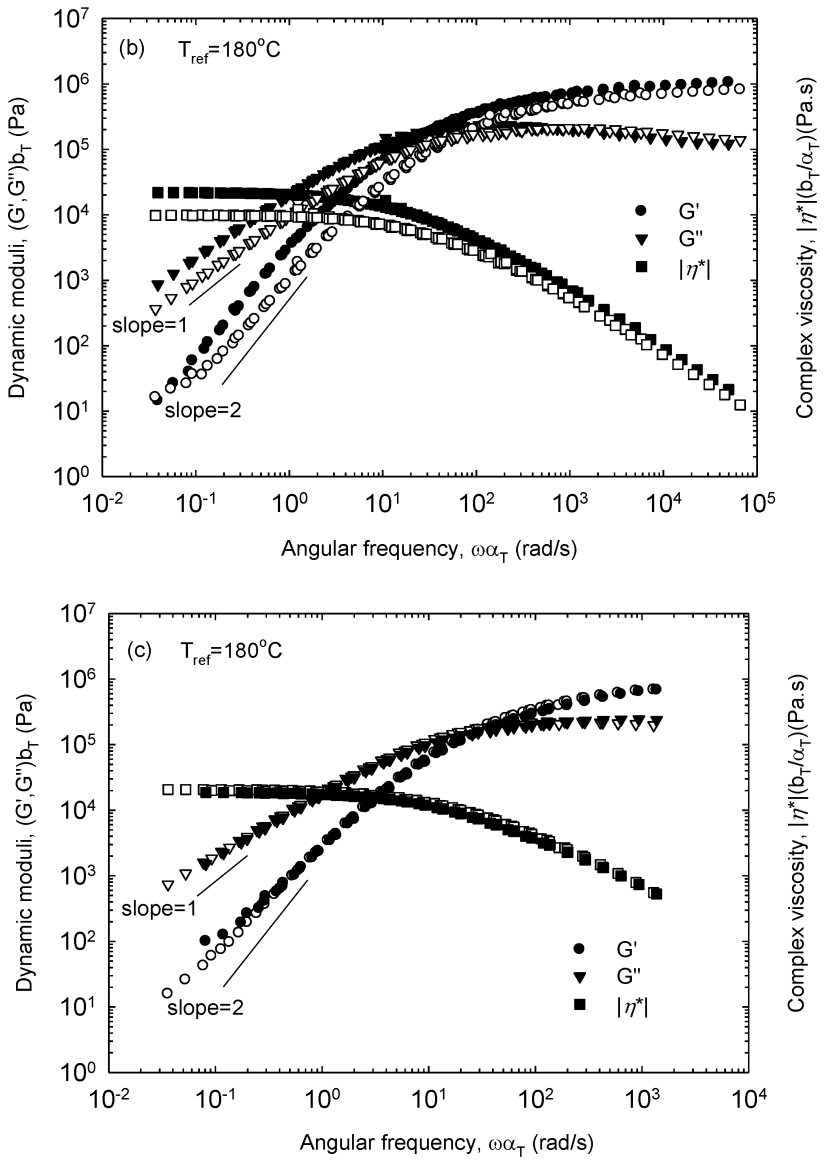

Figure 7.6: Master curve of the linear viscoelastic moduli, G' and G'' and complex viscosity $|\eta^*(\omega)|$ of diblocks (unfilled symbols) and the corresponding blends (filled symbols) (a)25L-b170-75LD and 25L90\75LD170 (b) 50L-b170-50LD and 50L190\50LD190 (c) 75L-b170-25LD and 75L200\25LD85 at the reference temperature of 180°C.

The terminal zone at low frequencies was reached for all homopolymers and their blends, where the well-known scalings of G' and G'' with ω^2 and ω, respectively have been obtained. The time-Temperature (t-T) superposition principle is applicable to the block copolymers and blends in this range of temperature, where these melts are in a disordered state. The disordered state was determined from the temperature independence of G' versus,

G'', (Figure 7.7 for the results plotted in Figure 7.6a). According to Han and coworker (Han and Kim, 1987), plots of log G' versus log G'' can be used to detect a critical temperature of possible phase transitions in copolymers and blends. Figure 7.7 shows temperature independency of diblock 25L-b170-75LD and 25L90\75LD170 blends at a temperature between 100 to 200°C. Similar temperature independencies are found for other diblock copolymers and blends at temperatures where t-T superposition was valid as discussed below.

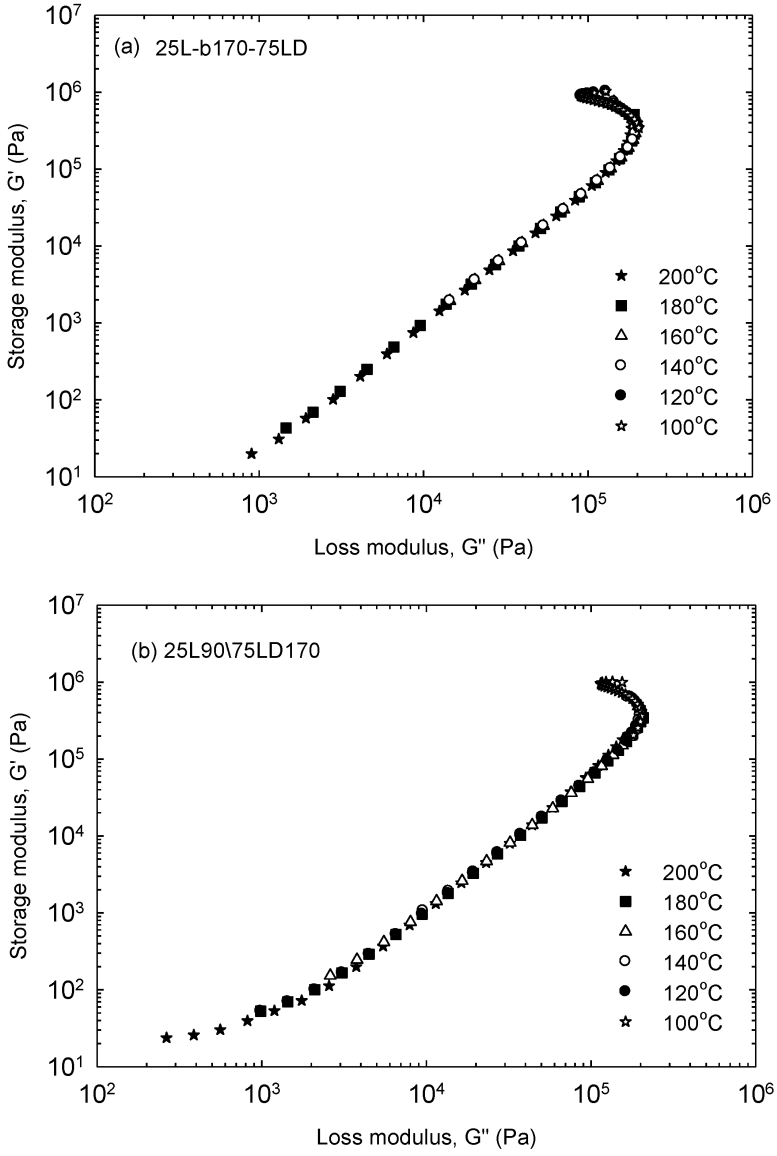

Figure 7.7: Plot of G' versus G'' at various temperatures for (a) diblock 25L-b170-75LD and (b) blend 25L90\75LD170.

The horizontal shift factors determined from the t-T superposition agreed well with reported observations in the literature for several PLA crystalline and amorphous homopolymers (see Figure 7.8) (Othman et al., 2011; Dorgan et al., 2005a). While all data appear to define a single line (WLF behavior), the data for blend with 50% and 75% in PLLA are off the WLF line. The blend of 50L190\50LD190 show a significant deviation starting at 120°C, whereas the blend of 75L200\25LD85 deviates slightly at the higher temperature of 140°C. This is due to phase separation exhibited by this blend as can be inferred by plotting log G' versus log G'' in Figure 7.9b and 7.10b. The moduli show temperature dependence at the temperature of 120°C and 140°C. This implies that the blend contains some microheterogeneity, which is due to existence of a small amount of a crystalline fraction that starts to crystallize at this temperature. In fact, this is the same temperature at which the t-T superposition starts to fail. Figure 7.9 and 7.10, show that the temperature dependencies of the blends were stronger as compared to corresponding diblock copolymers.

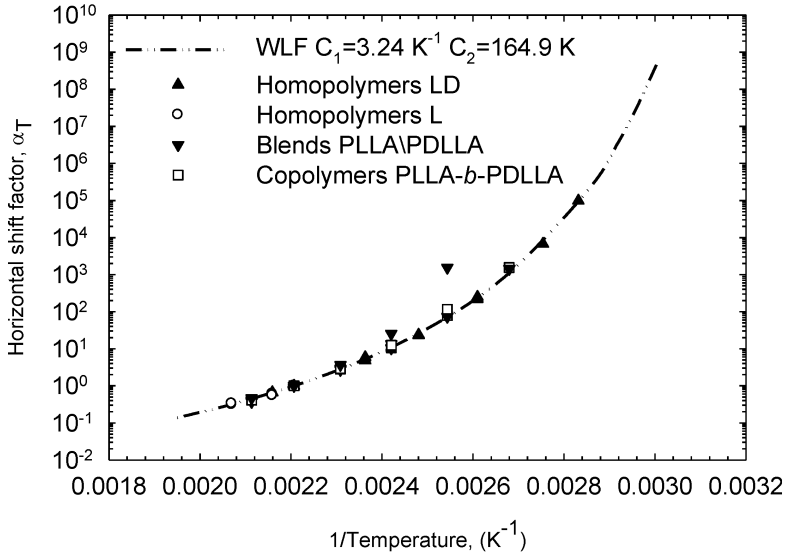

Figure 7.8: The horizontal shift factors, α_T of homopolymers, blends and diblock copolymers at the reference temperature of 180°C. The dotted line represents WLF fitting.

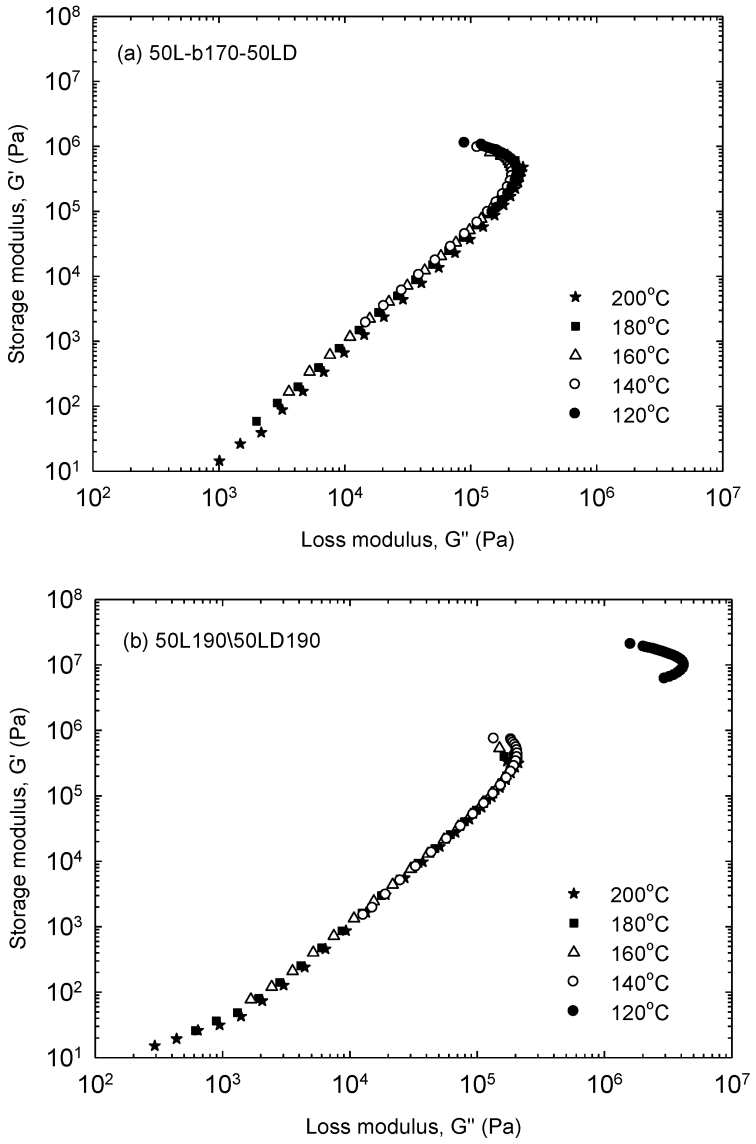

Figure 7.9: Plot of G' versus G'' at various temperatures for (a) diblock 50L-b17-50LD (b) blend 50L190\50LD190 to check for possible transitions.

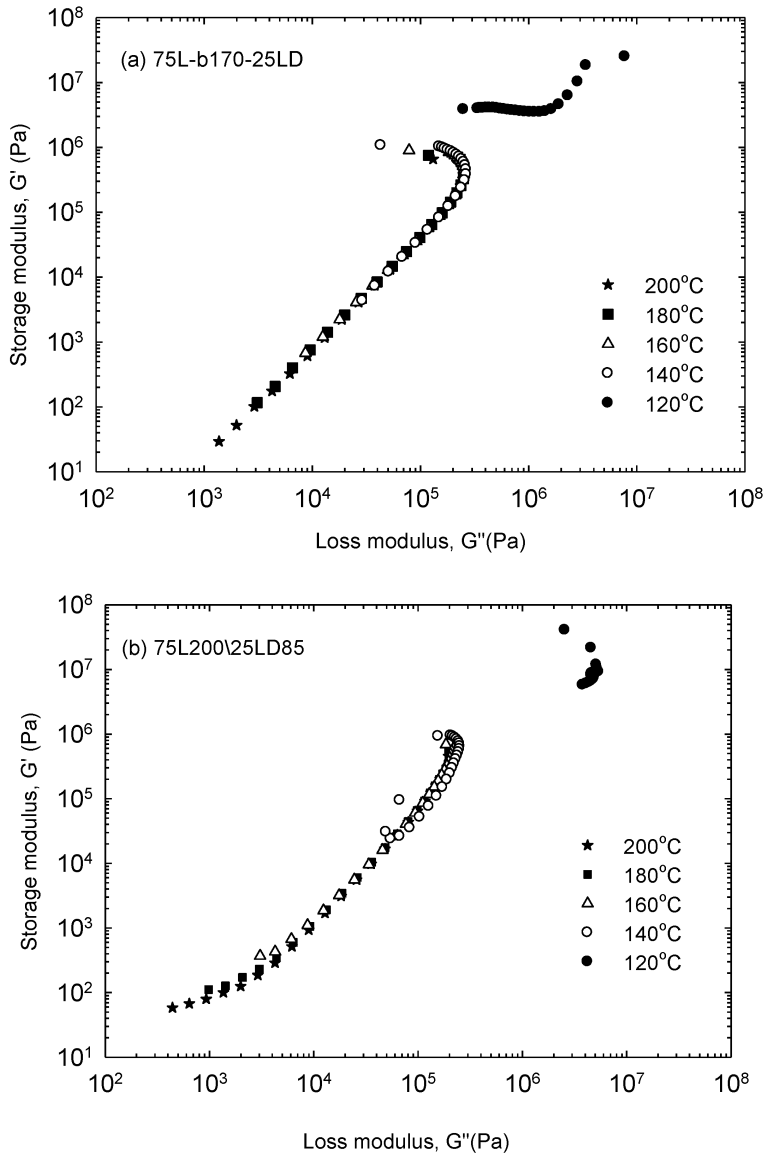

Figure 7.10: Plot of G' versus G'' at various temperatures for (a) diblock 75L-b170-25LD (b) blend 75L200\25LD85 to check for possible transitions.

Figure 7.11 depicts the complex viscosities of the diblock copolymers PLLA-*b*-P DLLA listed in Table 5.3. As expected the zero-shear viscosity scales with M_w (examined below). In fact the block copolymers listed in Table 5.3 entries 1-3 have the same molecular weight of about 170 kg/mol show almost the same zero shear viscosity as can also be seen in Figure 7.11.

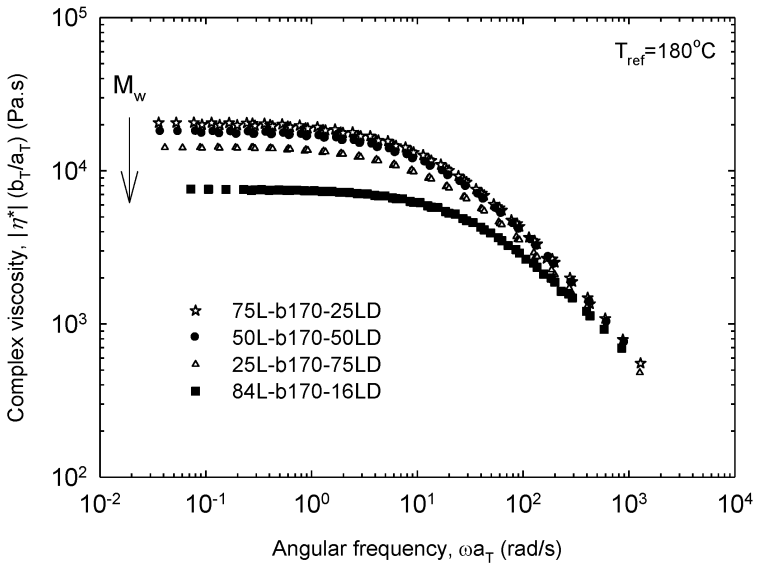

Figure 7.11: The complex viscosities of diblock copolymers listed in Table 5.3 (entries 1 to 4) at the reference temperature of 180°C.

7.2.3 Triblock copolymers

Figure 7.12 shows the master curves of the linear viscoelastic moduli and the complex viscosity of the triblock copolymers PLLA-*b*-PDLLA-*b*-PLLA (entries 1 and 2 in Table 5.4) with different PLLA and PDLLA length ratios. Similar linear viscoelastic behavior was found for these triblock copolymers, which are independent of PLLA and PDLLA length ratio. Small differences in the viscoelastic properties of the triblock copolymers in Figure 7.12 are due to small differences in the molecular weight. The terminal zone at low frequencies has been reached as indicated by slope of 1 and 2 of G'' and G', respectively.

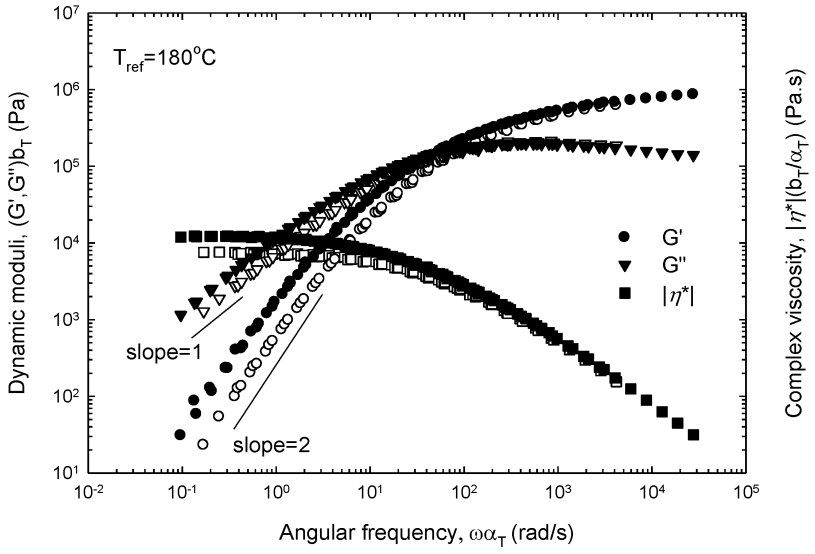

Figure 7.12: Master curve of the linear viscoelastic moduli, G' and G'' and complex viscosity $\left|\eta^*(\omega)\right|$ of 37.5L-25LD-37.5L (unfilled symbols) and 25L-50LD-25L (filled symbols) copolymers at the reference temperature of 180°C.

7.2.4 The zero-shear viscosity

The zero-shear viscosities of the blends, diblock copolymers PLLA-*b*-PDLLA as well as triblock copolymers PLLA-*b*-PDLLA-*b*-PLLA are plotted in Figure 7.13 as a function of molecular weight. The relationship between zero-shear viscosity can be described by the scaling law of $\eta_o \propto M_w^{3.4}$ which was determined previously by Othman et al. (2011) for a series of nearly monodisperse PLAs (similar results were obtained by Dorgan et al. (2005a)). The slope of 3.4 implies linear structure and it is also in agreement with the solution properties results discussed above for the diblock and triblock copolymers as well as crystalline and amorphous PLA homopolymers. The zero-shear viscosities of blends, diblocks and triblocks also agree with this scaling law implying the similarities in the behavior between PLA homopolymers, diblocks and triblocks of linear architecture.

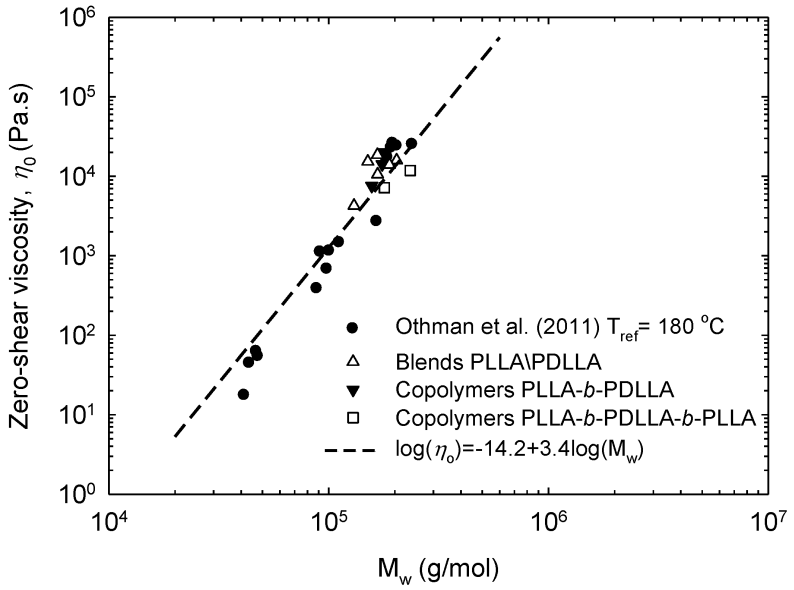

Figure 7.13: The scaling between the zero-shear viscosity and molecular weight of PLAs at the reference temperature of 180°C.

7.2.5 Sterecomplex structure

Figure 7.14 shows the zero-shear viscosities of PLLA (L190 as a reference) and diblock copolymers PLLA-*b*-PDLA (of two different compositions) plotted as a function of the reciprocal of temperature. At 230°C the viscosity of the diblock copolymers regardless of PLLA and PDLA length, are comparable to PLLA (L190) indicating no interaction between PLLA and PDLA above the melting point of stereocomplex which is around 210°C. Slightly higher viscosities of L190 are due to higher molecular weight of L190 as compared to diblock copolymers (~170 kg/mol). However, the viscosity of diblock copolymers 50L-b170-50D and 75L-b170-25D increase dramatically at about 210°C and 200°C respectively. This increase in the zero-shear viscosity indicates the occurrence of physical crosslinking that is caused by strong interaction between PLLA and PDLA and the existence of stereocomplex crystallite structure. The diblock 50L-b170-50D exhibits a stronger increase in its zero-shear viscosity as compared to diblock 75L-b170-25D due to higher sterecomplex content as a result of stronger interactions between PLLA and PDLA in the symmetric diblock. The ΔH_{m2} value of 50L-b170-50D is 19.5 Jg^{-1}, a value much higher than 10.0 Jg^{-1} of the 75L-b170-25D block copolymer.

Viscosity increments of PLLA\PDLA blends have been reported by Rahman et al. (2009) and Yamane et al. (2004) at 200°C and 190°C respectively at certain critical concentrations of PDLA added to PLLA. The blends of PLLA with low M_w PDLA showed a more pronounced increase in viscosity than high M_w PDLA. Blending of the low molecular weight polymers reduces the zero-shear viscosity. However, the results indicate that the PLLA\PDLA blends, whose molecular weights are lower than pure PLLA, show higher viscosities compared to that of pure PLLA. Similar observations have been made in the case of viscosity measurements of PLLA\PDLA blends in solution at room temperature (Tsuji et al., 1991b). The induction time at which the viscosity rise is short for equimolar blends and the time becomes longer as the blends deviates from equimolarity due to the fact that the most favorable composition for formation of stereocomplex is 1:1 (Tsuji et al., 1991a;1991b).

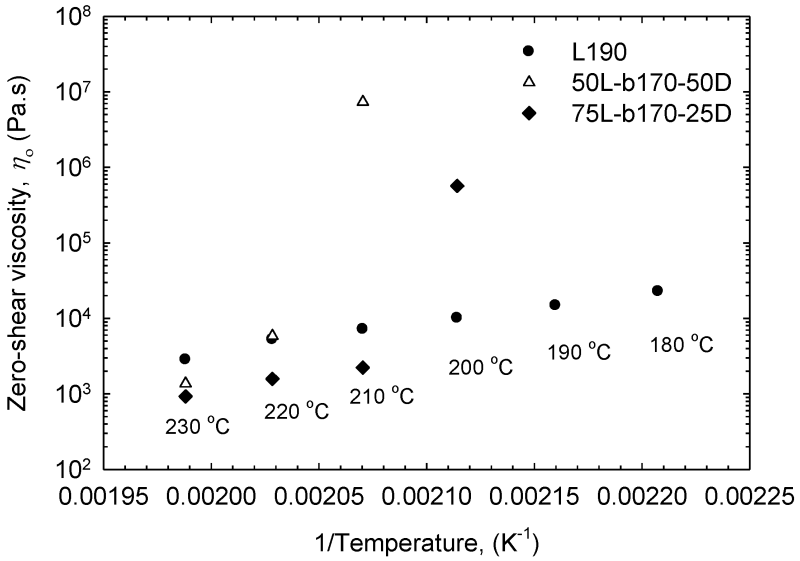

Figure 7.14: The zero-shear viscosities of PLLA and diblock copolymers PLLA-*b*-PDLA at various temperatures.

Viscosity enhancements were also found for the case of triblock copolymers of PLLA-*b*-PDLLA-*b*-PDLA and PLLA-*b*-aPHB-*b*-PDLA as seen in the case of diblock copolymers PLLA-*b*-PDLA (Figure 7.15). This indicates the existence of stereocomplex structure and strong interaction between PLLA and PDLA in the outer block as mentioned before. However, the viscosity increase for 37.5L-b-25LD-b-37.5D and 25L-b-50LD-b-25D delayed until 160°C and 140°C respectively, despite the existence of stereocomplex crystals

(see section 5.2.3). This could be attributed to the PDLLA middle block, which somehow interferes with the formation of sterecomplex crystals from the melt. Unfortunately no further detailed explanation could be found. The viscosities of triblock copolymers PLLA-*b*-aPHB-*b*-PDLA at 240°C were much lower than those of the other triblocks that have relatively the same M_w. This is due to possible degradation of PHB at high temperature as PHB suffered severe thermal degradation at a temperature beyond 175°C (Ramkumar and Bhattacharya, 1998; Yamaguchi and Arakawa, 2006).

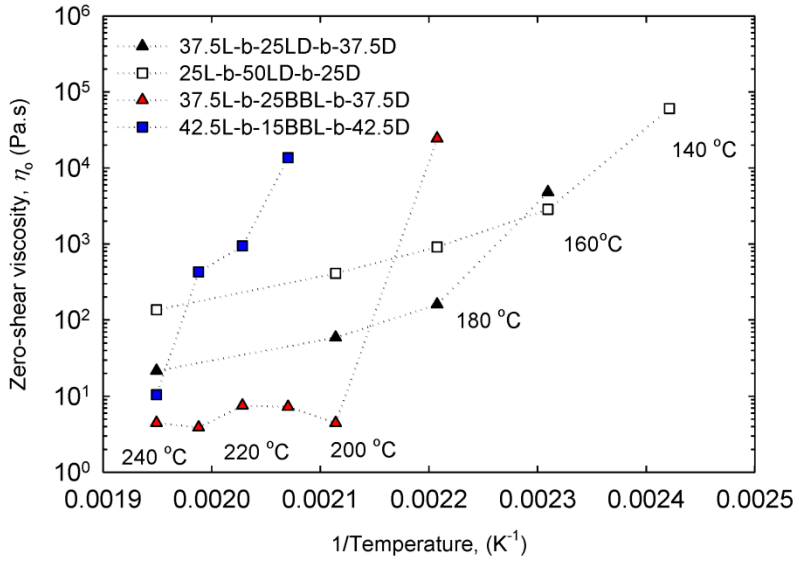

Figure 7.15: The zero-shear viscosities of triblock copolymers PLLA-*b*-PDLLA-*b*-PDLA and PLLA-*b*-aPHB-*b*-PDLA at various temperatures.

7.3 Tensile Properties

Figure 7.16 depicts typical stress-strain curves of a PLLA, a PDLLA and a PLLA-*b*-PDLLA copolymer. Linear behavior can be observed at low strains where the elastic modulus can be determined. Consequently, the linear region is followed by a nonlinear behavior before the yield point. The PLLA (L190) shows a clear brittle behavior, with no sign of necking. The tensile strength can be determined from the maximum of stress in the tensile curve. The tensile strengths of copolymers with 50% PLLA and 25% PLLA are comparable to that of pure PLLA with some increase of the elongation at break caused by the presence of the PDLLA block. However, the 75L-b170-25LD shows the highest values of maximum

(tensile) stress as well as the maximum strain over the other diblock copolymers and the pure PLLA and PDLLA.

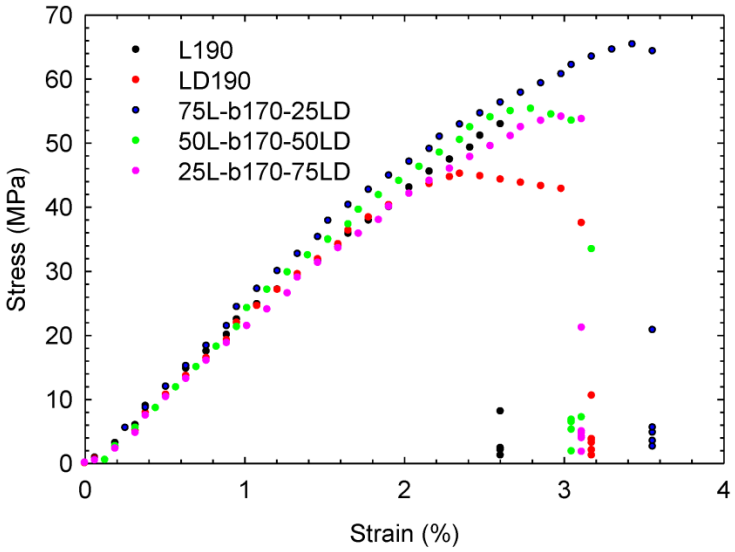

Figure 7.16: Tensile stress strain behavior of PLLA, PDLLA and diblock copolymers.

Figure 7.17 shows the elastic modulus of homopolymers L190 and LD190, blends (entries 1 to 3 in Table 5.2) and diblock copolymers as a function of DL (entries 1 to 3 in Table 5.3) or D (entries 5 and 6 in Table 5.3) weight fraction. The elastic modulus of the blends and diblock copolymers remain relatively unchanged as compared to PLLA and they are independent of molecular weight details at least for the range of M_w studied here. This implies that blending and copolymerizing of PDLLA or PDLA with PLLA to synthesize diblocks does not change the PLLA stiffness.

The DL or D fraction has an effect on the tensile strength. The tensile strength of the 75L200\25LD85 blends is lower by 12% compared to that of pure PLLA (Figure 7.18). On the other hand, the diblock copolymers in all composition show an improvement in tensile strength and elongation at break as compared to their counterpart homopolymers and blends. As mentioned earlier, the tensile strength and elongation at break exhibit a maximum for the diblock 75L-b170-25LD. The tensile strength improved by 15% and 32% compared to pure PLLA and 75L200\25LD85 blends respectively. Moreover, the elongation at break increased by 33% and 42% compared to PLLA and 75L200\25LD85 blends respectively (Figure 7.19).

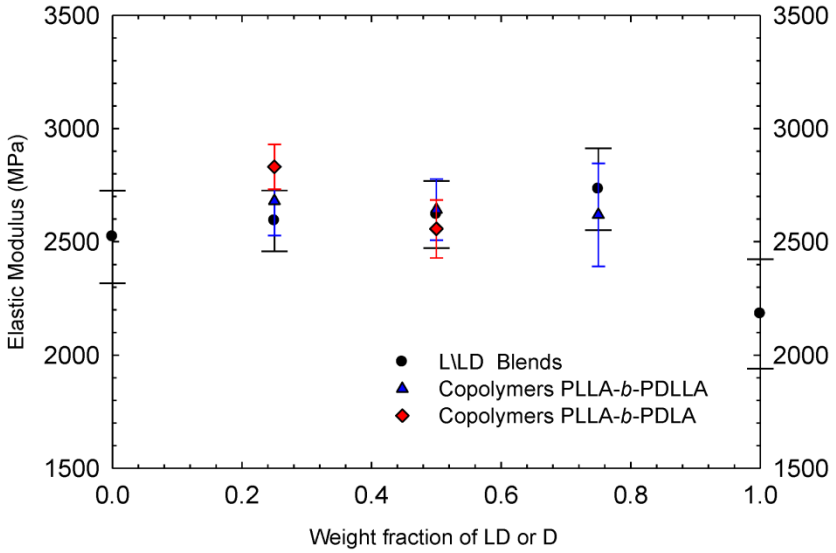

Figure 7.17: Elastic modulus of PLA homopolymers, blends and diblock copolymers as a function of the DL or the D composition.

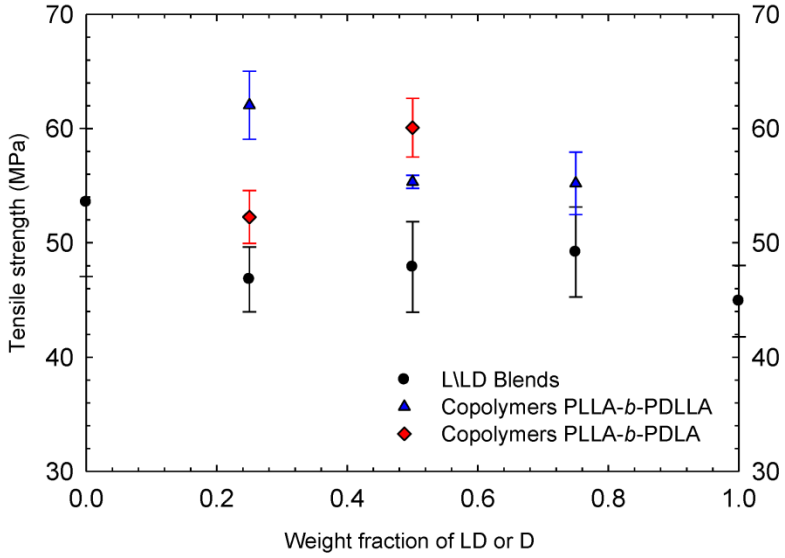

Figure 7.18: Tensile strength of PLA homopolymers, blends and diblock copolymers as a function of DL or D composition.

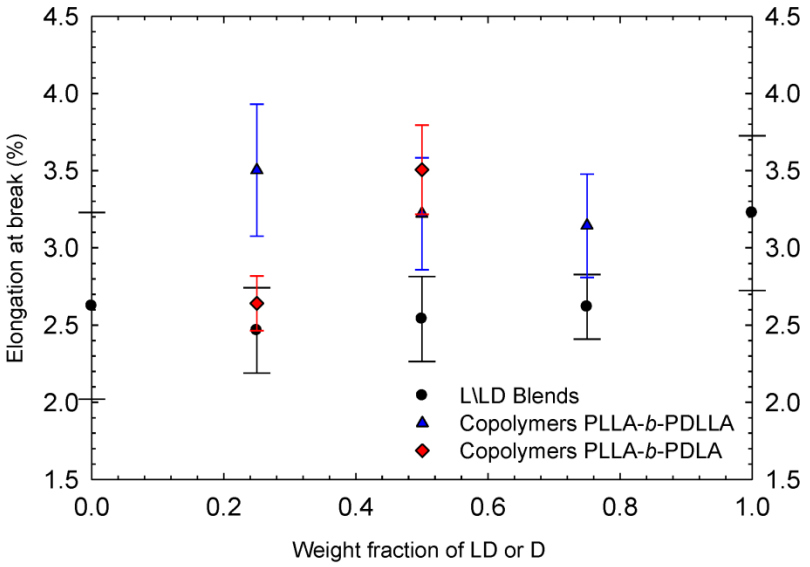

Figure 7.19: Elongation at break of PLA homopolymers, blends and diblock copolymers as a function of DL or D composition.

These results indicate that the diblock copolymers are capable to withstand higher stress before the samples fail in tensile mode. Synergistic effects of copolymerization of PLLA and PDLLA, and segmental connection in diblock copolymers contributes to this improvement. Bouapao et al. (2009) found that in PLLA\PDLLA blends, PLLA and PDLLA were phase separated when the samples were melt quenched to 0°C. This explained the low tensile strength and elongation at break of the blends. As mentioned in the experimental part, the films for the tensile test were prepared by melt compression of the sample followed by cooling using cold water. This might cause a small degree of phase separation and the reduced mechanical properties of blends compared to those of their pure counterparts.

Diblock 50L-b170-50D shows higher values of tensile strength and elongation at break than 75L-b170-25D. This is in agreement with reported results on higher cohesive properties found in the stereocomplex crystals over the homocrystallites PLA (Sarasua et al., 2005). Diblocks containing higher amount of stereocomplexity show a higher tensile strength and elongation at break. The tensile strength and elongation at break improved by 12% and 13% respectively compared to pure PLLA. Similar improvements in tensile properties have been reported by Tsuji and Ikada (1999*)* for PLLA\PDLA equimolar blends.

The tensile properties of the triblock copolymers are listed in Table 7.1. The elastic modulus of triblock copolymers remain unchanged regardless of the outer block and block

length ratio of PLA. The tensile strength of copolymers PLLA-*b*-PDLLA-*b*-PLLA and PLLA-*b*-PDLLA-*b*-PDLA with 25% PDLLA are comparable to that of PLLA, whereas the tensile strength of copolymers with 50% PDLLA decreases slightly with the value comparable to the tensile strength of PDLLA. The elongation at break for copolymers PLLA-*b*-PDLLA-*b*-PLLA improved about 85% and 77% as compared to that of PLLA. The values of elongation at break for PLLA-*b*-PDLLA-*b*-PDLA triblocks were also comparable to those of diblock PLA-*b*-PDLA. Higher elongation at break was observed for copolymers with high stereocomplex content.

On the other hand, dramatic drop of tensile properties were observed for the triblock with 25% amorphous PHB in the middle block. This copolymers showed poor tensile strength and elongation at break, 11.3 MPa and 1.8% respectively. It has been reported that PHB typically alters the final morphology of the stereocomplex crystals and hinders the crystallization of stereocomplex PLA in PHB\stereocomplex PLA blends and this is the reason for the significant drop of the mechanical properties (Chang and Woo, 2011).

However, these results contradict those reported in literature for triblock copolymers PLLA-*b*-aPHB-*b*-PLLA. It has been reported that due to atactic PHB which is elastomeric in nature, it can be used to prepare elastomeric polymers (Hiki et al., 2000; Albertsson et al., 2010). The elongation at break of PLLA-*b*-aPHB-*b*-PLLA copolymers improved about 10 times compared to pure PLLA. It worth to mention that, small molecular weight of PHB (M_n 31 kg/mol) was used in Hiki and coworkers study thus the PHB was miscible with PLLA. High molecular of PHB could be phase-separated even if they are linked in a block copolymer (Hiki et al., 2000). This could also be the reason of poor tensile properties observed for the triblock with 25% PHB.

Table 7.1: Tensile properties of homopolymers, diblock and triblock copolymers

Entry	*Samples*	*Tensile strength, MPa*	*Elastic modulus, MPa*	*Elongation at break, %*
1	L190	53.5±6.5	2521.4±204.2	2.6±0.6
2	LD190	44.9±3.1	2182.4±241.9	3.2±0.5
3	75L-b170-25LD	62.0±3.0	2679.6±153.2	3.5±0.4
4	50L-b170-50LD	55.3±0.6	2641.6±135.4	3.2±0.4
5	25L-b170-75LD	55.2±2.7	2618.8±227.0	3.1±0.3
6	75L-b170-25D	52.2±2.3	2830.4±99.5	2.6±0.2
7	50L-b170-50D	60.1±2.6	2556.8±127.2	3.5±0.3
8	37.5L-25LD-37.5L	56.1±2.0	2548.4±124.0	4.8±0.1
9	25L-50LD-25L	40.1±4.0	2673.5±117.7	4.6±0.3
10	37.5L-25LD-37.5D	58.4±3.8	2637.2±109.9	3.5±0.1
11	25L-50LD-25D	44.9±5.5	2654.0±102.2	2.8±0.1
12	42.5L-15BBL-42.5D	43.3±2.1	2300.2±36.3	2.3±0.1
13	37.5L-25BBL-37.5D	11.3±1.8	918.7±127.6	1.8±0.1

7.4 Summary

The solution and melt rheological as well as the mechanical properties of blends of homopolymer PLAs, and equivalent block copolymers have been investigated as functions of molecular characteristics. The good agreement of the solution properties with those nearly monodisperse PLAs indicated that the copolymers possess a linear molecular structure.

Linear viscoelastic behavior of block copolymers PLLA-*b*-PDLLA was independent of PLLA length in copolymers. The time-Temperature superposition principle is applicable to the block copolymers and blends up to a certain temperature. The terminal zone behavior at low frequency is reached with characteristic slope of 1 and 2 for G'' and G', respectively, indications of disordered state. The disordered state was confirmed by logarithmic plot of storage modulus, G' versus loss modulus, G'', at which the moduli become independent of temperature. Similar linear viscoelastic behaviors were observed for triblock copolymers of PLLA-*b*-PDLLA-*b*-PLLA regardless of block length ratio. The relationship between zero-

shear viscosities and molecular weight of blends and copolymers can be described by $\eta_o \propto M_w^{3.4}$.

In the presence of stereocomplex crystallites, diblock copolymers PLLA-*b*-PDLA show a viscosity enhancement at temperatures between the two melting temperatures. However the viscosity enhancement was delayed to a lower temperature in triblock where PDLLA located in the middle block.

Tensile testing shows that, diblock and triblock copolymers of PLLA and PDLLA or/and PDLA show promising improvements in tensile strength and elongation at break compared to the corresponding homopolymers and blends. However, PLLA\PDLLA blends show mechanical properties lower than those of their pure components due to phase separation that happens during quenching to room temperature. Moreover, the triblock copolymers of PLLA-*b*-aPHB-*b*-PDLA with atactic PHB in the middle block showed poor tensile strength and elongation at break.

8 Rheology and Processing of Commercial PLAs

In this chapter, four commercial PLAs with M_w in the range of 10^4 to 10^5 g/mol are studied in terms of their rheological and processing behavior. The results are compared with literature values for other PLAs. Their slip behavior as a function of wall shear stress and molecular weight is examined. Their processing behavior in capillary flow is also examined in terms of critical conditions for the onset of melt fracture. Finally, processing aids that can be used to postpone the onset of melt fracture to high shear rates are proposed (Achilleos et al., 2002; Amos et al., 2001).

8.1 Rheological Properties

8.1.1 Linear viscoelasticity

To confirm the thermal stability of PLA samples during rheological measurements, dynamic time sweeps were carried out for PLA 7001D at 180°C at the fixed frequency of 1 rad/s. The representative results are plotted in Figure 8.1. The time sweep data in terms of complex modulus indicate practically constant modulus over long periods of time, longer than typical duration of the rheological experiments.

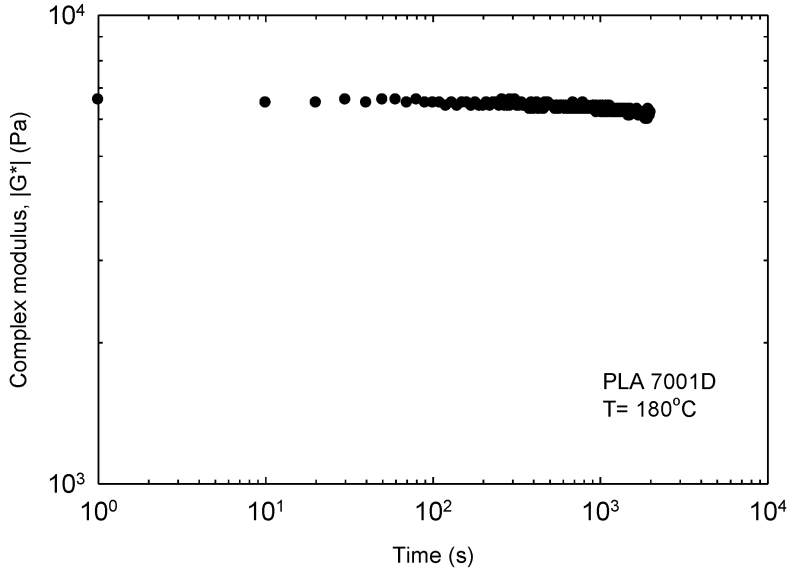

Figure 8.1: Time sweep experiment to check the thermal stability of PLA 7001D at 180°C.

Figure 8.2 show the master curves of linear viscoelastic moduli, G' and G'' and complex viscosity $\left|\eta^*(\omega)\right|$ of all commercial PLAs studied at the reference temperature of 180°C. The time-Temperature superposition was applied using RHEOPLUS software (MCR 501 rheometer of Anton Paar) to obtain the master curves. The continuous lines represent fits of parsimonious relaxation spectrum (PM) (g_i, λ_i) according to Equations 6-8 and 6-9. The generalized Maxwell model parameters for all commercial PLAs are listed in Table 8.1 at 180°C. Vertical, b_T and horizontal α_T shift factors were applied. Typical values of b_T were in the range of 0.98-1.03, which are close to 1 (typically found for other linear nearly monodisperse PLAs) (Othman et al., 2011).

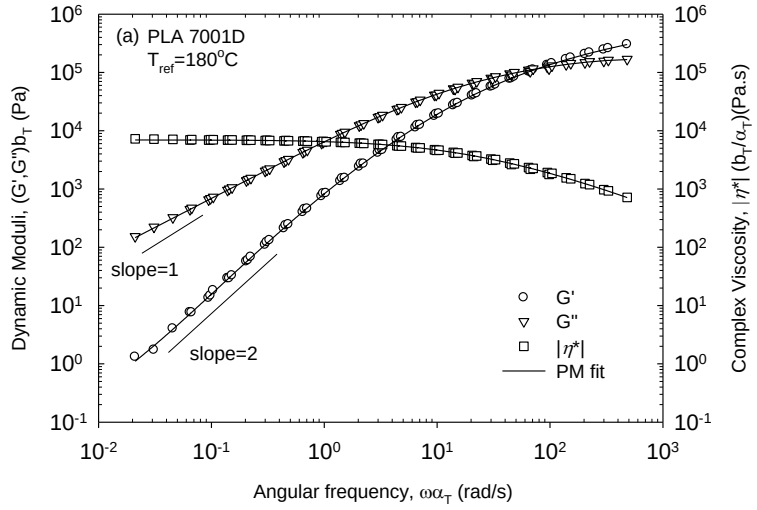

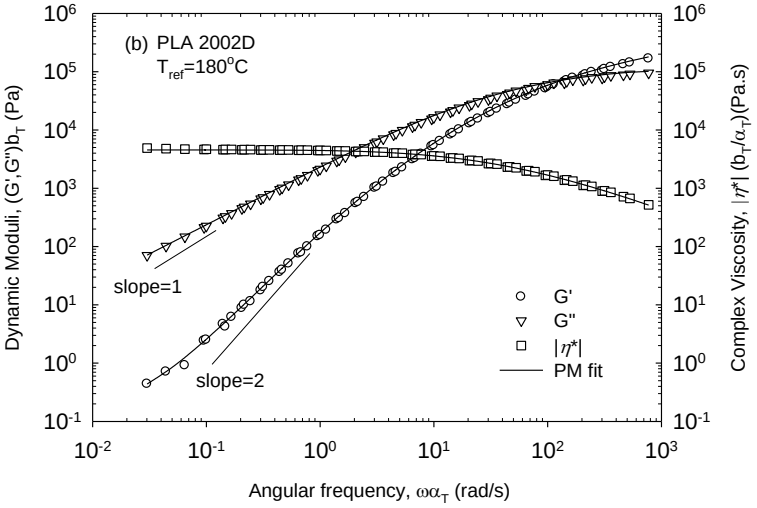

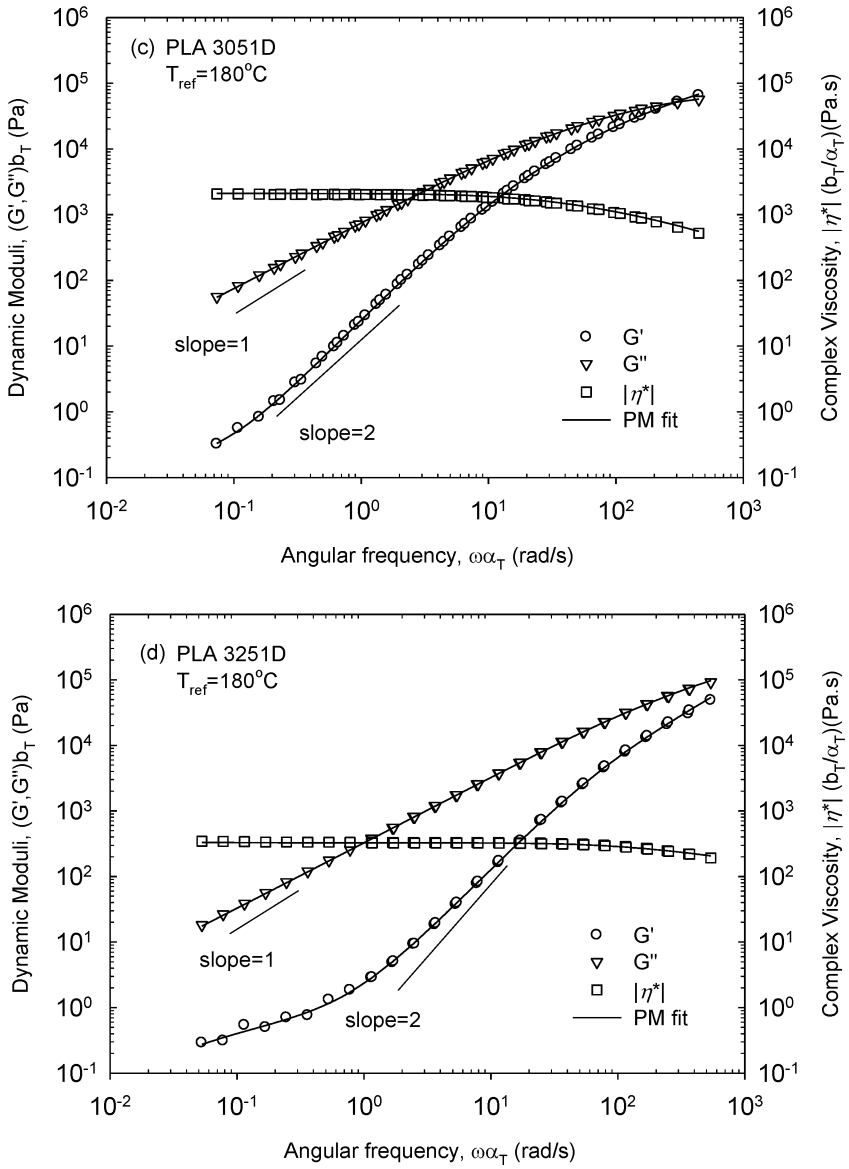

Figure 8.2: Master curve of the linear viscoelastic moduli, G' and G'', and complex viscosity $\left|\eta^*(\omega)\right|$ of all commercial PLAs (listed in Table 4.4) studied at the reference temperature of 180°C.

Table 8.1: Generalized Maxwell model parameters (g_i, λ_i) for all commercial PLAs at 180°C.

PLA 7001D		***PLA 2002D***		***PLA 3051D***		***PLA 3251D***	
g_i	λ_i	g_i	λ_i	g_i	λ_i	g_i	λ_i
3.39×10^{5}	2.07×10^{-3}	3.51×10^{5}	1.60×10^{-3}	1.17×10^{5}	1.30×10^{-3}	3.75×10^{5}	4.53×10^{-4}
1.35×10^{5}	2.55×10^{-2}	1.36×10^{5}	1.28×10^{-2}	3.40×10^{4}	8.92×10^{-3}	2.94×10^{4}	4.22×10^{-3}
7.97×10^{3}	3.13×10^{-1}	2.30×10^{4}	8.00×10^{-2}	5.49×10^{3}	4.47×10^{-2}	1.66×10^{3}	2.04×10^{-2}
5.08×10^{1}	3.85×10^{0}	6.61×10^{2}	5.99×10^{-1}	1.93×10^{2}	2.50×10^{-1}	9.70×10^{-1}	1.55×10^{0}
7.16×10^{-1}	4.73×10^{1}	5.92×10^{-1}	1.14×10^{2}	1.79×10^{-1}	1.08×10^{2}	4.55×10^{-1}	2.17×10^{1}

The horizontal shift factors, α_T determined here together with those determined by Othman et al. (2011) for a large number of crystalline and amorphous PLAs follow the WLF equation, where C_1=3.24 K^{-1}, C_2=164.9 K (Dorgan et al., 2005a). The PLAs considered in the present work are crystalline, and as such the temperature range for rheological characterization is narrow. The shift factors can be described by an Arrhenius equation resulting in a flow activation energy of 98.50 kJ/mol (lower range of 1/T in Figure 8.3). This value agrees with previously reported values on PLLA and PDLA (Conrad, 2009; Cooper-White and Mackay, 1999; Dorgan et al., 1999), whereas a higher value has been reported for PDLLA (these are typically amorphous). For example, Othman et al. (2011) reported the value of 177.65 kJ/mol for a series of nearly monodisperse PDLLA whose shift factors fall in the higher range of 1/T in Figure 8.3. However, Figure 8.3 shows that, the shift factors for all PLAs can be satisfactorily described by the WLF equation and a single value of flow activation energy is not representative for all PLAs.

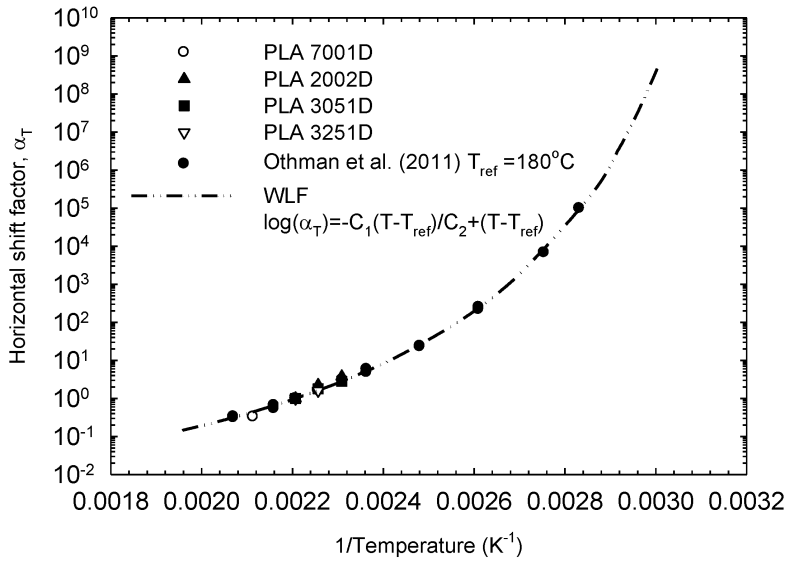

Figure 8.3: The horizontal shift factors, α_T for commercial PLAs as well a number of PLAs studied by Othman et al. (2011) at the reference temperature of 180°C. The continuous line represents fitting to the data of the WLF equation.

Figure 8.4 shows the complex viscosity material function of all the PLAs studied at the reference temperature of 180°C. It is shown that the terminal zone has been reached and the zero-shear viscosity can be obtained directly from the experimental data. The onset for shear thinning occurs at smaller frequencies as the molecular weight increases.

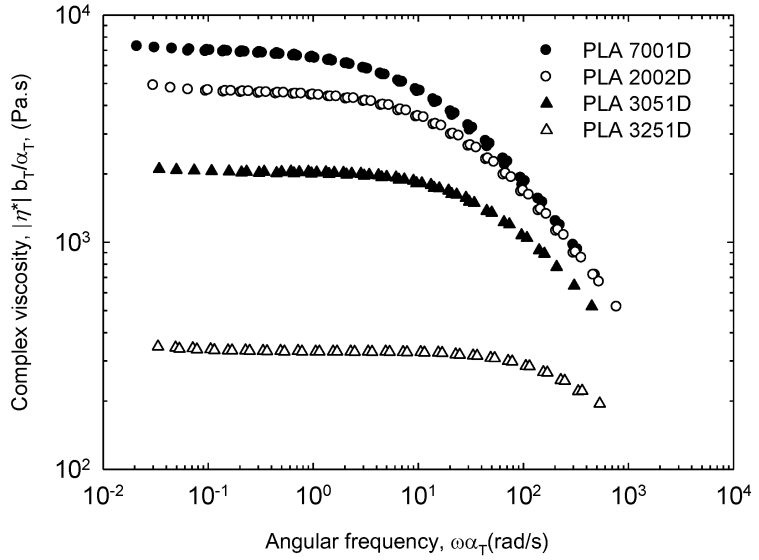

Figure 8.4: The complex viscosity of the commercial PLAs (listed in Table 4.4) studied at the reference temperature of 180°C.

The zero-shear viscosities as a function of molecular weight are plotted Figure 8.5. The relationship between the zero-shear viscosity and molecular weight can be described by:

$$\log(\eta_o) = -14.2 + 3.4\log(M_w) \qquad (8\text{-}1)$$

at the reference temperature of 180°C. This relationship was also determined by Othman et al. (2011) who studied a series of nearly monodisperse PLAs and the results presented in section 6.2.

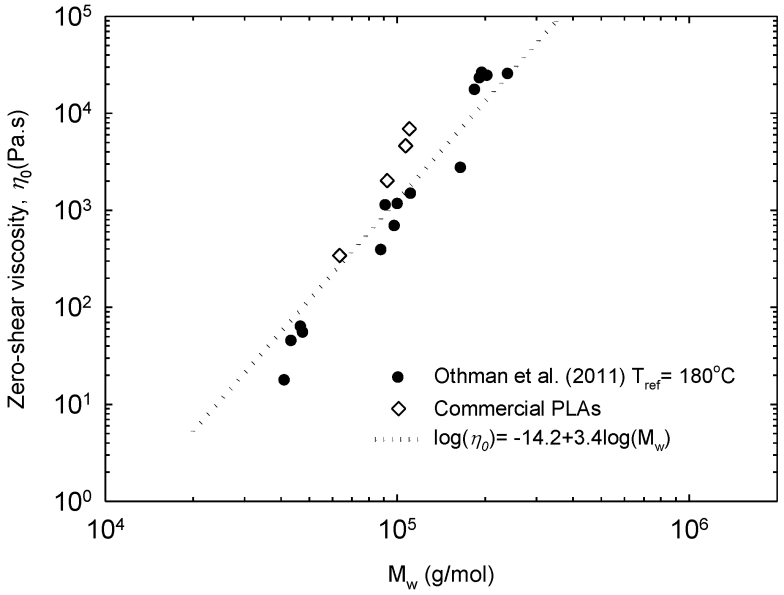

Figure 8.5: The scaling between the zero-shear viscosity of PLAs and M_w of PLAs at the reference temperature of 180°C.

8.1.2 Extensional rheology

Figure 8.6 plot the tensile stress growth coefficient of PLA 7001D in uniaxial extensions, at several extensional Hencky strain rates measured at 160°C and 170°C respectively using the SER-2 fixture. The dashed line represents the linear viscoelastic envelope (LVE) $3\eta^+(t)$, where $\eta^+(t)$ is the shear stress growth coefficient obtained in linear viscoelasticity. In the present case the coefficient $\eta^+(t)$ was calculated from the parsimonious relaxation spectrum (g_i, λ_i) fitted to linear viscoelastic moduli (G' and G'') using Equation 6-11. The values of g_i and λ_i for PLA 7001D at 160°C and 170°C are listed in Table 8.2.

Table 8.2: Generalized Maxwell model parameters (g_i, λ_i) for PLA 7001D at 160 and 170°C.

160 °C		***170°C***	
g_i	λ_i	g_i	λ_i
1.72×10^{5}	2.87×10^{-2}	3.09×10^{5}	2.27×10^{-3}
5.43×10^{4}	1.68×10^{-1}	1.85×10^{5}	1.44×10^{-2}
4.57×10^{3}	9.81×10^{-1}	6.10×10^{4}	9.06×10^{-2}
1.77×10^{2}	5.74×10^{0}	4.86×10^{3}	5.71×10^{-1}
2.25×10^{0}	3.35×10^{1}	1.42×10^{2}	3.61×10^{0}

Figure 8.6(a) and Figure 8.6(b) show that at Hencky strain rates of 0.1, 1 and 10 s^{-1} and short times, the extensional data are superposed well with the LVE, indicating the consistency between shear and extensional experimental data. No strain hardening is observed, which agrees with the linear structure of the polymers concluded from their shear rheology and the GPC-LS measurements. Strain softening at higher times are due to sagging that occurs due to low melt strength of PLAs.

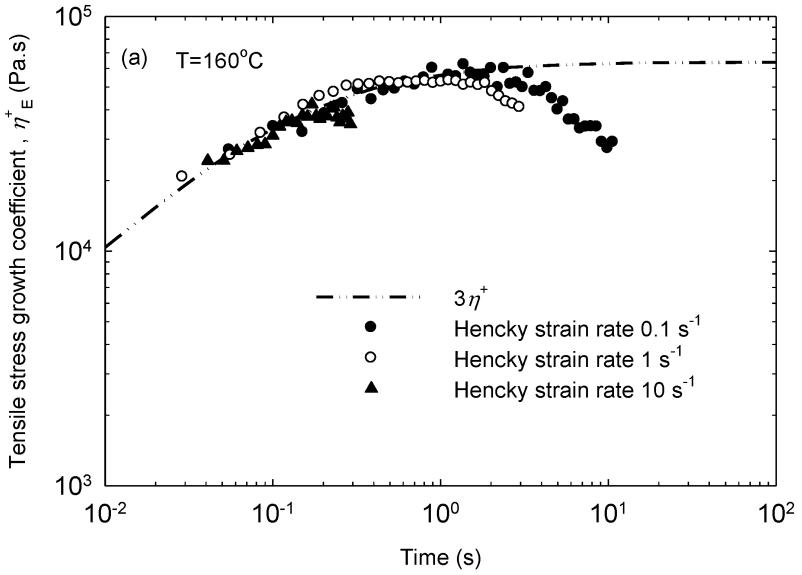

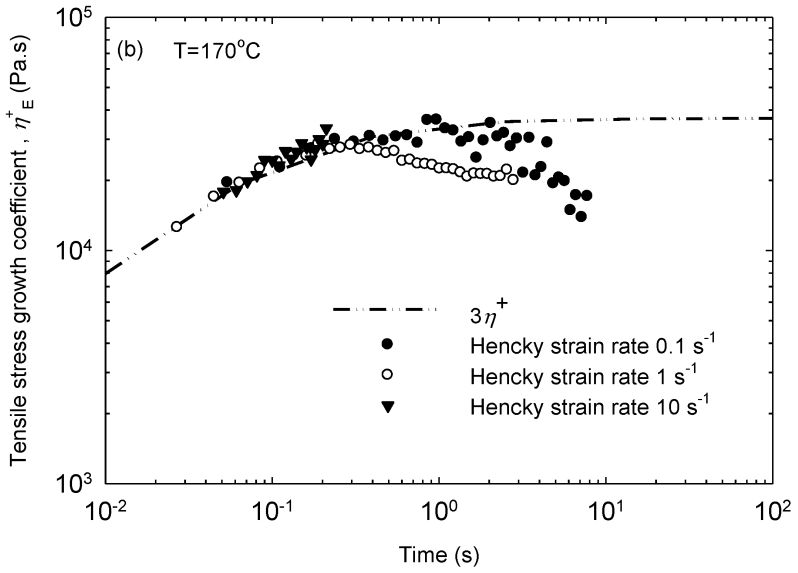

Figure 8.6: The tensile stress growth coefficient as a function of time measured at various Hencky strain rates for PLA 7001D at (a) 160°C and (b) 170°C.

Strain hardening for linear PLA polymers has been observed by Palade et al. (2001), Yamane et al. (2004) and recently by Othman et al. (2011) and discussed in section 6.4. It has been reported that the strain hardening was due to wide polydispersity and present of long chain tail in the molecular weight distribution (Palade et al., 2001). In the case of nearly monodisperse PLA, that strain hardening occurs when the longest relaxation time is smaller than the characteristic deformation time (inverse of the rate of deformation) (Othman et al., 2011). In the present study the uniaxial extensional measurement was conducted at a temperature above the melting point and the longest relaxation times are 0.0227 s and 0.0155 s at 160^{o}C and 170^{o}C respectively. These longest relaxation times were obtained by analyzing the linear viscoelastic data in terms of their discrete relaxation spectrum using the method discussed by Baumgaertel and Winter (1989) and Baumgaertel et al. (1990) (see section 6.3 for detail). As these relaxation times are smaller than the characteristic times (0.1 s to 10 s) of Hencky strain rates from 0.1 s^{-1} to 10 s^{-1}, strain hardening effects are not expected.

8.2 Capillary Rheometry

The capillary rheometry of all commercial PLAs has been studied to assess possible slip effects as well as melt fracture phenomena. The raw data obtained from such a piece of equipment (pressure drop, Δp versus volumetric flow rate, Q) can be transformed into fundamental rheological data (shear stress and shear rate) by the following two equations. First, the apparent wall shear stress is given by:

$$\sigma_{w,a} = \frac{\Delta p D}{4L} \tag{8-2}$$

where $\sigma_{w,a}$ is the apparent shear stress, *L/D* is the length-to-diameter ratio of the capillary die and Δp is the total pressure drop. The apparent shear rate is given by:

$$\dot{\gamma}_A = \frac{32Q}{\pi D^3} \tag{8-3}$$

where Q is the volumetric flow rate. To obtain the true shear stress along the capillary wall and the true shear rate, the entry pressure, Δp_{end} (Bagley correction) and Rabinowitsch corrections should be applied (Dealy and Wissbrun, 1999).

Figure 8.7 depicts the flow curves of PLA 7001D determined by using capillary dies having D=0.76 mm and four different length-to-diameter (*L/D*) ratios. The flow curves do not superpose well due to the entry pressure drop, which has to be taken into account. This seems to be significant particularly for the short dies.

Figure 8.8 is the Bagley plot used to determine the entry pressure drop at several values of the apparent shear rate. Linear regression was applied to obtain the entry pressure that seems to represent the experimental data very well. In fact, the experimental data fall almost perfectly on a straight line indicating that the absence of viscous heating and that the effect of pressure on viscosity is minimal.

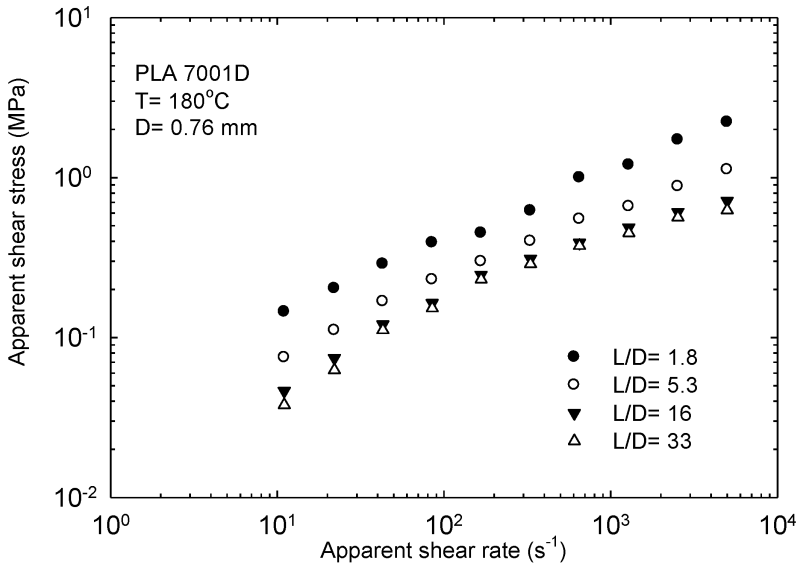

Figure 8.7: The apparent flow curves of PLA 7001D for several dies having the same diameter (0.76 mm) and various *L/D* ratios at 180°C.

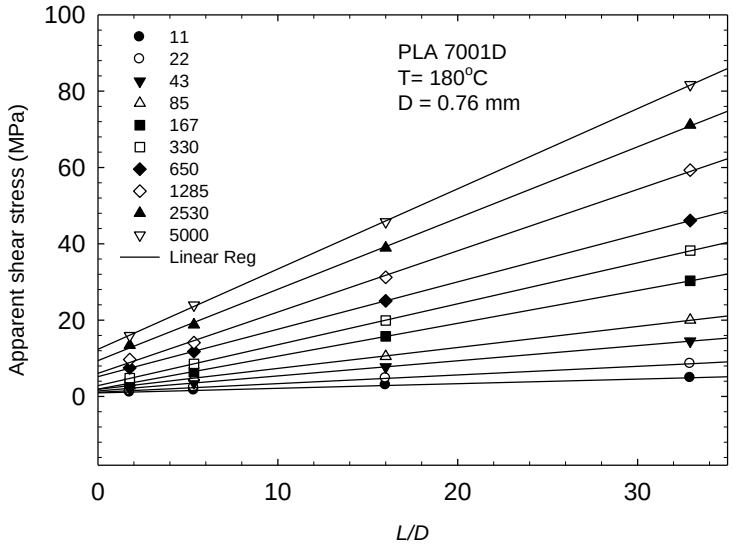

Figure 8.8: Bagley plot to determine the end pressure correction for PLA 7001D at 180°C.

Application of the entry pressure drop to the data plotted in Figure 8.7 results in an excellent superposition that now defines the flow curve of this polymer in terms of the true shear stress (Equation 8-4) versus the apparent shear rate $\dot{\gamma}_A$ (Figure 8.9).

$$\sigma_w = \frac{\left(\Delta p - \Delta p_{end}\right)}{4\left(L/D\right)} \tag{8-4}$$

Since the data for various *L/D* superpose well, it implies that the effect of pressure on viscosity is negligible (also concluded by the linearity of the Bagley plot). Similar results were obtained for all polymers studied in this work which are plotted in Figure 8.9a, b, c and d.

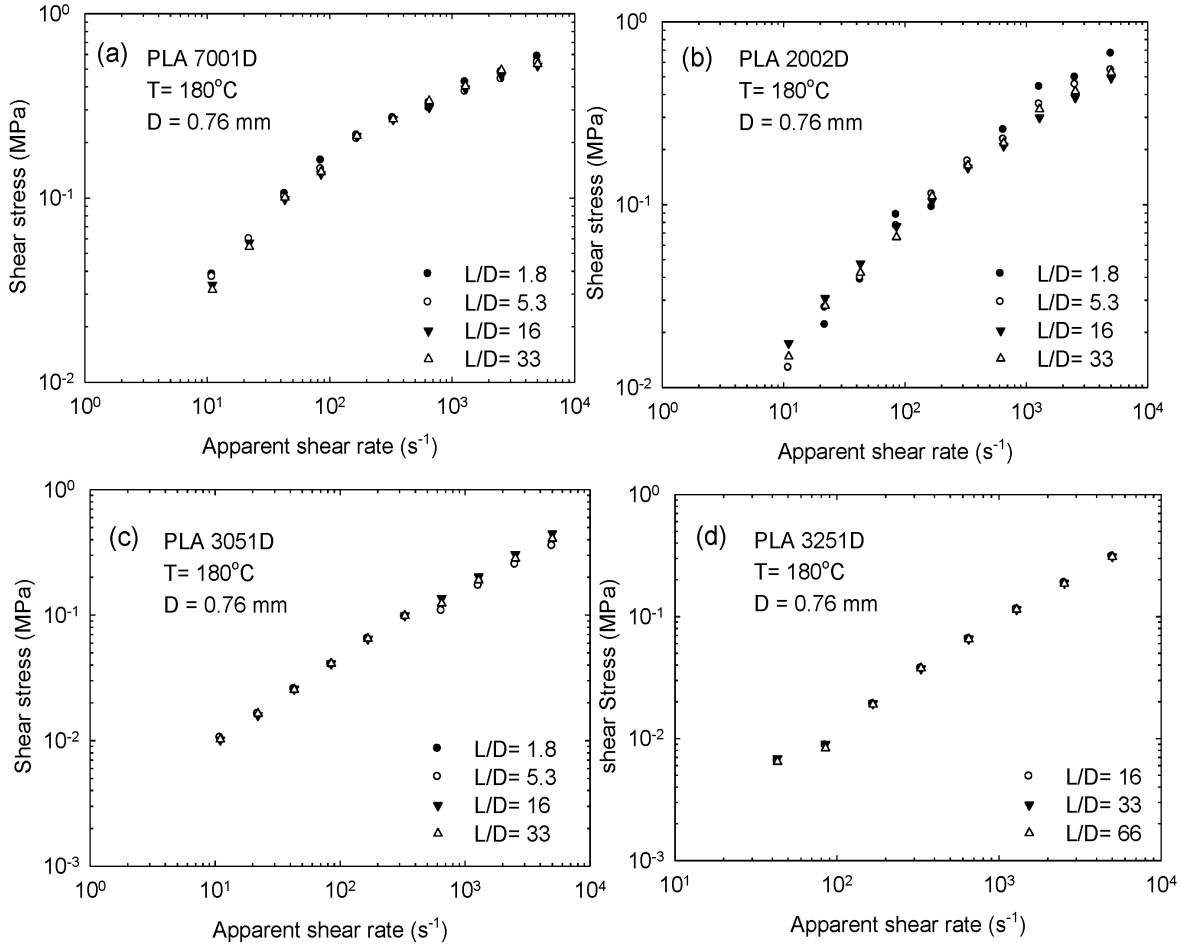

Figure 8.9: The flow curves of all PLAs for several dies having the same diameter and various *L/D* ratios at 180°C. These are essentially the apparent flow curves plotted in Figure 8.7 with the application of end pressure correction determined from Figure 8.8.

Figure 8.10 and Figure 8.11 plot the end pressure as a function of wall shear stress and apparent shear rate respectively for all PLAs studied at 180°C. The end pressure of PLA 7001D and PLA 2002D are slightly lower than the others (PLA 3051D and PLA 3251D). Beyond a certain shear stress and an apparent shear rate the end pressure of all PLAs start to converge and superpose within the experimental error. The experimental results at these

small shear stress and apparent shear rate values are subject to relatively large experimental error that might be contributed to the accuracy of the data.

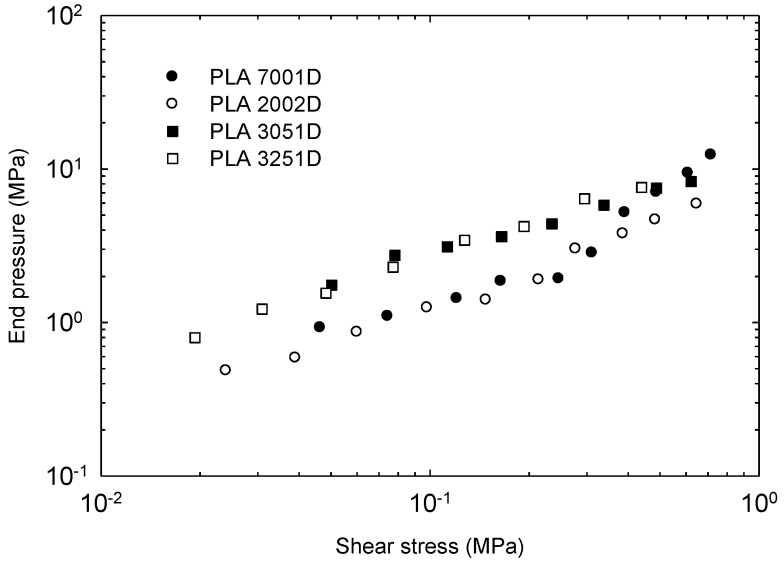

Figure 8.10: End pressure versus shear stress of all PLAs at 180°C

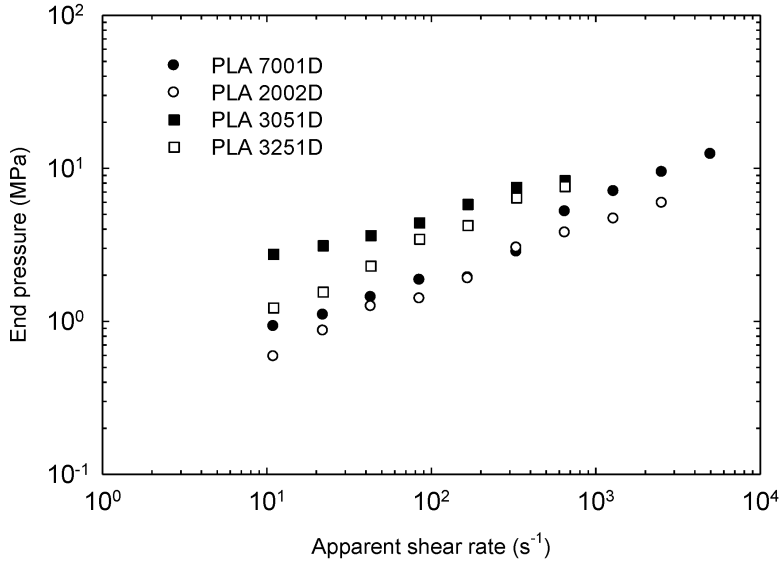

Figure 8.11: End pressure versus apparent shear rate of all PLAs at 180°C

8.2.1 Wall slip

The Mooney technique has been used here to determine the wall slip for all PLAs (Mooney 1931). Figure 8.12 shows the Bagley-corrected apparent flow curves of all PLAs for three dies having the same *L/D*=16 and different diameters (*D*=1.22 mm, 0.76 mm, and 0.43 mm).

The dynamic complex modulus is also plotted in Figure 8.12 as a function of angular frequency ($G^* \equiv \sqrt{(G'^2 + G''^2)}$ versus ω), which represents the flow curve of the polymers under no slip. The diameter dependency of the flow curves or deviation of the flow curves from the curve indicated as LVE (failure of the Cox-Merz rule) implies wall slip (Ansari et al., 2011). In fact, such deviations from the LVE curve and diameter dependence has been obtained for the three PLAs (see Figure 8.12a, b and c), whereas for the PLA having the smallest molecular weight, the no-slip boundary condition seems to apply (Figure 8.12d).

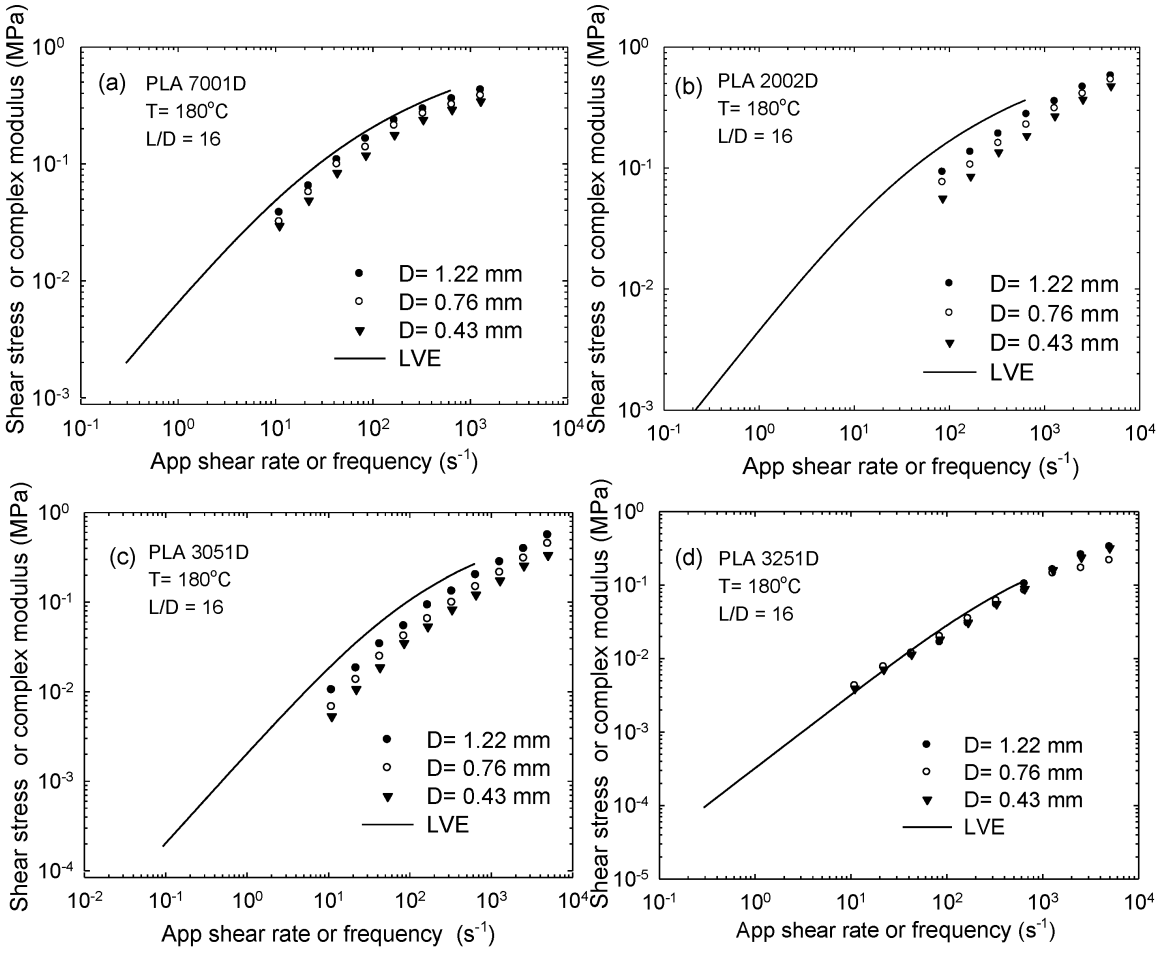

Figure 8.12: Diameter dependence of the flow curve and deviation of these from the LVE curve implies the occurrence of wall slip. As seen all PLAs slip except PLA3251D having the smallest molecular weight (a) PLA 7001D, (b) PLA 2002D, (c) PLA 3051D and (d) PLA 3251D

The Mooney technique has been used to determine wall slip as a function of wall shear stress according to the following relationship:

$$\dot{\gamma}_A = \dot{\gamma}_{A,s} + \frac{8u_s}{D} \tag{8-5}$$

where $\dot{\gamma}_{A,s}$ is the apparent shear rate corrected for the effect of slip and u_s is slip velocity. The slip velocity and true shear rate can be obtained from the slope and intercept respectively from the plot of the apparent shear rate versus 1/*D* at a fixed value of shear stress (Figure 8.13).

The deviation of each flow curve that corresponds to a different diameter from the LVE curve can also be interpreted as wall slip as discussed above. The following relationship can be used to calculate slip from the deviation of each flow curve from LVE:

$$\dot{\gamma}_A = \frac{4n_{LVE}}{3n_{LVE}+1}\omega + \frac{8u_s}{D} \tag{8-6}$$

where n_{LVE} is the local slope of the LVE curve defined as $n_{LVE} \equiv \log(G^*)/\log(\omega)$, and ω is the frequency that corresponds to a shear stress (modulus) at which the slip is calculated. If the experimental data are consistent, the slip velocities from the two methods should be the same which was the case in the present study.

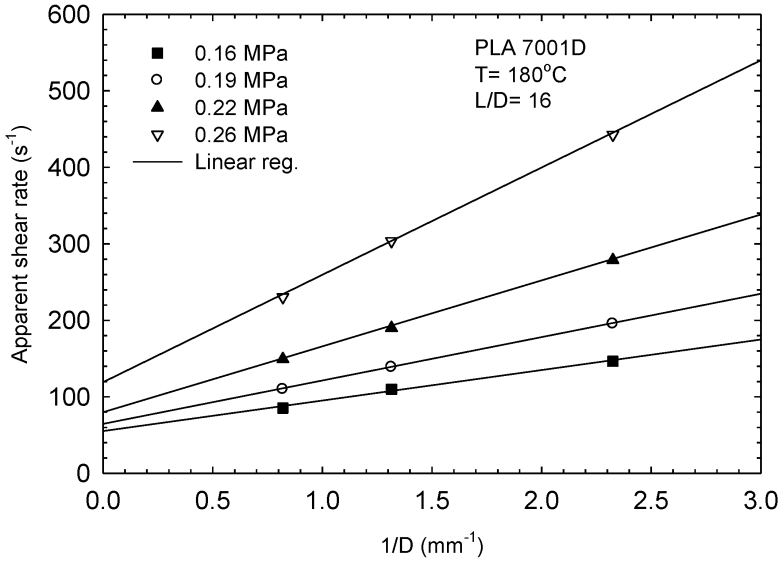

Figure 8.13: The Mooney plot for PLA7001D at 180°C, constructed to determine its slip velocity.

Figure 8.14 plots the slip velocity of PLA 7001D obtained from Mooney technique (Equation 8-5) and from the deviations of each flow curve in Figure 8.12 from the corresponding LVE curve using Equation 8-6. All four sets of data agree well and in fact the slip velocity obtained from the Mooney method is an average of the values obtained from the deviation of the three flow curves from the LVE.

The slip velocities of three PLAs are plotted in Figure 8.15. The PLA with the smallest molecular weight, namely PLA 3251D, does not slip as the flow curves did not exhibit diameter dependence (Figure 8.12d) and the flow curves agreed with the LVE data. PLA 3051D has the highest slip velocity as compared to PLA 7001D and PLA 2002D, which have higher molecular weights. It appears that the slip velocity increases with decrease of molecular weight. However, below a certain molecular weight where the molecular size is comparable to characteristic size of the asperities the slip velocity becomes zero. Previous studies have shown the same molecular weight dependence of slip velocity for nearly monodisperse or narrow molecular weight distribution polymers. Mhetar and Archer (1998a;1998b) for the case of nearly monodisperse polybutadienes, and Awati et al. (2000) and Mackay and Henson (1998) for nearly monodisperse polystyrenes have shown that slip velocity increases with decrease of molecular weight. Considering the convective constraint release mechanism for bulk and tethered chains, Joshi et al. (2001) proposed some scaling relationships that are in agreement with these experimental observations.

Figure 8.16 plots the data of Figure 8.12 corrected for slip effects in order to determine the slip corrected flow curves of all PLAs (true rheological behavior). Good agreements are obtained between the capillary and linear viscoelastic (LVE) data provided that the Rabinowitsch correction is applied on the capillary data as well. This agreement also shows the validity of the Cox–Merz rule once slip effects are accounted for.

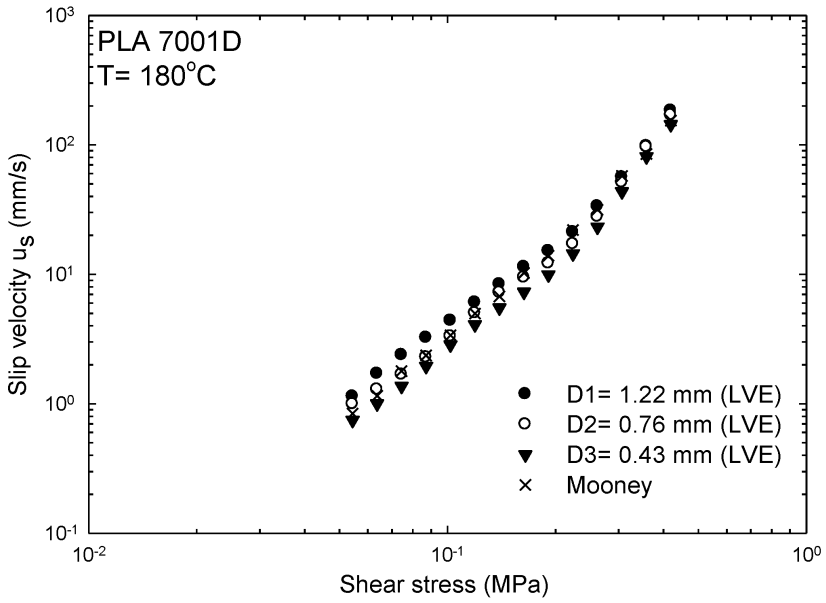

Figure 8.14: The slip velocity, u_s of resin PLA7001D determined from Mooney analysis and from deviation of various apparent flow curves from the LVE data at 180°C. Reasonable agreement between the various sets of data shows consistency of the results.

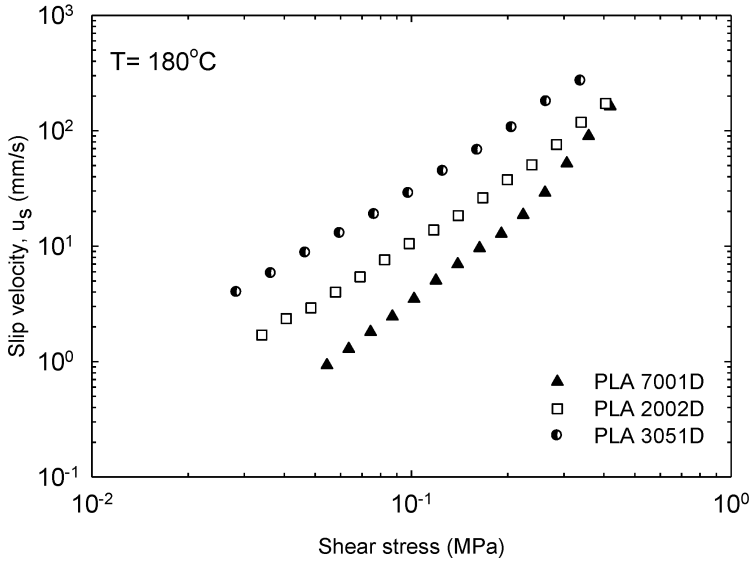

Figure 8.15: The slip velocity, u_s as a function of wall shear stress for three PLAs at 180°C.

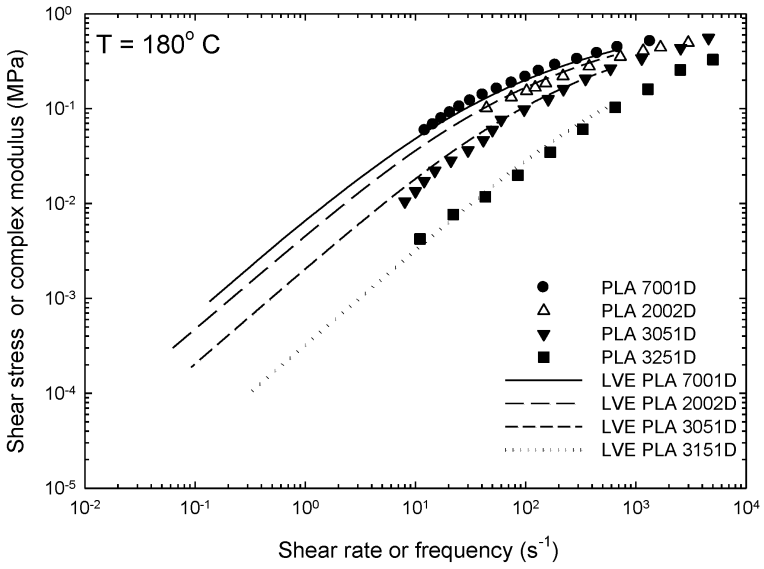

Figure 8.16: The slip corrected flow curves show an excellent agreement with the LVE data, also showing the applicability of the Cox-Merz rule once slip effects are accounted for.

8.2.2 Melt fracture

Figure 8.17 shows images of extrudates of PLA7001D obtained by extrusion through a capillary die having D=0.76 mm and *L/D*=16 at 180°C, 200°C and 220°C at various shear rates. First at 180°C, the extrudate at the shear rate of 650 s^{-1} has a relatively smooth surface (Figure 8.17). As the apparent shear rate increases, surface irregularities appear at 1285 s^{-1}, which become gross distortions at 2530 s^{-1}. Table 8.3 and Table 8.4 list the critical shear stresses and rates for the onset of extrudate distortion at the temperature of 180°C for PLA 7001D and PLA 2002D respectively. The critical shear rate depends significantly on the diameter of the die. Namely the critical shear rate for the onset of extrudate distortion decreases with increase of diameter, in accordance with the scaling of

$$\dot{\gamma}_{A,c} \propto D^{-1} \tag{8.12}$$

proposed by Howells and Benbow (1962). However, the critical condition for the onset of melt fracture is not sensitive to *L/D* ratio (Migler, 2005). No instabilities were observed for PLA 3051D and PLA 3251D at the temperature of 180°C even the highest shear rates reached in this study (about 5,000 s^{-1}). The critical stresses are slightly dependent on the

diameter and relatively independent of molecular weight, with most of the critical shear stress values in the range of 0.2-0.3 MPa.

Table 8.3: Critical shear stress and critical apparent shear rates for the onset of melt fracture of PLA 7001D at 180°C as a function of the geometrical characteristics of capillary dies.

Diameter (mm)	***L/D***	**Shear stress MPa**	**Apparent shear rate s^{-1}**
0.43	16	0.33	914
0.76	1.8	0.30	463
0.76	5.3	0.29	463
0.76	16	0.29	463
0.76	33	0.30	463
1.22	16	0.20	119

Table 8.4: Critical shear stress and critical apparent shear rates for the onset of melt fracture of PLA 2002D at 180°C as a function of the geometrical characteristics of capillary dies.

Diameter (mm)	***L/D***	**Shear stress MPa**	**Apparent shear rate s^{-1}**
0.43	16	0.31	914
0.76	1.8	0.26	914
0.76	5.3	0.26	914
0.76	16	0.25	914
0.76	33	0.26	914
1.22	16	0.23	463

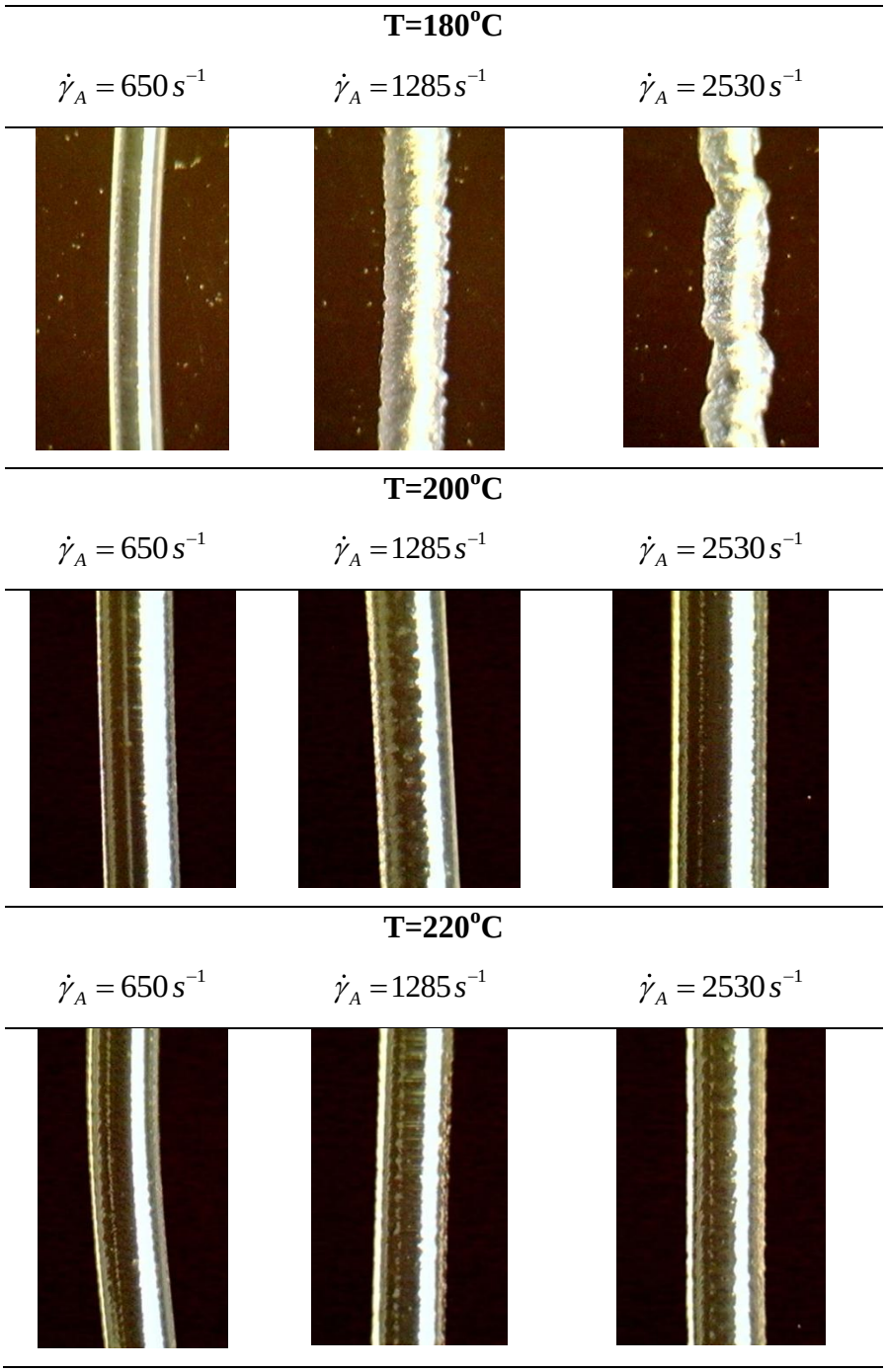

Figure 8.17: Images of PLA 7001D extrudates at different apparent shear rates and various temperatures ranging from 180°C to 220°C.

It has been reported by Howells and Benbow (1962) that two potential easy cures for extrudate distortion are either to increase or decrease the temperature (hot or cold extrusion)! They pointed out that it might only be necessary to change the boundary conditions at the exit in order to postpone the occurrence of extrudate distortion at higher rates (Migler, 2005).

Non-uniform temperature is also a possible route to eliminate melt fracture (Miller and Rothstein, 2004; Miller et al., 2006). An increase of temperature from 180^{o}C to 200^{o}C and furthermore to 220^{o}C improved extrudate appearance significantly as shown in Figure 8.17.

Figure 8.18 plots the apparent flow curves of PLA 7001D at three temperatures, namely 180^{o}C, 200^{o}C and 220^{o}C. The degree of drop in the wall shear stress scale is according to the time-Temperature superposition obtained from the linear viscoelastic measurements. Although the appearance improves as the temperature increases, the critical shear stress for the onset of these irregularities remains approximately the same.

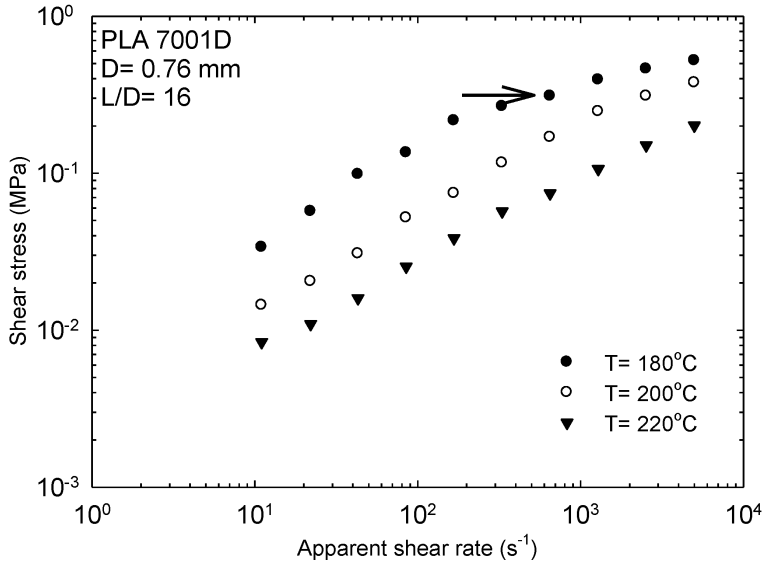

Figure 8.18: The flow curves of PLA7001D at various temperatures from 180°C to 220°C.

8.2.3 Processing aids

In order to overcome extrudate distortions and to render the processes economically feasible, polymer processing aids (PPAs) are frequently used (Achilleos et al., 2002; Amos et al., 2001; Hatzikiriakos et al., 1995; Priester et al., 1993; Rosenbaum et al., 1995). PPAs can eliminate melt fracture phenomena such as sharkskin or postpone them to higher shear (flow) rates. The end result is an increase of the productivity as well as an energy cost reduction, while high product quality is maintained. The additives mostly used are fluoropolymers (Amos et al., 2001; Priester et al., 1993) especially designed for polyolefin extrusion

processes. Amos et al. (2001) and Achilleos et al. (2002) have reviewed the formulation, applications and performance of various processing aids. As stressed by Rosenbaum et al. (1995) a potential polymer to work as a processing aid for the extrusion of another polymer should first be immiscible and have an interfacial tension with the polymer under flow smaller than the interfacial tension of the polymer under flow with the wall. Such a candidate might be a poly(ε-caprolactone) (PCL) polymer of similar viscosity, which is immiscible with PLA (Arraiza et al., 2007; Sarazin et al., 2008; Takayama and Todo, 2006; Wu et al., 2006).

Extrusion experiments were performed for PLA 7001D (most severe melt fracture behavior) with addition of 0.5 wt% of commercial PCL, Capa® 6500 (see section 4.1 for more details). The two polymers were grinded and mixed in dry form and then loaded into the barrel of the capillary rheometer. Figure 8.19 depicts a transient experiment illustrating the process of wall coating by the presence of PCL. First, Figure 8.19 (left) shows the pressure transient for the capillary extrusion of pure PLA 7001D by using a die having a diameter equal to 0.76 cm and *L/D* ratio of 16. The pressure drop increases slowly and after a certain time assumes a steady-state value. When the blend of PLA+ 0.5 wt% PCL is extruded through a die (Figure 8.19 right), the pressure drop passes through a maximum and as the PCL gradually coats the interface of the die, slip becomes a factor and as a result the pressure drop starts decreasing. The steady-state value is obtained after filling the reservoir four times. The steady-state value of the apparent shear stress in the presence of 0.5 wt% of PCL is significantly lower compared to that in the absence of PCL. This is clearly due to the occurrence of slip.

Figure 8.20 shows the apparent flow curves obtained at 180^{o}C for pure PLA 7001D and that of a blend of PLA 7001D with 0.5 wt% of the finely dispersed PCL. No end pressure (Bagley) correction was applied in this plot. The presence of the PCL dramatically decreases the shear stress practically over the whole range of apparent shear rates up to 5,000 s^{-1}.

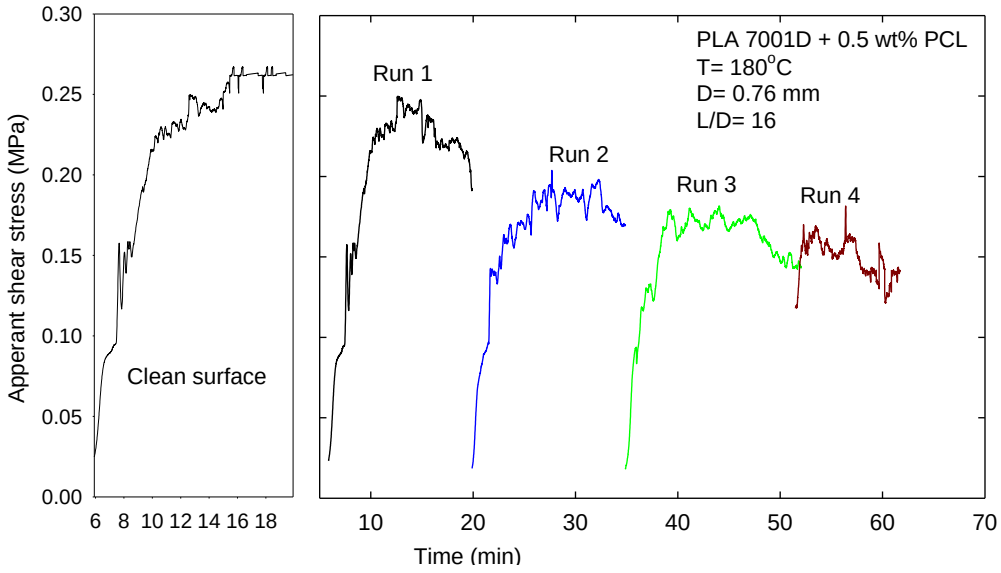

Figure 8.19: The effect of the addition of 0.5 wt % of a poly(ε-caprolactone) (PCL) on the transient response in the capillary extrusion of PLA7001D at 180°C.

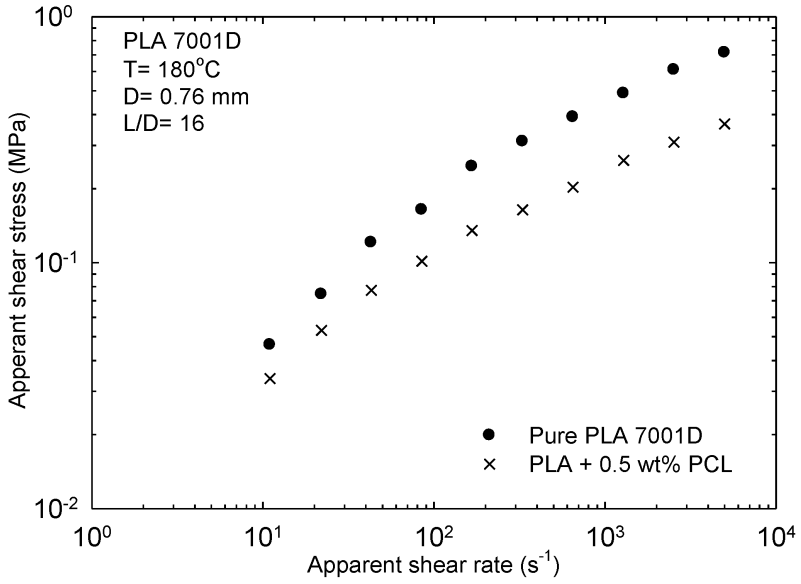

Figure 8.20: The effect of the addition of 0.5 wt % of a poly(ε-caprolactone) (PCL) on the flow curve of resin PLA 7001D at 180°C using a die with D=0.76 mm and L/D=16.

The presence of PCL completely eliminates melt fracture. Thus, the extrudates appear relatively smooth up to the shear rates of 5000 s^{-1} as can be seen from Figure 8.21. The fracture elimination by PCL arises from interfacial slip which decreases the effective

deformation of the melt significantly particularly at the exit where surface melt fracture originates (Migler, 2005).

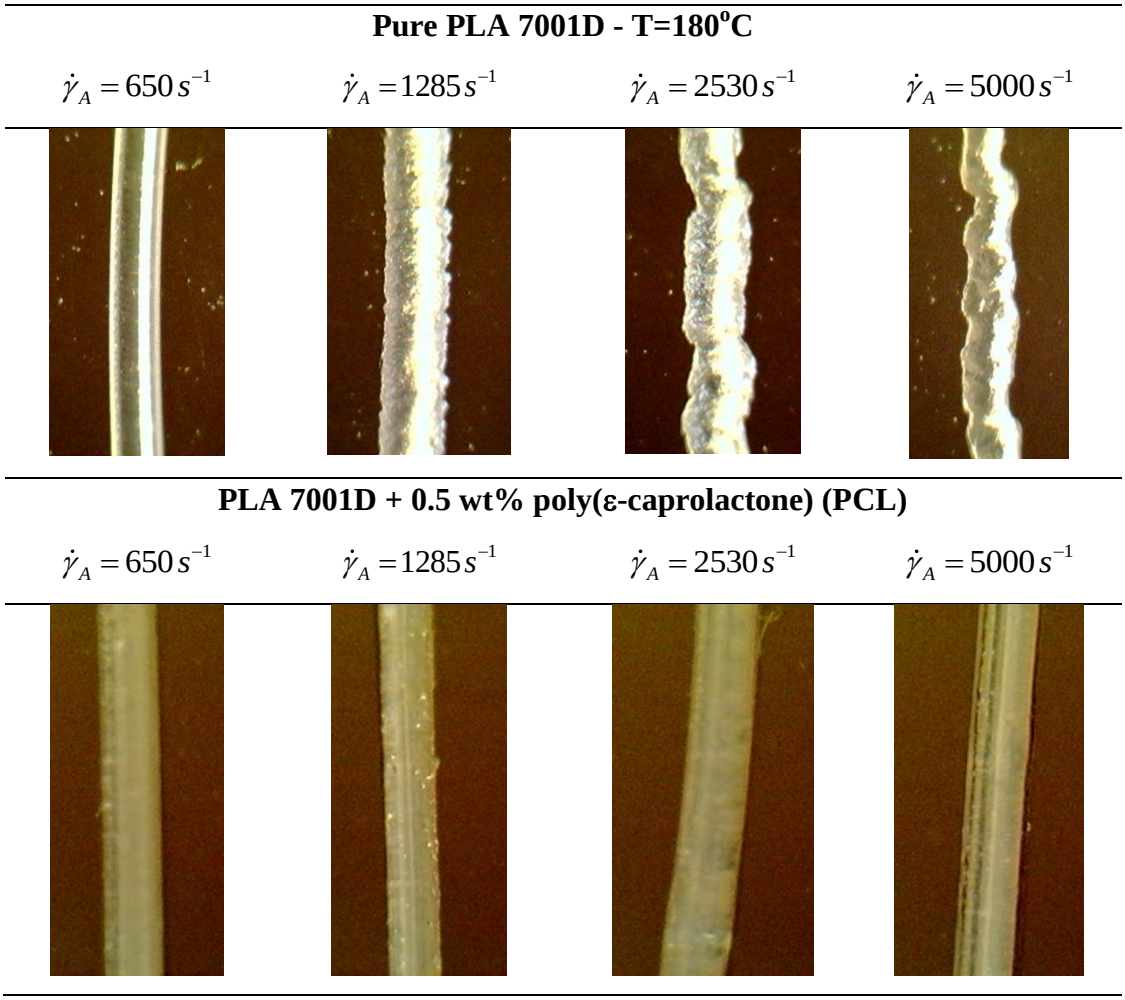

Figure 8.21: Images of PLA 7001D extrudates at different apparent shear rates extruded with and without 0.5 wt% of a PCL at 180°C. The addition of a PCL is an effective way to eliminate melt fracture in the extrusion of PLA.

8.3 Summary

The wall slip and melt fracture behavior of four commercial PLAs as well as their rheological properties under shear and extensional have been investigated. The linear viscoelastic and extensional behavior of melts has indicated linear structure behavior. This property was in agreement with data previously reported in the literature in terms of the variation of the zero-shear viscosity with molecular weight.

PLAs with molecular weights greater than a certain value slipped significantly, with the slip velocity to increase with decrease of molecular weight. While this finding seems counterintuitive, it appears to be consistent with findings on the slip behavior of other nearly monodisperse polymers such as polybutadienes and polystyrenes. The capillary data agreed well with linear viscoelastic envelope (LVE) once correction for slip effects was applied and thus the Cox-Merz rule appears applicable.

The onset of melt fracture for the high molecular weight PLAs occurred at around 0.2 to 0.3 MPa, depending on the geometrical characteristics of the dies, and nearly independent of temperature. The critical shear rate for the onset of melt fracture scales inversely with the die diameter consistent with observations on the melt fracture of other polymers such as polyethylenes. Finally, addition of 0.5 wt% PCL was effective in eliminating and delaying the onset of melt fracture to higher shear rates. Thus, a small amount of PCL may be used as a processing aid for the processing of PLAs.

9 Conclusions, Contribution to Knowledge and Recommendations

9.1 Conclusions

The thermal, solution and melt rheological properties of newly synthesized PLA have been investigated for different optical compositions and molecular weights. First, regarding the solution properties, the values of the Mark-Houwink parameters and characteristic radii agreed with values reported for other PLA as well as other linear flexible polymers. From linear viscoelasticity, the time-Temperature superposition applies well on the linear viscoelastic data of stabilized PLA indicating that the PLA are themorheologically simple fluids. The molecular weight between entanglements of approximately 4,400 g/mol was calculated from the plateau modulus of 0.9 MPa ± 0.2 that independent of optical composition. The scaling of zero-shear viscosities and longest relaxation times of nearly monodisperse are consistent with those reported for other well-entangled linear macromolecules. Strain hardening was observed at low temperature and high Hencky strain rate. This behavior disappears when the longest relaxation time is smaller than the characteristic time of deformation. Increase of chain mobility at high temperature ease the chain relaxation, thus low degree of chain orientation occurs. Nevertheless the strain hardening is possible for these linear polymers for cases when the longest relaxation time is larger than the characteristic time of deformation. The strain hardening behavior of PLAs was successfully predicted by K-BKZ constitutive equation and proved that such behavior (strain hardening) was due solely to the dynamic of molecular relaxation.

The thermal, rheological and mechanical properties of blends of homopolymer PLAs, and equivalent diblock copolymers have also been investigated as functions of molecular characteristics. Addition of amorphous PLA decreased the crystalline content in the blends of homopolymer PLAs; however the melting points remain unchanged. The crystallization of diblock copolymers was different from that of equivalent blends as a result of the covalent connection between PLLA and PDLLA block that restricts molecular flexibility for ease of molecular orientation. As a result, the crystallinity of diblocks decreases compared to that of the corresponding blends. For PLLA-*b*-PDLA diblocks, formation of stereocomplex crystallites lead to a high melting point (>200 °C). Block copolymers PLLA-*b*-PDLLA-*b*-PDLA crystallized into exclusively stereocomplex crystal where only one melting temperature can be observed. The linear viscoelastic behavior of copolymers was

independent of block length ratio. Han's method was used to confirm the disordered state which also indicated by the terminal zone of slope 1 and 2 of G'' and G'. The relationship between zero-shear viscosities and molecular weight can be described by $\eta_o \propto M_w^{3.4}$ which also agrees with nearly monodisperse homopolymers PLAs reported previously. In the presence of stereocomplex crystallites (double melting peaks), diblock copolymers PLLA-*b*-PDLA show a viscosity enhancement at high temperatures between the two peak temperatures compared to pure homopolymers. Interestingly, the viscosity enhancement of triblock copolymers PLLA-*b*-PDLLA-*b*-PDLA with PDLLA located in the middle block was delayed to lower temperature despite having a single high melting temperature (~210°C).

From tensile testing, diblock and triblock copolymers of PLLA and PDLLA as well as PLLA and PDLA show promising improvements in tensile strength and elongation at break compared to the corresponding homopolymers and blends. However, PLLA\PLDLA blends show mechanical properties lower than those of their pure components due to phase separation that possibly happens during quenching to room temperature. Triblock of PLLA-*b*-aPHB-*b*-PDLA with middle block of atactic PHB showed poor tensile properties even though amorphous PHB is known as an elastomeric polymer. The PHB hindered the crystallization of stereocomplex thus deteriorated the tensile properties of the copolymers.

The wall slip and melt fracture behavior of commercial PLAs as well as their rheological properties under shear and extensional have been investigated. The solution properties and linear viscoelastic behavior of melts have indicated linear structure behavior. These properties were in agreement with such as solution properties and melt properties in terms of the variation of the zero-shear viscosity with molecular weight previously reported in the literature. The end pressure and slip corrections have been applied to the capillary data. After a certain value of molecular weights the PLAs were slipped significantly, with the slip velocity to increase with decrease of the molecular weight. While this finding seems counterintuitive, it appears to be consistent with findings on the slip behavior of other nearly monodisperse polymers such as polybutadienes and polystyrenes. The Cox-Merz rule is satisfied once the capillary data have been corrected for slip effects and the data agreed well with linear viscoelastic envelope (no slip effects). The onset of melt fracture for PLA 7001D and PLA 2002D occurred at around 0.2 to 0.3 MPa, depending on the geometrical characteristics of the dies, and nearly independent of temperature. The critical shear rate for

the onset of melt fracture scaled inversely proportional with the die diameter consistent with observations on the melt fracture of other polymers such as polyethylenes. Finally, addition of 0.5 wt% poly(ε-caprolactone) (PCL) was effective in eliminating and delaying the onset of melt fracture to higher shear rates. Thus, a small amount of PCL may be used as a processing aid for the processing of PLAs.

9.2 Contributions to Knowledge

The present work has yielded the following contribution to knowledge

1. The thermorheological properties of newly synthesized PLA with moderated isotacticity have been studied as a function of molecular weight and optical composition. Despite having moderated isotacticity, P_m value of about 0.6, the thermorheological properties are similar to PLA reported in literature.
2. Extensional rheology of PLA has been studied over a wide range of temperatures and Hencky strain rates. Using nearly monodisperse PLA proves that polydispersity contributed to strain hardening suggested in previous studies. It is confirmed that strain hardening is possible for linear polymers for cases when the longest relaxation time is larger than the characteristic time of deformation. This behavior was due to the dynamic of molecular relaxation and was successfully predicted by the K-BKZ constitutive equation.
3. Block copolymerization of PLA with its enantiomers can be used to improve mechanical properties to some extent. Despite having similar melt properties, the thermal and mechanical properties can be manipulated by changing the block length ratio. Block copolymers of PLLA-*b*-PDLLA-*b*-PLLA improved PLA brittleness. Exclusively stereocomplex crystals can be obtained by block copolymers PLLA-*b*-PDLLA-*b*-PDLA.
4. A detailed study on the processing of commercials PLA as a function of molecular weight was performed in a systematic manner. The slip and melt fracture phenomena were studied as a functions of molecular weight. The slip velocity of PLAs has been quantified as a function of the wall shear stress and molecular weight and such data

can be directly used in simulations of various processes. Small amount of PCL can be used as a processing aid to PLA processing.

9.3 Recommendations for Future Work

There are several aspects of this work that could be investigated in the future. Some suggestion and recommendations on future studies are as follows:

1. A detailed, systematic study using an *in-situ* crystallization apparatus (*e.g.* wide-angle X-ray scattering (WAXS)) can be carried out to gain better understanding of the crystallization of moderate-isotaciticy PLA under flow. In other words, shear induced crystallization studies are needed and ways of enhancing the crystallization of PLAs are desirable to be identified.
2. A detailed study of the crystallization kinetics and mechanism of crystallization of diblock and triblock copolymers can be performed to understand and explain some of thermal behavior observed in the present study *i.e.* formation of exclusively stereocomplex crystals.
3. Synthesis and thermorheological study of triblock copolymers of PLA with different middle blocks, specifically crystalline biodegradable polymer *e.g.* crystalline PHB.
4. An additional study on the effect of polydispersity on the slip behavior of PLA is needed. At this point synergistic effects of molecular weight and its distributions is not known. Furthermore, a study of the occurrence of stick-slip in the case of PLAs could also be carried out (Hatzikiriakos, 2012).
5. Identify more polymers and/or additives that are immiscible with PLA and investigate their performance as possible processing aids for the extrusion of PLA.

Bibliography

Abe, H., Doi, Y., Satkowski, M. M., Noda, I. (1994). Miscibility and morphology of blends of isotactic and atactic poly(3-hydroxybutyrate). *Macromolecules, 27*(1), 50-54.

Achilleos, E., Georgiou, G., Hatzikiriakos, S. (2002). Role of processing aids in the extrusion of molten polymers. *Journal of Vinyl & Additive Technology, 8*(1), 7-24.

Acosta-Ramirez, A., Douglas, A. F., Yu, I., Patrick, B. O., Diaconescu, P. L., Mehrkhodavandi, P. (2010). Synthesis and structural studies of chiral indium(III) complexes supported by tridentate diaminophenol ligands. *Inorganic Chemistry, 49*(12), 5444-5452.

Agrawal, A., Bhalla, R. (2003). Advances in the production of poly(lactic acid) fibers. A review. *Journal of Macromolecular Science-Polymer Reviews, 43*(4), 479-503.

Albertsson, A., Varma, I. K., Lochab, B., Finne-Wistrand, A., Kumar, K. (2010). Design and synthesis of different types of poly(lactic acid). In Auras, R., Lim, L. T., Selke, S. E. M., Tsuji H. (Eds.1), *Poly(lactic acid): Synthesis, structure, properties, processing and applications*. New Jersey: John Wiley & Son, Inc.

Amos, S. E., Giacoletto, G. M., Horns, J. H., Lavallee, C., Woods, S. S. (2001). *Polymer processing aids (PPA) in plastic additives*. Munich: Hanser.

Ansari, M., Hatzikiriakos, S. G., Sukhadia, A. M., Rohlfing, D. C. (2011). Rheology of ziegler-natta and metallocene high-density polyethylenes: Broad molecular weight distribution effects. *Rheologica Acta, 50*(1), 17-27.

Archer, L. A. (2005). Wall slip: Measurement and modelling issues. In S. G. Hatzikiriakos, K. B. Migler (Eds.), *Polymer processing instabilities*. New York: Marcel Dekker.

Arraiza, A. L., Sarasua, J. R., Verdu, J., Colin, X. (2007). Rheological behavior and modeling of thermal degradation of poly(epsilon-caprolactone) and poly(L-lactide). *International Polymer Processing, 22*(5), 389-394.

Auhl, D., Kaschta, J., Munstedt, H., Kaspar, H., Hintzer, K. (2006). Molecular characterization of semi-fluorinated copolymers with a controlled amount of long-chain branching. *Macromolecules, 39*(6), 2316-2324.

Auras, R., Harte, B., Selke, S. (2004). An overview of polylactides as packaging materials. *Macromolecular Bioscience, 4*(9), 835-864.

Awati, K., Park, Y., Weisser, E., Mackay, M. (2000). Wall slip and shear stresses of polymer melts at high shear rates without pressure and viscous heating effects. *Journal of Non-Newtonian Fluid Mechanics, 89*(1-2), 117-131.

Baumgaertel, M., Schausberger, A., Winter, H. H. (1990). The relaxation of polymers with linear flexible chains of uniform length. *Rheologica Acta, 29*(5), 400-408.

Baumgaertel, M., Winter, H. H. (1989). Determination of the discrete relaxation time spectrum from dynamic mechanical data. *ANTEC 89*, 1652-1655.

Bigg, D. (1996). Effect of copolymer ratio on the crystallinity and properties of polylactic acid copolymers. *ANTEC 96, 42*, 2028-2039.

Blundell, D., Mahendrasingam, A., Martin, C., Fuller, W., MacKerron, D., Harvie, J., et al. (2000). Orientation prior to crystallisation during drawing of poly(ethylene terephthalate). *Polymer, 41*(21), 7793-7802.

Bouapao, L., Tsuji, H., Tashiro, K., Zhang, J., Hanesaka, M. (2009). Crystallization, spherulite growth, and structure of blends of crystalline and amorphous poly(lactide)s. *Polymer, 50*(16), 4007-4017.

Burchard, W. (1999). Solution properties of branched macromolecules. *Advances in Polymer Science*, 113-113.

Carlson, D., Dubois, P., Nie, L., Narayan, R. (1998). Free radical branching of polylactide by reactive extrusion. *Polymer Engineering and Science*, 38(2), 311-321.

Cicero, J. A., Dorgan, J. R., Dec, S. F., Knauss, D. M. (2002). Phosphite stabilization effects on two-step melt-spun fibers of polylactide. *Polymer Degradation and Stability, 78*(1), 95-105.

Chang, L., Woo, E. M. (2011). Effects of molten poly(3-hydroxybutyrate) on crystalline morphology in stereocomplex of poly(L-lactic acid) with poly(D-lactic acid). *Polymer*, 52(1), 68-76.

Cheung, M., Carduner, K., Golovoy, A., Vanoene, H. (1990). Studies on the role of organophosphites in polyester blends .2. The inhibition of ester-exchange reactions. *Journal of Applied Polymer Science*, 40(5-6), 977-987.

Coates, G. W., Ovitt, T. M. (1999). Synthesis of new poly(lactic acid) microstructures. *Abstracts of Papers of the American Chemical Society, 218*, 207.

Conrad, J. D. (2009). The Rheology, Degradation, Processing and Characterization of Renewable Resource Polymers. (PhD, Chemical Engineering, Clemson University).

Cooper-White, J., Mackay, M. E. (1999). Rheological properties of poly(lactides). effect of molecular weight and temperature on the viscoelasticity of poly(l-lactic acid). *Journal of Polymer Science, Part B: Polymer Physics, 37*(15), 1803-1814.

de Jong, S., van Dijk-Wolthuis, W., Kettenes-van den Bosch, J., Schuyl, P., Hennink, W. (1998). Monodisperse enantiomeric lactic acid oligomers: Preparation, characterization, and stereocomplex formation. *Macromolecules*, 31(19), 6397-6402.

Dealy, J. M., Wissbrun, K. F. (1999). *Melt rheology and its role in plastic processing*. New York: Van Nostrand Reinhold.

Dealy, J. M., Kim, S. (2005). Gross melt fracture in extrusion. In S. G. Hatzikiriakos, K. B. Migler (Eds.1), *Polymer processing instabilities*. New York: Marcel Dekker.

Dechy-Cabaret, O., Martin-Vaca, B., Bourissou, D. (2004). Controlled ring-opening polymerization of lactide and glycolide. *Chemical Reviews, 104*(12), 6147-6176.

Doi, M., Edwards, S.F. (1986). *The theory of Polymer Dynamics.* New York: Oxford University Press.

Dorgan, J. R., Williams, J. S., Lewis, D. N. (1999). Melt rheology of poly(lactic acid): Entanglement and chain architecture effects. *Journal of Rheology, 43*(5), 1141-1155.

Dorgan, J. R., Janzen, J., Clayton, M. P., Hait, S. B., Knauss, D. M. (2005a). Melt rheology of variable L-content poly(lactic acid). *Journal of Rheology, 49*(3), 607-619.

Dorgan, J. R., Janzen, J., Knauss, D. M., Hait, S. B., Limoges, B. R., Hutchinson, M. H. (2005b). Fundamental solution and single-chain properties of polylactides. *Journal of Polymer Science, Part B: Polymer Physics, 43*(21), 3100-3111.

Dorgan, J. R., Janzen, J., Knauss, D., Braun, B. (2004). Melt rheology of polylactides. *ANTEC 2004, 2,* 1740-1743.

Dorgan, J., Lehermeier, H., Mang, M. (2000). Thermal and rheological properties of commercial-grade poly(lactic acid)s. *Journal of Polymers and the Environment, 8*(1), 1-9.

Douglas, A. F., Patrick, B. O., Mehrkhodavandi, P. (2008). A highly active chiral indium catalyst for living lactide polymerization. *Angewandte Chemie - International Edition, 47*(12), 2290-2293.

Ferry, J. D. (1980). Viscoelastic properties of polymers. 3rd edition. New York: John Wiley & Sons, Inc.

Fuchs, K., Friedrich, C., Weese, J. (1996). Viscoelastic properties of narrow-distribution poly(methyl methacrylates). *Macromolecules, 29*(18), 5893-5901.

Fukushima, K., Furuhashi, Y., Sogo, K., Miura, S., Kimura, Y. (2005). Stereoblock poly(lactic acid): Synthesis via solid-state polycondensation of a stereocomplexed mixture of poly(L-lactic acid) and poly(D-lactic acid). *Macromolecular Bioscience, 5*(1), 21-29.

Fukushima, K., Kimura, Y. (2006). Stereocomplexed polylactides (neo-PLA) as high-performance bio-based polymers: Their formation, properties, and application. *Polymer International, 55*(6), 626-642.

Fukushima, K., Hirata, M., Kimura, Y. (2007). Synthesis and characterization of stereoblock poly(lactic acid)s with nonequivalent D/L sequence ratios. *Macromolecules, 40*(9), 3049-3055.

Garlotta, D. (2001). A literature review of poly(lactic acid). *Journal of Polymers and the Environment, 9*(2), 63-84.

Georgiou, G. (2005). Stick-slip instability. In S. G. Hatzikiriakos, K. B. Migler (Eds.1), *Polymer processing instabilities*. New York: Marcel Dekkar.

Gevgilili, H., Kalyon, D.M. (2001). Step-strain flow: Wall slip effects and other error sources. *Journal of Rheology*, 45, 467-475.

Grijpma, D., Penning, J., Pennings, A. (1994). Chain entanglement, mechanical-properties and drawability of poly(lactide). *Colloid and Polymer Science, 272*(9), 1068-1081.

Groot, W., van Krieken, J., Sliekersl, O., de Vos, S. (2010). Production and purification of lactic acid and lactide. In Auras, R., Lim, L. T., Selke S. E. M., Tsuji H. (Eds.1), *Poly(lactic acid): Synthesis, structure, properties, processing and applications*. New Jersey: John Wiley & Son, Inc.

Gupta, A. P., Kumar, V. (2007). New emerging trends in synthetic biodegradable polymers - polylactide: A critique. *European Polymer Journal, 43*(10), 4053-4074.

Han, C., Kim, J. (1987). Rheological technique for determining the order - disorder transition of block copolymers. *Journal of Polymer Science Part B-Polymer Physics, 25*(8), 1741-1764.

Hatzikiriakos, S. G., Dealy, J. (1991). Wall slip of molten high-density polyethylene .1. sliding plate rheometer studies. *Journal of Rheology, 35*(4), 497-523.

Hatzikiriakos, S. G., Dealy, J. (1992a). Wall slip of molten high-density polyethylenes .2. capillary rheometer studies. *Journal of Rheology, 36*(4), 703-741.

Hatzikiriakos, S. G., Dealy J. (1992b). Role of slip and fracture in the oscillating flow of HDPE in a capillary. *Journal of Rheology*, 36, 845-884.

Hatzikiriakos, S. G., Hong, P., Ho, W., Stewart, C. (1995). The effect of teflon coatings in polyethylene capillary extrusion. *Journal of Applied Polymer Science, 55*(4), 595-603.

Hatzikiriakos, S. G., Kapnistos, M., Vlassopoulos, D., Chevillard, C., Winter, H. H., Roovers, J. (2000). Relaxation time spectra of star polymers. *Rheologica Acta, 39*(1), 38-43.

Hatzikiriakos, S.G., Migler, K. B. (2005). Overview of processing instabilities In S. G. Hatzikiriakos, K. B. Migler (Eds.1), *Polymer processing instabilities*. New York: Marcel Dekker.

Hatzikiriakos, S. G. (2012). Wall Slip of Molten Polymers, *Progress in Polymer Science*, 37, 624-643.

Hiki, S., Miyamoto, M., Kimura, Y. (2000). Synthesis and characterization of hydroxy-terminated [RS]-poly(3-hydroxybutyrate) and its utilization to block copolymerization with L-lactide to obtain a biodegradable thermoplastic elastomer. *Polymer, 41*(20), 7369-7379.

Hoogsteen, W., Postema, A., Pennings, A., Tenbrinke, G., Zugenmaier, P. (1990). Crystal-structure, conformation, and morphology of solution-spun poly(L-lactide) fibers. *Macromolecules, 23*(2), 634-642.

Hormnirun, P., Marshall, E., Gibson, V., White, A., Williams, D. (2004). Remarkable stereocontrol in the polymerization of racemic lactide using aluminum initiators

supported by tetradentate aminophenoxide ligands. *Journal of the American Chemical Society*, *126*(9), 2688-2689.

Howells, E. R., Benbow, J. J. (1962). Flow defects in polyethylene melts. *Transactions and Journal Plastics Institute* , 30, 240–253.

Ikada, Y., Jamshidi, K., Tsuji, H., Hyon, S. (1987). Stereocomplex formation between enantiomeric poly(lactides). *Macromolecules*, *20*(4), 904-906.

Ikada, Y., Tsuji, H. (2000). Biodegradable polyesters for medical and ecological applications. *Macromolecular Rapid Communications*, *21*(3), 117-132.

Jackson, J. K., De Rosa, M. E., Winter, H. H. (1994). Molecular weight dependence of relaxation time spectra for the entanglement and flow behavior of monodisperse linear flexible polymers. *Macromolecules*, *27*(9), 2426-2631.

Joshi, Y., Lele, A., Mashelkar, R. (2001). Molecular model for wall slip: Role of convective constraint release. *Macromolecules*, *34*(10), 3412-3420.

Kainthan, R. K., Muliawan, E. B., Hatzikiriakos, S. G., Brooks, D. E. (2006). Synthesis, characterization, and viscoelastic properties of high molecular weight hyperbranched polyglycerols. *Macromolecules*, *39*(22), 7708-7717.

Kalika, D., Denn, M.M. (1987). Wall slip and extrudate distortion in linear low-density polyethylene. *Journal of Rheology*,31, 815-834.

Kalyon, D.M., Gevgilili, H. (2003). Wall slip and extrudate distortion of three polymer melts. *Journal of Rheology,* 47, 683-699.

Kanev, D., Takacs, E., Vlachopoulos, J. (2007). Rheological evaluation and observations of extrusion instabilities of biodegradable polyesters. *International Polymer Processing*, *22*(5), 395-401.

Kasehagen, L. J., Macosko, C. W. (1998). Nonlinear shear and extensional rheology of long-chain randomly branched polybutadiene. *Journal of Rheology, 42*(6), 1303-1327.

Keith, H. D., Padden Jr., F. J. (1987). Sperulitic morphology in polyethylene and isotactic polystyrene: influence of diffusion of segregated species. *Journal of Polymer Science, Part B: Polymer Physics, 25*(11), 2371-2392.

Keith, H. D., Padden, J., F.J. (1964). Spherulitic crystallization from melt. *Journal of Applied Physics, 35*(4), 1270-1296.

Komazawa, Y., Tang Z. (2008). Process for producing polylactic acid block copolymer. *Patent Application*, PCT/JP2007/065778.

Lehermeier, H. J., Dorgan, J. R. (2001). Melt rheology of poly(lactic acid): Consequences of blending chain architectures. *Polymer Engineering and Science, 41*(12), 2172-2184.

Li, L., Zhong, Z., De Jeu, W. H., Dijkstra, P. J., Feijen, J. (2004). Crystal structure and morphology of poly(L-lactide-b-D-lactide) diblock copolymers. *Macromolecules, 37*(23), 8641-8646.

Lim, L., Auras, R., Rubino, M. (2008). Processing technologies for poly(lactic acid). *Progress in Polymer Science (Oxford), 33*(8), 820-852.

Mackay, M., Henson, D. (1998). The effect of molecular mass and temperature on the slip of polystyrene melts at low stress levels. *Journal of Rheology, 42*(6), 1505-1517.

Mahendrasingam, A., Blundell, D., Martin, C., Fuller, W., MacKerron, D.H., Harvie, J.L., Oldman, R.J., Riekel, C. (2000). Influence of temperature and chain orientation on the crystallization of poly(ethylene terephthalate) during fast drawing. *Polymer, 41*(21), 7803-7814.

Mahendrasingam, A., Blundell, D., Parton, M., Wright, A., Rasburn, J., Narayanan, T., Fuller, W. (2005). Time resolved study of oriented crystallisation of poly(lactic acid) during rapid tensile deformation. *Polymer, 46*(16), 6009-6015.

Mahendrasingam, A., Blundell, D., Wright, A., Urban, V., Narayanan, T., Fuller, W. (2003). Observations of structure development during crystallisation of oriented poly(ethylene terephthalate). *Polymer*, *44*(19), 5915-5925.

Majerska, K., Duda, A. (2004). Stereocontrolled polymerization of racemic lactide with chiral initiator: Combining stereoelection and chiral ligand-exchange mechanism. *Journal of the American Chemical Society, 126*(4), 1026-1027.

Mhetar, V., Archer, L. (1998a). Slip in entangled polymer melts. 1. General features. *Macromolecules, 31*(24), 8607-8616.

Mhetar, V., Archer, L. (1998b). Slip in entangled polymer solutions. *Macromolecules, 31*(19), 6639-6649.

Migler, K.B., Hervet, H., Leger, L. (1993) Slip transition of a polymer melt under shear stress. *Physical Review Letters,* 70, 287-290.

Migler, K. B. (2005). Sharkskin instability in extrusion In S. G. Hatzikiriakos, K. B. Migler (Eds.1), *Polymer processing instabilities*. New York: Marcel Dekker.

Miller, E., Rothstein, J. (2004). Control of the sharkskin instability in the extrusion of polymer melts using induced temperature gradients. *Rheologica Acta, 44*(2), 160-173.

Miller, E., Lee, S. J., Rothstein, J. P. (2006). The effect of temperature gradients on the sharkskin surface instability in polymer extrusion through a slit die. *Rheologica Acta, 45*(6), 943-950.

Miyaki, Y., Einaga, Y., Fujita, H., Fukuda, M. (1980). Flory viscosity factor for the system polystyrene + cyclohexane at 34.5°C. *Macromolecules, 13*(3), 588-592.

Mooney, M. (1931). Explicit formulas for slip and fluidity. *Journal of Rheology,* 2, 210-222.

Nampoothiri, K. M., Nair, N. R., John, R. P. (2010). An overview of the recent developments in polylactide (PLA) research. *Bioresource Technology, 101*(22), 8493-8501.

Numata, K., Srivastava, R. K., Finne-Wistrand, A., Albertsson, A., Doi, Y., Abe, H. (2007). Branched poly(lactide) synthesized by enzymatic polymerization: Effects of molecular branches and stereochernistry on enzymatic degradation and alkaline hydrolysis. *Biomacromolecules, 8*(10), 3115-3125.

Opaprakasit, P., Opaprakasit, M. (2008). Thermal properties and crystallization behaviors of polylactide and its enantiomeric blends. *Macromolecular Symposia*, 264(1), 113-120.

Othman, N., Acosta-Ramirez, A., Mehrkhodavandi, P., Dorgan, J. R., Hatzikiriakos, S. G. (2011). Solution and melt viscoelastic properties of controlled microstructure poly(lactide). *Journal of Rheology, 55*(5), 987-1005.

Othman, N., Jazrawi, B., Mehrkhodavandi, P., Hatzikiriakos, S.G. (2012). Wall slip and melt fracture of poly(lactides). *Rheologica Acta*, 51,357-369.

Ovitt, T., Coates, G. (2002). Stereochemistry of lactide polymerization with chiral catalysts: New opportunities for stereocontrol using polymer exchange mechanisms. *Journal of the American Chemical Society, 124*(7), 1316-1326.

Palade, L., Lehermeier, H. J., Dorgan, J. R. (2001). Melt rheology of high L-content poly(lactic acid). *Macromolecules, 34*(5), 1384-1390.

Papanastasiou, A. C., Scriven, L. E., Macosko, C. W. (1983). Integral constitutive equation for mixed flows: viscoelastic characterization. *Journal of Rheology, 27*(4), 387-410.

Pearce, R., Marchessault, R. (1994). Multiple melting in blends of isotactic and atactic poly(beta-hydroxybutyrate). *Polymer, 35*(18), 3990-3997.

Pearson, D.S., Muller, L., Fetters J., Hadjichristidis, N. (1983). Comparison of the rheological properties of linear and star-branched polyisoprenes in shear and elongational flow. *Journal of Polymer Science Part B: Polymer Physics,* 21, 2287-2298.

Perego, G., Cella, G., Bastioli, C. (1996). Effect of molecular weight and crystallinity on poly(lactic acid) mechanical properties. *Journal of Applied Polymer Science, 59*(1), 37-43.

Perego, G., Cella, G. (2010). Mechanical properties. In Auras, R., Lim, L. T., Selke, S. E. M., Tsuji H. (Eds.1), *Poly(lactic acid): Synthesis, structure, properties, processing and applications.* New Jersey: John Wiley & Son, Inc.

Podzimek, S. (1994). Use of GPC coupled with a multiangle laser light scattering photometer for the characterization of polymers. on the determination of molecular weight, size, and branching. *Journal of Applied Polymer Science, 54*(1), 91-103.

Priester, D., Stika, K., Chapman, G., McMinn, R., Ferrandez, P. (1993). Quality-control techniques for processing additives. *ANTEC 93, 39*, 2528-2533.

Radano, C., Baker, G., Smith, M. (2000). Stereoselective polymerization of a racemic monomer with a racemic catalyst: Direct preparation of the polylactic acid stereocomplex from racemic lactide. *Journal of the American Chemical Society*, 122(7), 1552-1553.

Rahman, N., Kawai, T., Go M., Koji, N., Kanaya, T., Watanabe, H., Okamoto, H., Kato, M., Usuki, A., Matsuda, M., Nakajima, K., Honma, N. (2009). Effect of polylactide stereocomplex on the crystallization behavior of poly(L-lactic acid). *Macromolecules, 42*(13), 4739-4745.

Ramamurthy, A. (1986). Wall slip in viscous fluids and influence of materials of construction. *Journal of Rheology, 30*(2), 337-357.

Ramkumar, D. H. S., Bhattacharya, M. (1998). Steady shear and dynamic properties of biodegradable polyesters. *Polymer Engineering and Science, 38*(9), 1426-1435.

Rasal, R. M., Janorkar, A. V., Hirt, D. E. (2010). Poly(lactic acid) modifications. *Progress in Polymer Science, 35*(3), 338-356.

Ray, S., Bousmina, M. (2005). Biodegradable polymers and their layered silicate nano composites: In greening the 21st century materials world. *Progress in Materials Science, 50*(8), 962-1079.

Reeve, M., McCarthy, S., Downey, M., Gross, R. (1994). Polylactide stereochemistry - effect on enzymatic degradability. *Macromolecules, 27*(3), 825-831.

Ren, J., Adachi, K. (2003). Dielectric relaxation in blends of amorphous poly(DL-lactic acid) and semicrystalline poly(L-lactic acid). *Macromolecules, 36*(14), 5180-5186.

Rosenbaum, E., Hatzikiriakos, S., Stewart, C. (1995). Flow implications in the processing of Tetrafluoroethylene/hexafluoropropylene copolymers. *International Polymer Processing, 10*(3), 204-212.

Rosenbaum, E. (1998). Rheology and processability of Teflon FEP resins for wire coating. (PhD, Chemical Engineering, The University of British Columbia).

Sarasua, J., Arraiza, A., Balerdi, P., Maiza, I. (2005). Crystallinity and mechanical properties of optically pure polylactides and their blends. *Polymer Engineering and Science, 45*(5), 745-753.

Sarazin, P., Li, G., Orts, W. J., Favis, B. D. (2008). Binary and ternary blends of polylactide, polycaprolactone and thermoplastic starch. *Polymer, 49*(2), 599-609.

Sawai, D., Takahashi, K., Sasashige, A., Kanamoto, T., Hyon, S. (2003a). Preparation of oriented beta-form poly(L-lactic acid) by solid-state coextrusion: Effect of extrusion variables. *Macromolecules, 36*(10), 3601-3605.

Sawai, D., Takahashi, K., Sasashige, A., Kanamoto, T., Hyon, S. (2003b). Preparation of oriented beta-form poly(L-lactic acid) by solid-state coextrusion: Effect of extrusion variables. *Macromolecules, 36*(10), 3601-3605.

Sawai, D., Tsugane, Y., Tamada, M., Kanamoto, T., Sungil, M., Hyon, S. (2007). Crystal density and heat of fusion for a stereo-complex of poly(L-lactic acid) and poly(D-lactic acid). *Journal of Polymer Science Part B-Polymer Physics, 45*(18), 2632-2639.

Sentmanat, M. (2004). Miniature universal testing platform: From extensional melt rheology to solid-state deformation behavior. *Rheologica Acta, 43*(6), 657-669.

Sentmanat, M., Wang, B. N., McKinley, G. H. (2005). Measuring the transient extensional rheology of polyethylene melts using the SER universal testing platform. *Journal of Rheology, 49*(3), 585-606.

Sodergard, A., Stoclet, G. (2010). Industrial production of high molecular weight poly(lactic acid). In Auras, R., Lim, L., Selke, S. E., Tsuji H. (Eds.1), *Poly(lactic acid) synthesis, structure, properties, processing and applications*. New Jersey: John Wiley & Sons, Inc.

Spassky, N., Wisniewski, M., Pluta, C., LeBorgne, A. (1996). Highly stereoelective polymerization of rac-(D,L)-lactide with a chiral schiff's base/aluminium alkoxide initiator. *Macromolecular Chemistry and Physics, 197*(9), 2627-2637.

Stamboulides, C., Hatzikiriakos, S. G. (2006). Rheology and processing of molten poly(methyl methacrylate) resins. *International Polymer Processing, 21*(2), 155-163.

Takahashi, M., Isaki, T., Takigawa, T., Masuda, T. (1993). Measurement of biaxial and uniaxial extensional flow behavior of polymer melts at constant strain rates. *Journal of Rheology, 37*(5), 827-846.

Takayama, T., Todo, M. (2006). Improvement of impact fracture properties of PLA/PCL polymer blend due to LTI addition. *Journal of Materials Science, 41*(15), 4989-4992.

Tang, H.S., Kalyon, D.M, (2004). Estimation of the parameters of Herschel-Bulkley fluid under wall slip using a combination of capillary and squeeze flow viscometers. *Rheologica Acta*, 43, 80-88.

Thomas, C. M. (2010). Stereocontrolled ring-opening polymerization of cyclic esters: Synthesis of new polyester microstructures. *Chemical Society Reviews, 39*(1), 165-173.

Trinkle, S., Friedrich, C. (2001). Van gurp-palmen-plot: A way to characterize polydispersity of linear polymers. *Rheologica Acta, 40*(4), 322-328.

Tsenoglou, C. (1988). Network architecture and modulus of miscible heteropolymer blends. *Journal of Polymer Science Part B-Polymer Physics, 26*(11), 2329-2339.

Tsuji, H. (2005). Poly(lactide) stereocomplexes: Formation, structure, properties, degradation, and applications. *Macromolecular Bioscience, 5*(7), 569-597.

Tsuji, H., Ikada, Y. (1999). Stereocomplex formation between enantiomeric poly(lactic acid)s. XI. Mechanical properties and morphology of solution-cast films. *Polymer, 40*(24), 6699-6708.

Tsuji, H., Takai, H., Saha, S. (2006). Isothermal and non-isothermal crystallization behavior of poly(L-lactic acid): Effects of stereocomplex as nucleating agent. *Polymer, 47*(11), 3826-3837.

Tsuji, H., Horii, F., Hyon, S., Ikada, Y. (1991a). Stereocomplex formation between enantiomeric poly(lactic acid)s. 2. Stereocomplex formation in concentrated solutions. *Macromolecules, 24*(10), 2719-2724.

Tsuji, H., Hyon, S., Ikada, Y. (1991b). Stereocomplex formation between enantiomeric poly(lactic acid)s. 3. Calorimetric studies on blend films cast from dilute solution. *Macromolecules, 24*(20), 5651-5656.

Tsuji, H., Hyon, S., Ikada, Y. (1991c). Stereocomplex formation between enantiomeric poly(lactic acid)s. 4. Differential scanning calorimetric studies on precipitates from mixed solutions of poly(D-lactic acid) and poly(L-lactic acid). *Macromolecules, 24*(20), 5657-5662.

Tsuji, H., Hyon, S., Ikada, Y. (1992). Stereocomplex formation between enantiomeric poly(lactic acid)s. 5. Calorimetric and morphological studies on the stereocomplex formed in acetonitrile solution. *Macromolecules, 25*(11), 2940-2946.

Tsuji, H., Ikada, Y. (1993). Stereocomplex formation between enantiomeric poly(lactic acid)s. 9. Stereocomplexation from the melt. *Macromolecules, 26*(25), 6918-6926.

Tsuji, H., Ikada, Y. (1995a). Blends of isotactic and atactic poly(lactide). I. Effects of mixing ratio of isomers on crystallization of blends from melt. *Journal of Applied Polymer Science, 58*(10), 1793-1802.

Tsuji, H., Ikada, Y. (1995b). Properties and morphologies of poly(L-lactide): 1. Annealing condition effects on properties and morphologies of poly(L-lactide). *Polymer, 36*(14), 2709-2716.

Tsuji, H., Ikada, Y. (1996). Blends of isotactic and atactic poly(lactide)s: 2. Molecular-weight effects of atactic component on crystallization and morphology of equimolar blends from the melt. *Polymer, 37*(4), 595-602.

Tsuji, H., Wada, T., Sakamoto, Y., Sugiura, Y. (2010). Stereocomplex crystallization and spherulite growth behavior of poly(l-lactide)-b-poly(d-lactide) stereodiblock copolymers. *Polymer, 51*(21), 4937-4947.

Utracki, L. A. (1986). Analysis of polymer blends by rheological techniques. *Journal of Elastomers and Plastics, 18*(3), 177-186.

van Ruymbeke, E., Muliawan, E. B., Hatzikiriakos, S. G., Watanabe, T., Hirao, A., Vlassopoulos, D. (2010). Viscoelasticity and extensional rheology of model cayley-tree polymers of different generations. *Journal of Rheology, 54*(3), 643-662.

Witzke, D. R. (1997). Introduction to properties, engineering and prospects of polylactide polymers. (PhD, Chemical Engineering, Michigan State University).

Woo, E. M., Chang, L. (2011). Crystallization and morphology of stereocomplexes in nonequimolar mixtures of poly(L-lactic acid) with excess poly(D-lactic acid). *Polymer, 52*(26), 6080-6089.

Wu, D., Zhang, Y., Zhang, M., Zhou, W. (2008). Phase behavior and its viscoelastic response of polylactide/poly(e-caprolactone) blend. *European Polymer Journal*, 44, 2171-2183.

Wu, J., Yu, T., Chen, C., Lin, C. (2006). Recent developments in main group metal complexes catalyzed/initiated polymerization of lactides and related cyclic esters. *Coordination Chemistry Reviews, 250*(5-6), 602-626.

www.rcbc.bc.ca

Xu, C. (2012). Living and immortal polymerization of cyclic esters with a dinuclear indium catalyst. (Master, Chemistry, The University of British Columbia).

Xu, J., Guo, B., Zhou, J., Li, L., Wu, J., Kowalczuk, M. (2005). Observation of banded spherulites in pure poly(L-lactide) and its miscible blends with amorphous polymers. *Polymer, 46*(21), 9176-9185.

Yamaguchi, M., Arakawa, K. (2006). Effect of thermal degradation on rheological properties for poly(3-hydroxybutyrate). *European Polymer Journal, 42*(7), 1479-1486.

Yamane, H., Sasai, K. (2003). Effect of the addition of poly(D-lactic acid) on the thermal property of poly(L-lactic acid). *Polymer, 44*(8), 2569-2575.

Yamane, H., Sasai, K., Takano, M., Takahashi, M. (2004). Poly(D-lactic acid) as a rheological modifier of poly(L-lactic acid): Shear and biaxial extensional flow behavior. *Journal of Rheology, 48*(3), 599-609.

Yui, N., Dijkstra, P., Feijen, J. (1990). Stereo block copolymers of L-lactides and D-lactides. *Makromolekulare Chemie-Macromolecular Chemistry and Physics, 191*(3), 481-488.

Zhang, X., Schneider, K., Liu, G., Chen, J., Bruning, K., Wang, D., Stamm, M. (2011). Structure variation of tensile-deformed amorphous poly(L-lactic acid): Effects of deformation rate and strain. *Polymer*, 52, 4141-4149.

Zhong, Z., Dijkstra, P., Feijen, J. (2002). [(Salen)al]-mediated, controlled and stereoselective ring-opening polymerization of lactide in solution and without solvent: Synthesis of highly isotactic polylactide stereocopolymers from racemic D,L-lactide. *Angewandte Chemie-International Edition*, 41(23), 4510.

Appendix A-Linear Viscoelastic Properties of PLA Homopolymers.

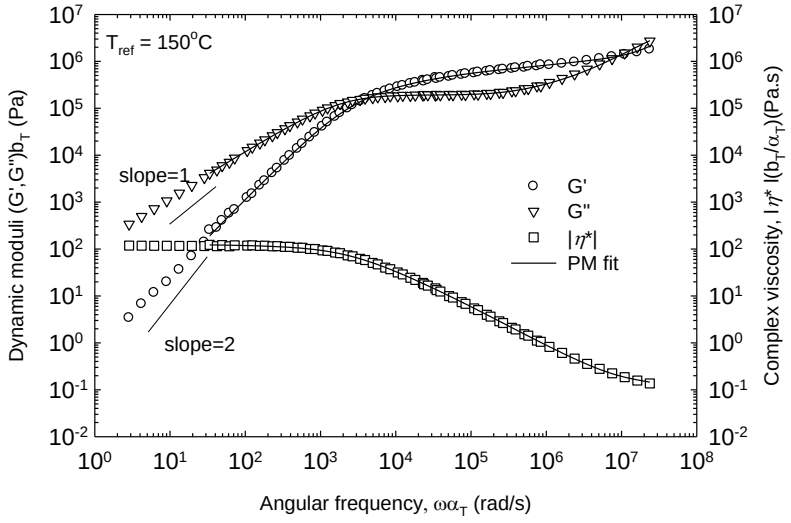

Figure A. 1: Master curve of LD40 at the reference temperature of 150°C.

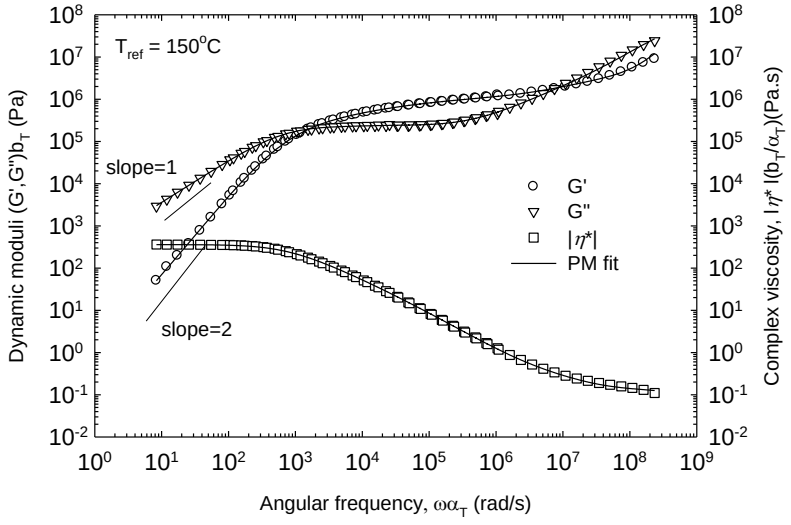

Figure A. 2: Master curve of LD50 at the reference temperature of 150°C.

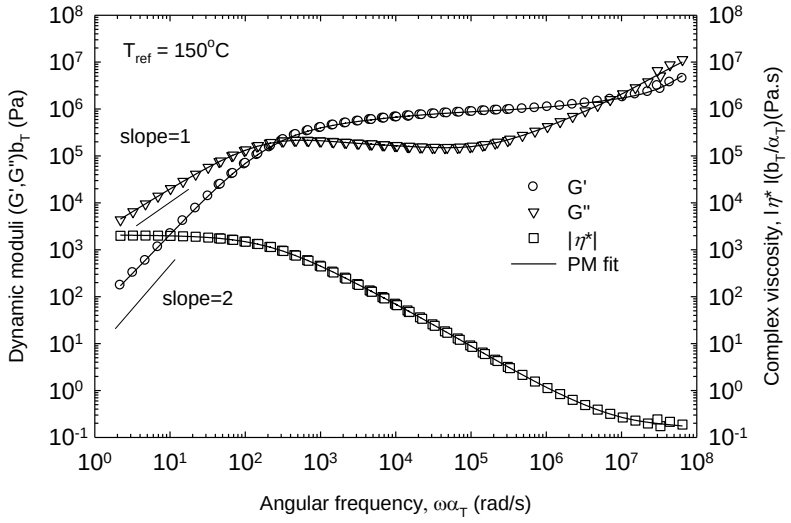

Figure A. 3: Master curve of LD100 at the reference temperature of 150°C.

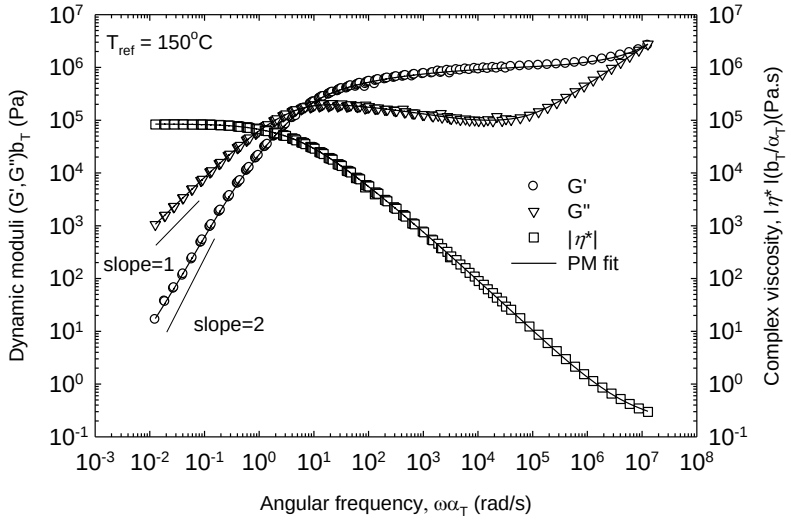

Figure A. 4: Master curve of LD190 at the reference temperature of 150°C.

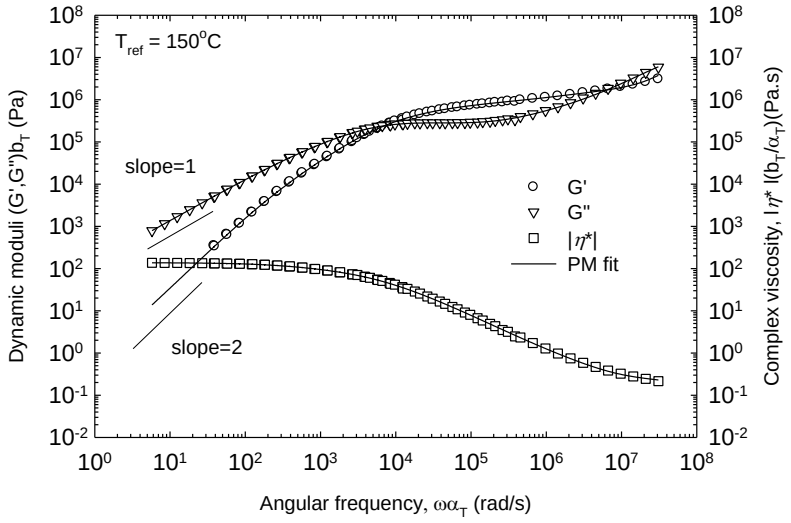

Figure A. 5: Master curve of LD50 A at the reference temperature of 150°C.

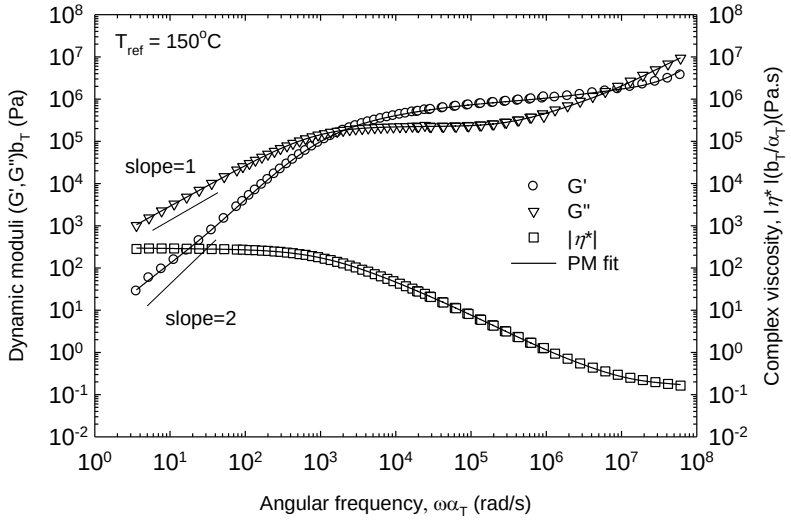

Figure A. 6: Master curve of L75D40 at the reference temperature of 150°C.

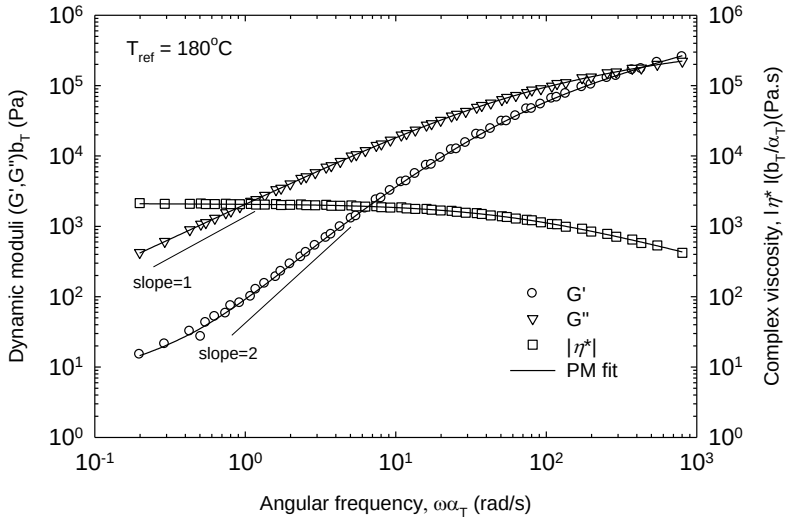

Figure A. 7: Master curve of L130 at the reference temperature of 180°C.

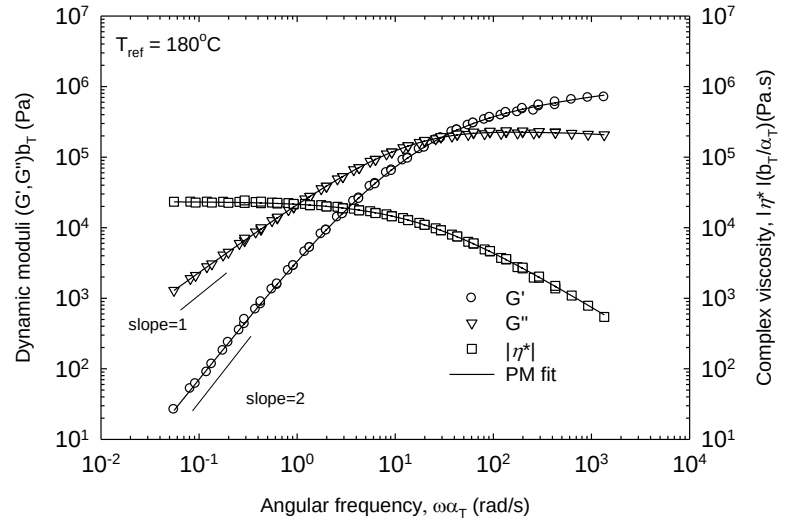

Figure A. 8: Master curve of L190 at the reference temperature of 180°C

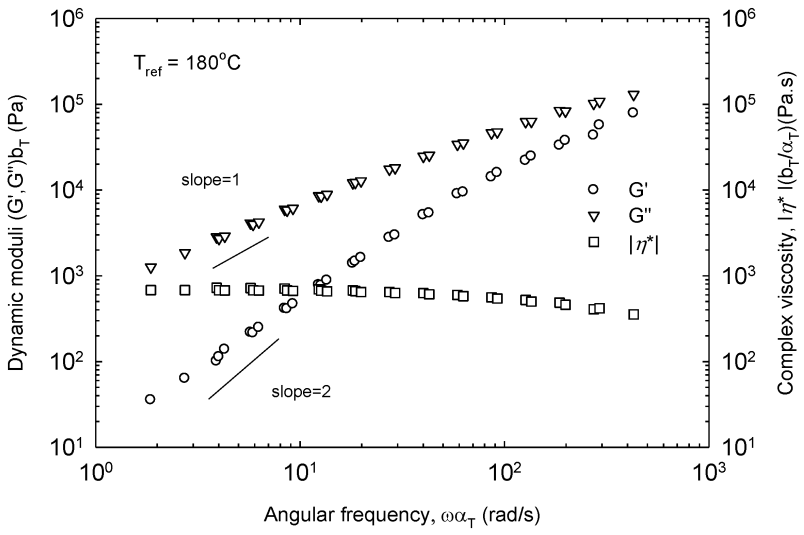

Figure A. 9: Master curve of D100 at the reference temperature of 180°C.

Appendix B-Extensional Rheology of PLA Homopolymers

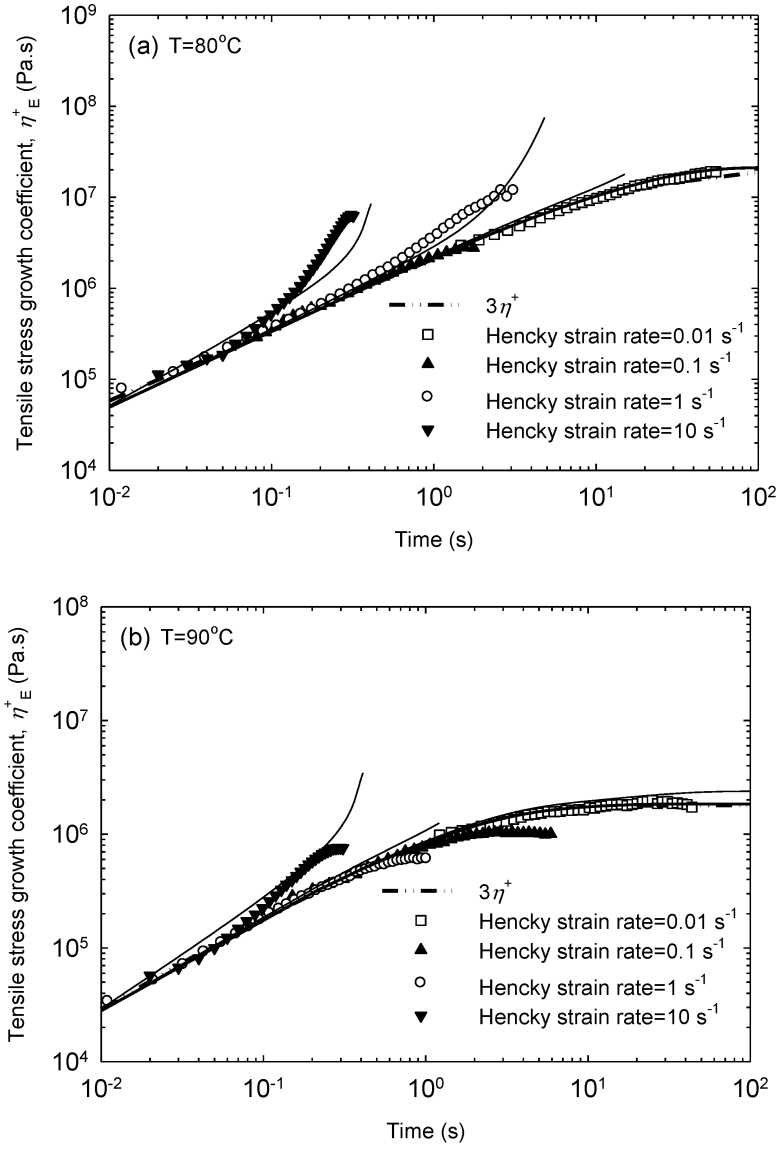

Figure B. 1: Tensile stress growth coefficient as a function of time measured at various Hencky strain rates for LD50 at (a) 80°C and (b) 90°C.

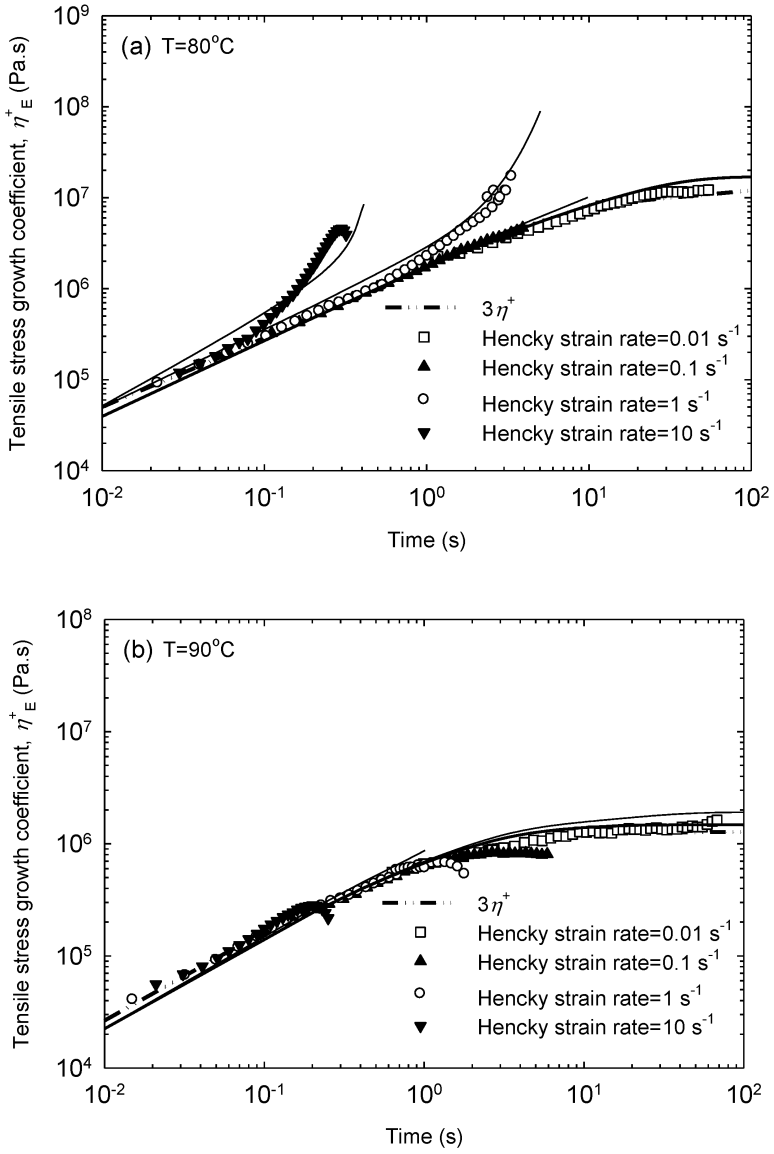

Figure B. 2: Tensile stress growth coefficient as a function of time measured at various Hencky strain rates for L75D40 at (a) 80°C and (b) 90°C.

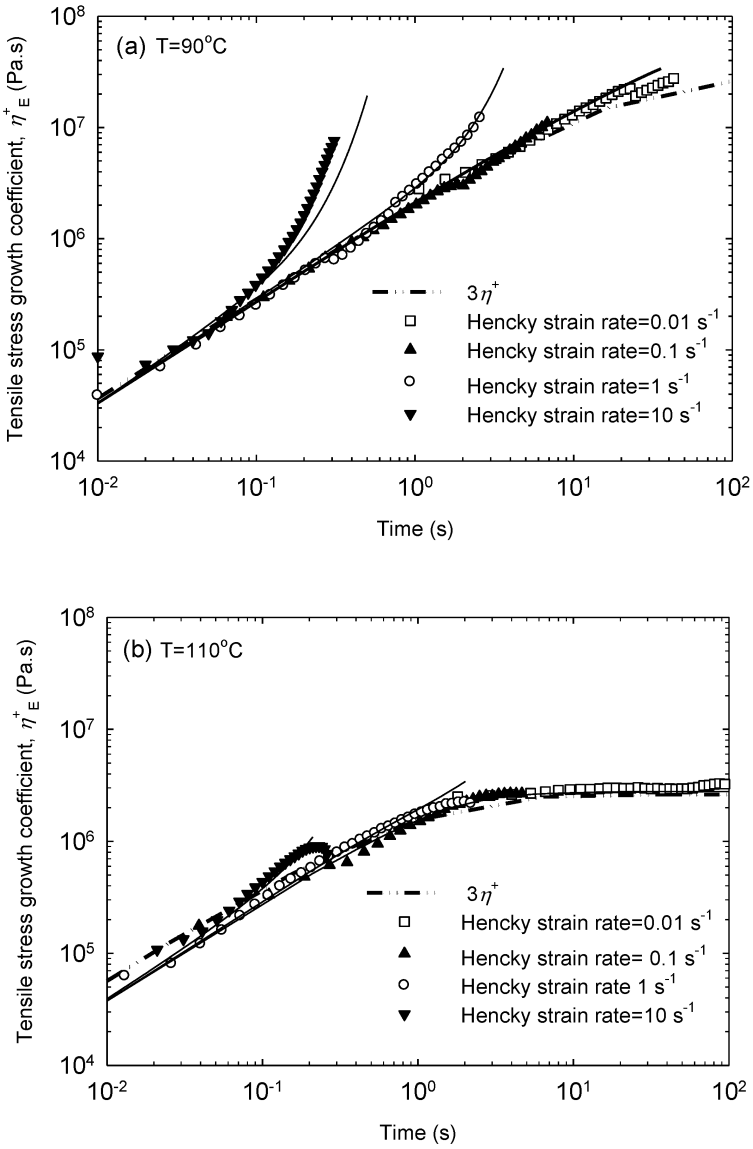

Figure B. 3: Tensile stress growth coefficient as a function of time measured at various Hencky strain rates for L75D100 at (a) 90°C and (b) 110°C.

Appendix C-Linear Viscoelastic Properties of Block Copolymers.

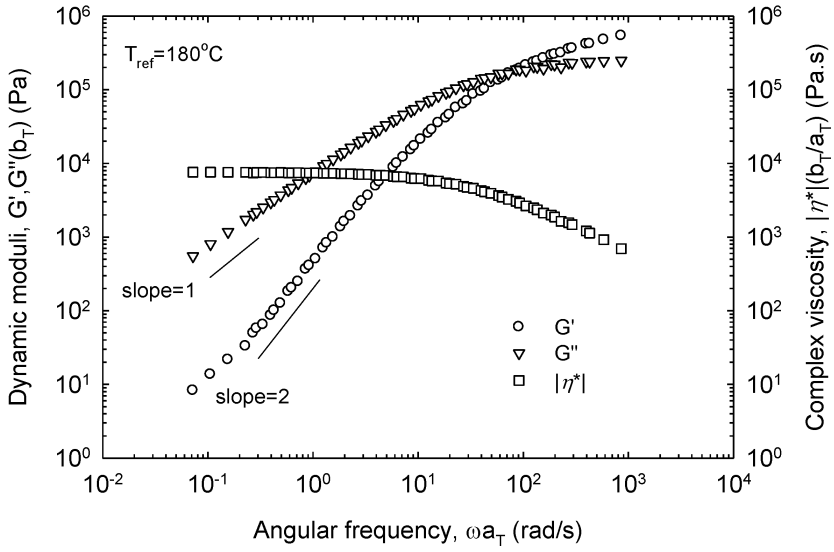

Figure C. 1: Master curve of diblock copolymers 84L-b170-16LD at the reference temperature of 180°C

Appendix D-Capillary Rheometer Studies

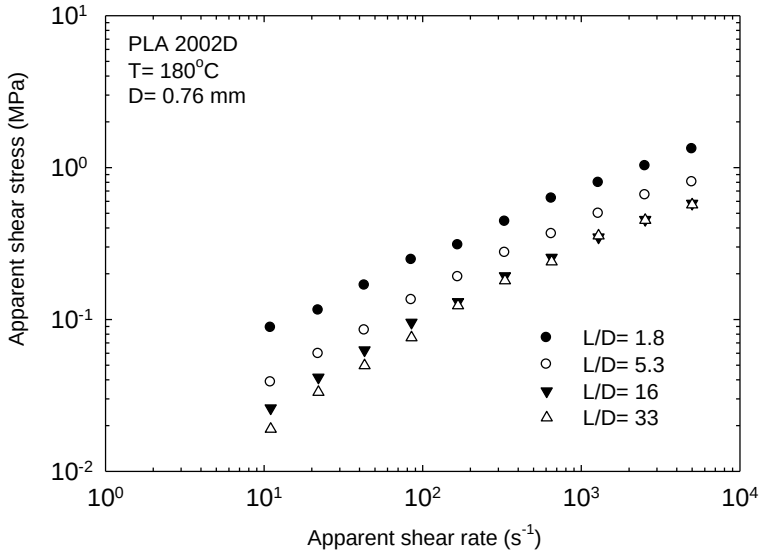

Figure D. 1: The apparent flow curves of PLA 2002D for several dies having the same diameter and various L/D ratio at 180°C.

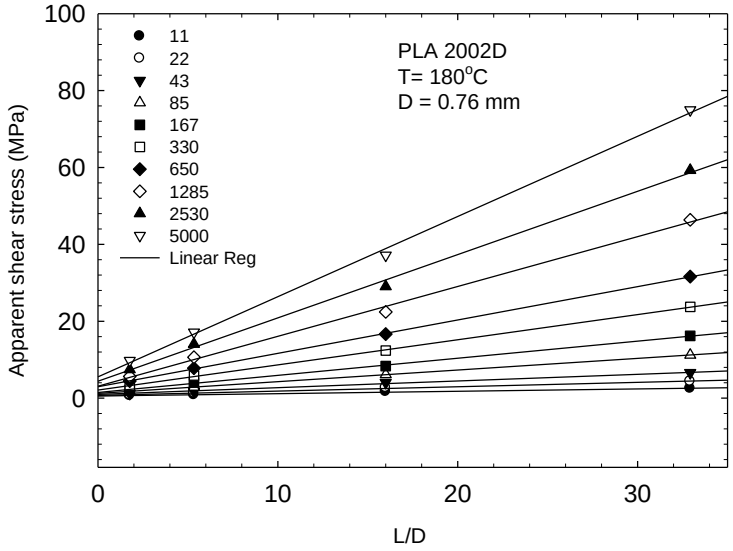

Figure D. 2: Bagley plot for PLA 2002D at 180°C.

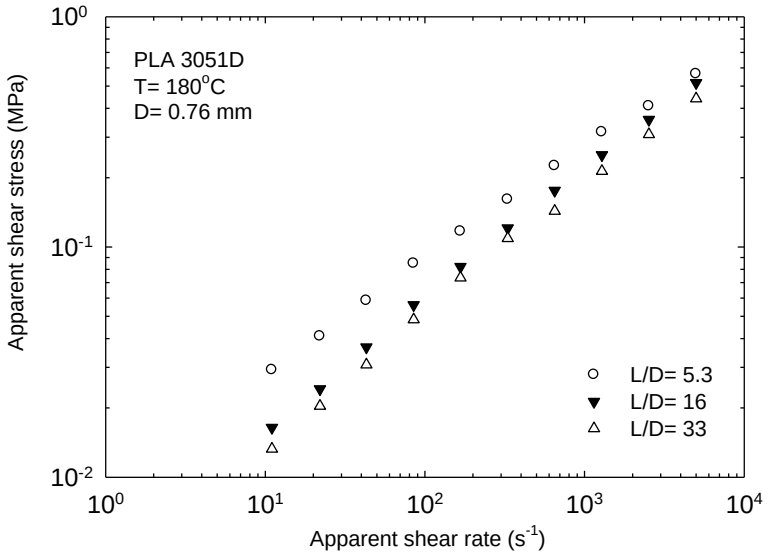

Figure D. 3: The apparent flow curves of PLA 3051D for several dies having the same diameter and various L/D ratio at 180°C.

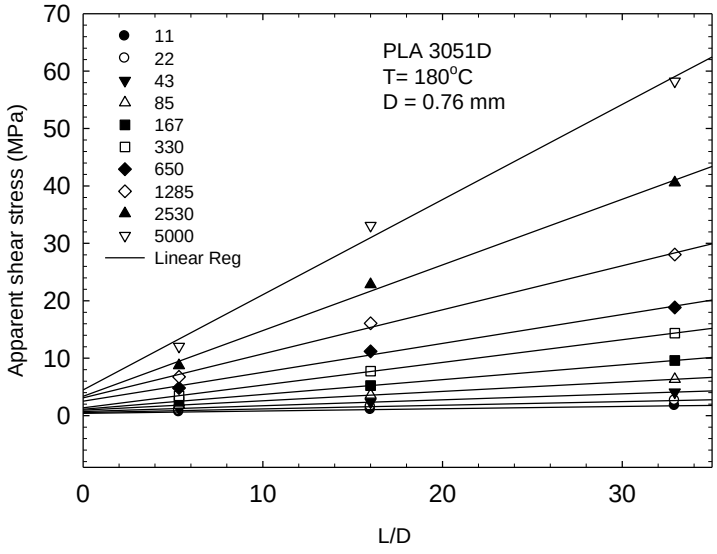

Figure D. 4: Bagley plot for PLA 3051D at 180°C.

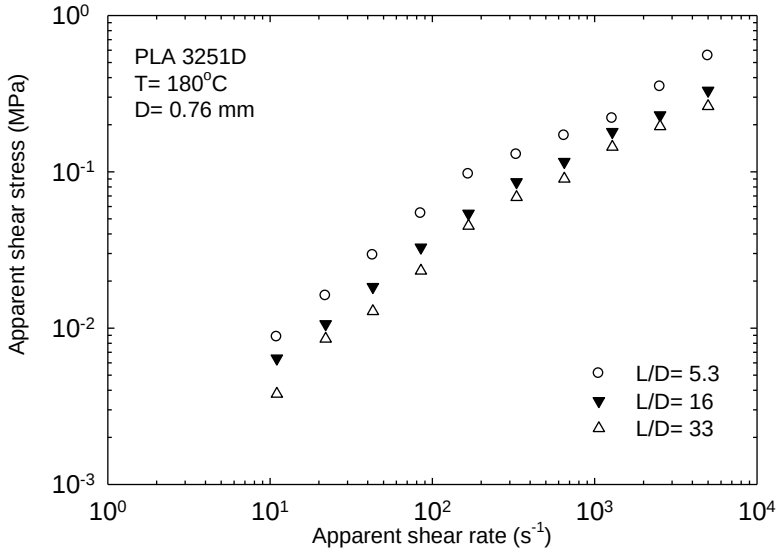

Figure D. 5: The apparent flow curves of PLA 3251D for several dies having the same diameter and various L/D ratio at 180°C.

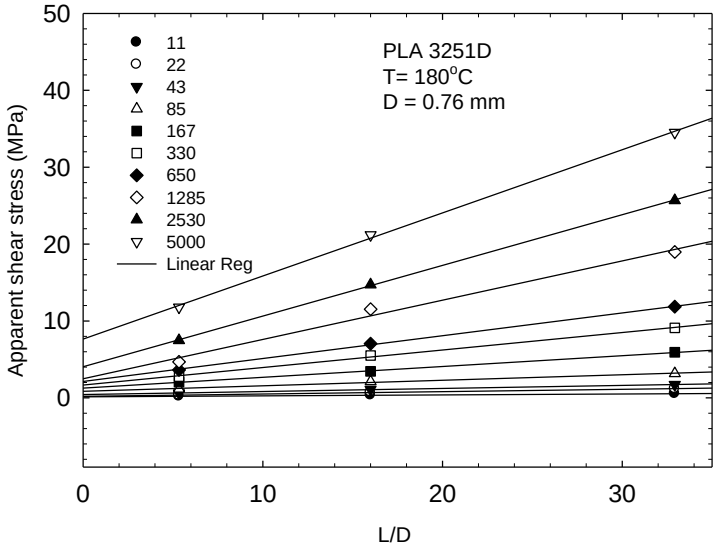

Figure D. 6: Bagley plot for PLA 3251D at 180°C.

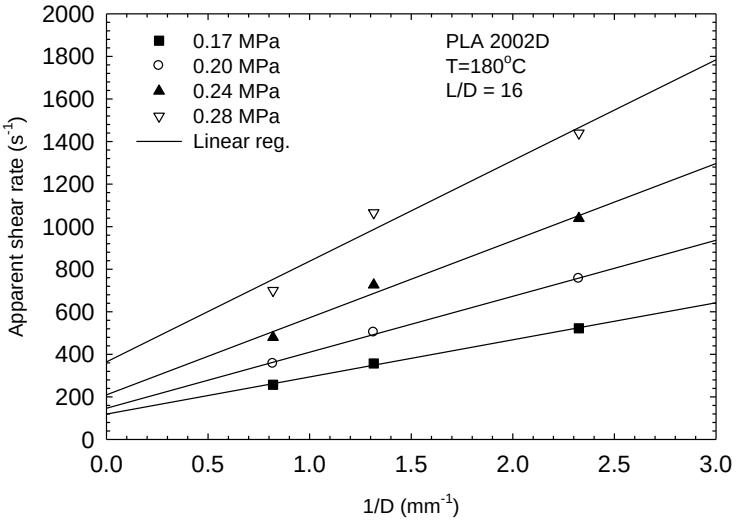

Figure D. 7: The Mooney plot for PLA 2002D at 180°C, constructed to determine its slip velocity.

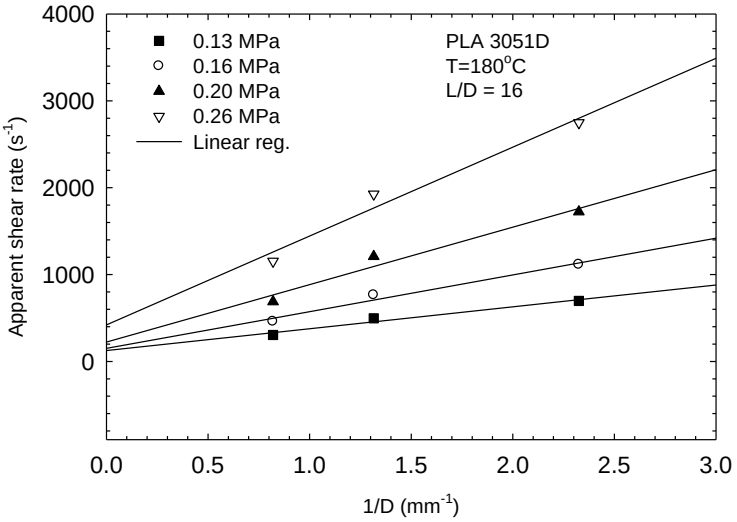

Figure D. 8: The Mooney plot for PLA 3051D at 180°C, constructed to determine its slip velocity.

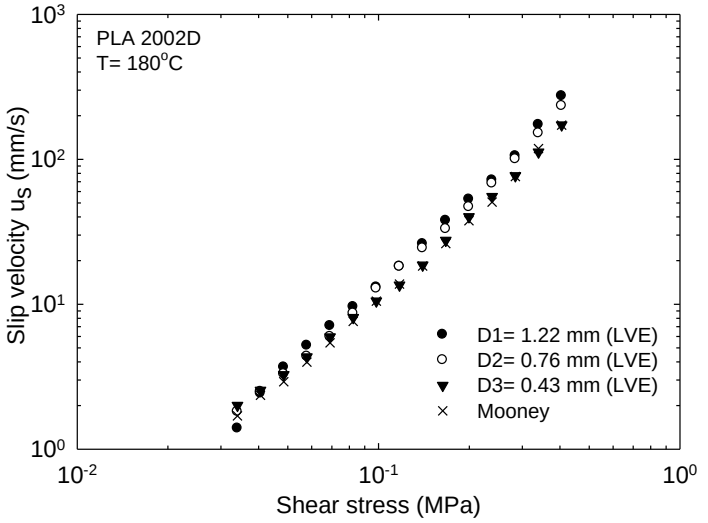

Figure D. 9: The slip velocity, u_s of resin PLA 2002D determined from Mooney analysis and from deviation of various apparent flow curves from the LVE data at 180°C.

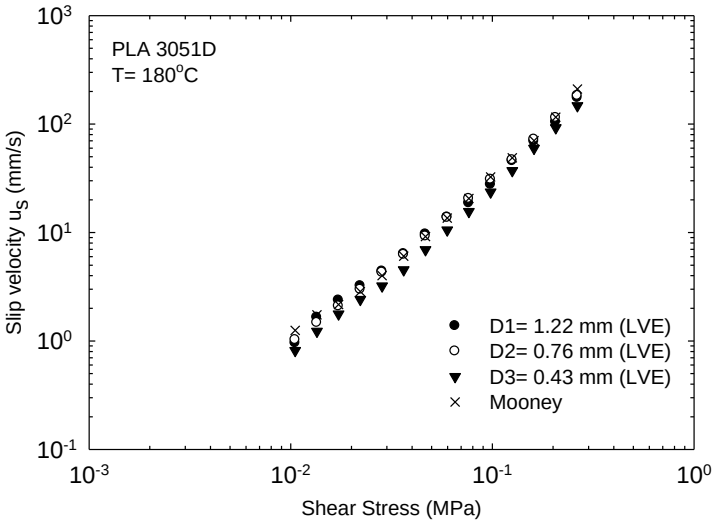

Figure D. 10: The slip velocity, u_s of resin PLA3051D determined from Mooney analysis and from deviation of various apparent flow curves from the LVE data at 180°C.